HOKKAIDO UNIVERSITY

Title	Novel Approaches to NMR Analysis of Complicated Organic Molecules
Author(s)	Fukushi, Eri
Degree Grantor	北海道大学
Degree Name	博士(農学)
Dissertation Number	乙第4989号
Issue Date	1996-03-25
DOI	https://doi.org/10.11501/3112178
Doc URL	https://hdl.handle.net/2115/51348
Type	doctoral thesis
File Information	000000297370.pdf

Hokkaido University Collection of Scholarly and Academic Papers : HUSCAP

Novel Approaches to NMR Analysis of Complicated Organic Molecules

特異な構造を有する有機化合物のための あたらしいNMR法の開発

Eri FUKUSHI

福士 江里

①

Novel Approaches to NMR Analysis of Complicated Organic Molecules

特異な構造を有する有機化合物のための
あたらしいNMR法の開発

Eri FUKUSHI
福士　江里

Novel Approaches to NMR Analysis of Complicated Organic Molecules

Contents

1 General introduction 1
- 1.1 Introduction 1
- 1.2 General experimental conditions 9

2 Structure elucidation of C_2 symmetric molecules 11
- 2.1 Introduction 11
- 2.2 The non-equivalency of equivalent nuclei in NMR 11
- 2.3 Connectivity between equivalent carbons 13
- 2.4 NOEs between equivalent protons 21
- 2.5 *J* couplings between equivalent protons 29
- 2.6 Introduction of paired satellite selection (PASS) and its product operator analysis 41
- 2.7 Two long-range J_{CH} values between one carbon and two equivalent protons 51
- 2.8 Discrimination of intra- and inter-unit NOEs 58
- 2.9 Experimental 69

3 NMR analysis of consecutive quaternary carbon systems 77
- 3.1 Introduction 77
- 3.2 1D DEPT C-C relay 79
- 3.3 2D DEPT C-C COSY 89
- 3.4 Measurement of long-range C-C coupling 95
- 3.5 Experimental 101

4 Discrimination of C-H connectivities via two and three bonds 105
- 4.1 Introduction 105
- 4.2 1D heteronuclear $^{13}C\{^1H\}$ NOE 108
- 4.3 Experimental 113

5 Summary 115

6 References 118

7 Summary in Japanese 123

1. General introduction

1.1 Introduction

Nuclear magnetic resonance (NMR) spectroscopy is one of the most important instrumental analysis methods in structural chemistry. In 1995, NMR spectroscopy reached the 50th anniversary. In the 1950's, it was the chemical shifts and the spin couplings (*J* couplings) that NMR had attracted chemists. The early ^{1}H NMR spectrum of ethanol showed three signals whose ratio of area was 3:2:1, corresponding to the CH_3-CH_2-OH (*1*). It is easy to imagine that this spectrum so excited the chemists of those days. In the 1960's, the nuclear Overhauser effects (NOEs) were begun to use for determination of spatial arrangement of nuclei. The chemical shifts, *J* couplings, and NOEs are the basic and main information from NMR as far as the structure elucidation of organic molecules. In the 1970's, the idea of two-dimensional (2D) NMR, first suggested by Jeener (*2*), was realized by Ernst (*3*). The application of NMR took a great leap forward by development of 2D methods. It should be noted that the Nobel prize for chemistry was awarded to Ernst in 1991 for his building up the base of modern NMR by introducing FT and 2D NMR.

NMR is now an indispensable tool for structure elucidation of natural products. Complex structure of compounds will be determined by various routine 1D and 2D NMR methods, by both improvement of the hardware and development of multipulse sequences. There are, however, some limitations in the conventional NMR methods. As far as my experience for these several years, following structural problems were left unsolved because of these inherent limitations.

1. Distinction of equivalent nuclei in symmetric molecules.
2. Analysis of highly proton-deficient molecules.

3. Discrimination of C-H connectivities via two and three bonds.

In order to solve these problems, I tried to develop some new techniques as well as modification of conventional methods.

1. Distinction of equivalent nuclei in symmetric molecules.

A C_2 symmetric molecule has a symmetry axis of second order and two equivalent units. The structure elucidation of such symmetric compounds by NMR methods is problematic because of the presence of two equivalent units in the molecule. Each pair of equivalent nuclei gives same signals in ^{1}H and ^{13}C NMR. Thus, it is almost impossible to distinguish between equivalent nuclei in the conventional NMR methods.

This inherent problem of structure elucidation of C_2 symmetric molecules has been established from the viewpoint of isotopomeric asymmetry utilizing the low natural abundance (1.11 %) of NMR detectable ^{13}C. Regarding one pair of equivalent carbons in a C_2 symmetric system , an isotopomer consisted of $\{^{12}C, ^{12}C\}$ is predominant (97.8%), whereas $\{^{13}C, ^{12}C\}$ (2.20%) and $\{^{13}C, ^{13}C\}$ (0.01%) isotopomers are minor. In ^{13}C NMR the major isotopomer is undetectable, and is therefore excluded. Furthermore, in the detectable two minor isotopomers, the $\{^{13}C, ^{13}C\}$ species can also be neglected because of its low natural abundance. Hence, the only isotopomer to be considered is the $\{^{13}C, ^{12}C\}$ species, which is not symmetrical (Fig.1.1). Concerning the heteronuclear coupling, the ^{13}C-bonded proton splits into a doublet by remarkable large $^{1}J_{CH}$ (> 120 Hz) whereas the ^{12}C-bonded proton is observed as a singlet or a doublet by small long-range coupling ($^{LR}J_{CH}$ < 15 Hz). These heteronuclear couplings are decoupled in most of the conventional NMR methods. Novel or modified pulse sequences

without heteronuclear decoupling solved structural problems characteristic of symmetric molecules (*4*).

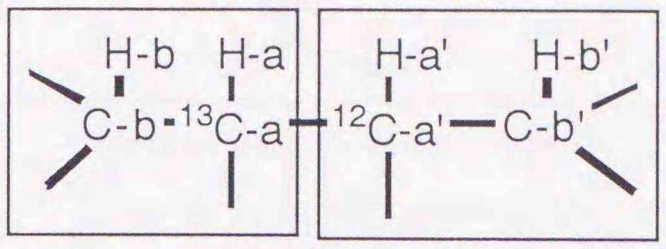
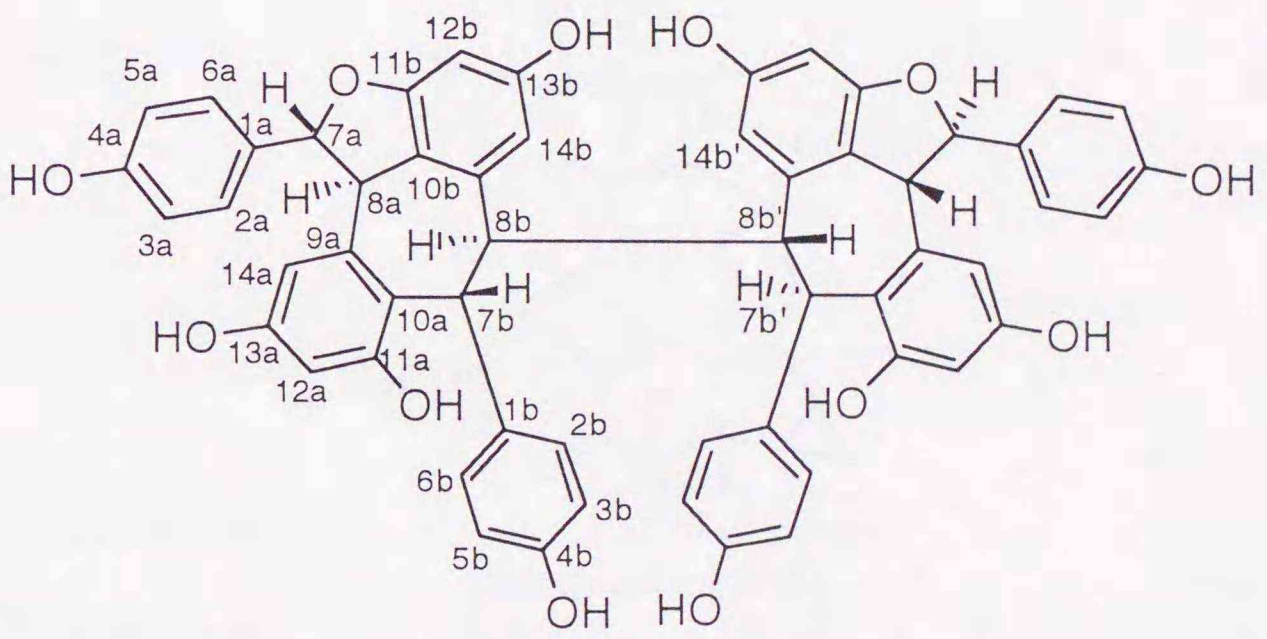


Fig.1.1. Symmetric structural fragment. Equivalent units are boxed in each other. Each pair of equivalent nuclei are given same labels. The labels without prime are given to the unit containing a ^{13}C, and that with prime to the ^{12}C counterpart.

Connectivity between equivalent carbons, C-a and C-a' in Fig.1.1, will be confirmed by detecting long-range couplings between ^{13}C-a and H-a'. In the case of hopeaphenol (**1**), connectivity between C-8b and C-8b' was confirmed (*4*) by detecting long-range couplings between C-8b and H-8b' separately from direct connection of C-8b and H-8b in the LSPD (*5*), modified COLOC (*6*), and HMBC (*7*, *8*) spectra. The acronyms are listed in the section 1.2.



hopeaphenol (**1**)

NOEs between equivalent protons H-a and H-a' as shown in Fig.1.2, were detected for the first time by the detection of the negative cross-

peaks at the center of the split HMQC correlations in the ^{13}C-coupled HMQC-NOESY (*9*) and (ROESY) (*10*) spectra.

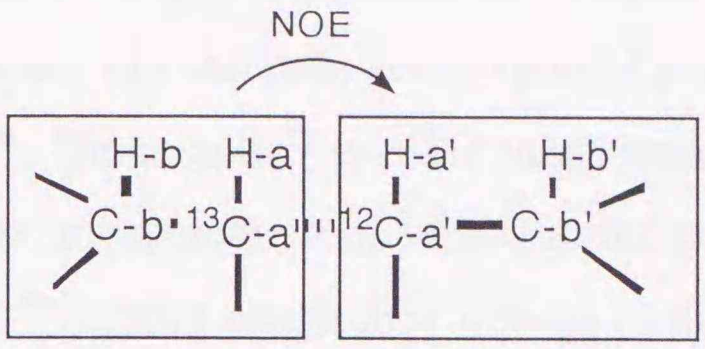
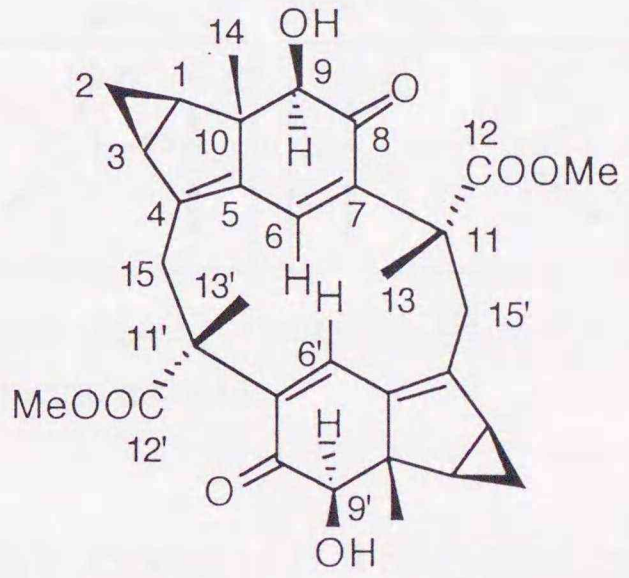


Fig.1.2. NOE between equivalent protons (H-a/H-a').
Direct connectivity between C-a and C-a' is not essential.

In the case of the ^{13}C-coupled HMQC-NOESY spectrum of cycloshizukaol A (**2**), the NOE between H-9 and H-9' made it possible to determine conformation of the flexible twelve-membered ring and stereochemistry on C-11 (*11*). Moreover, the ^{13}C-coupled HMQC-ROESY sequence was constructed to apply to molecules of intermediate size such as **1**. The molecular conformation was deduced from the presence of the ROE between H-7b and H-7b' (*12*).



cycloshizukaol A (**2**)

In addition, the measurement of spin-spin couplings between equivalent protons was achieved by ω_1 hetero half-filtered DQF-COSY

without interference of long-range CH couplings. The obtained ^{3}J(H-8b/H-8b') value also supported the conformation of **1**.

Next, as a novel concept for conversion of 2D ω_1 hetero half-filtered methods to their 1D variants, PASS (*pa*ired *s*atellite *s*election) has been introduced (*13*). The resulting two 1D subspectra are equivalent to the two slices used for measurement of $^{LR}J_{CH}$ in the corresponding 2D experiment (*14*, *15*). The long-range J_{CH} appears as displacement of signals in those two 1D spectra. In **1**, J couplings between C-8b and H-7b ($^{2}J_{CH}$) and between C-8b and H-7b' ($^{3}J_{CH}$) could be measured separately. The value of $^{3}J_{CH}$ was consistent with the conformation determined above.

Discrimination of intra-unit (H-a/H-b) and inter-unit (H-a/H-b') NOEs (Fig.1.3) would be established by PASS-NOESY and PASS-ROESY provided that long-range J(C-a/H-b) and J(C-a/H-b') are different.

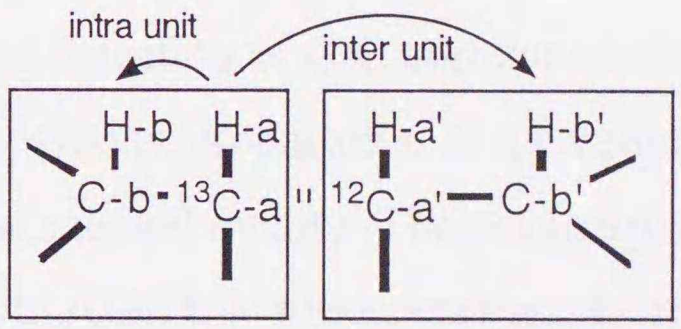


Fig.1.3. Intra- (H-a/H-b) and inter- (H-a/H-b') unit NOEs in a C_2 symmetric molecule.

The PASS-NOESY spectra at H-9 of cycloshizukaol A (**2**) detected the intra-unit NOE between H-9 and H-1. In the similar manner, the PASS-ROESY spectra at H-8b of hopeaphenol (**1**) indicated the presence of an intra-unit ROE between H-8b and H-14b.

2. Analysis of highly proton-deficient molecules.

As for the structure elucidation of molecules containing sequential quaternary carbons, detection of ^{13}C-^{13}C connectivity is a necessity. One of the most popular methods for detecting C-C direct connectivities is INADEQUATE (*16*, *17*) despite the two major disadvantages. Those are the inherent low sensitivity because of detecting low population (0.01%) of isotopomers containing ^{13}C-^{13}C bonds at natural abundance and the resonance-offset effects of the radio frequency (RF) pulses. I proposed a new detection method for ^{13}C-^{13}C coupling, DEPT C-C relay (*18*), which enabled sensitivity enhancement by DEPT polarization transfer and observation of ^{13}C-^{13}C satellites without any resonance-offset variation of phase distortion through the wide range of ^{13}C resonance. By this phase-distortionless sequence, it has become possible to apply DEPT spectrum editing to the relayed spectra to discriminate CH_3-, CH_2-, CH-C connectivities. Furthermore, accurate J_{CC} values could be determined since constant phase results were available (*19*).

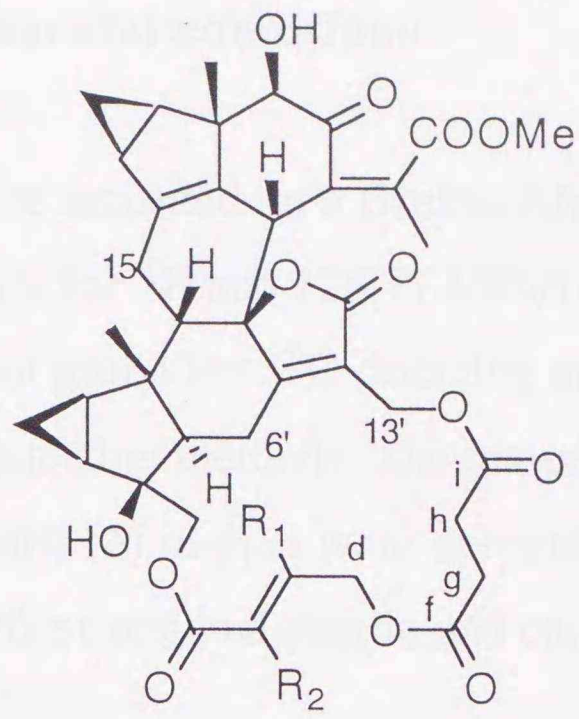
In addition, a 2D variant of the sequence was also proposed, which enabled well-resolved detection of C-C correlations including those between protonated carbons. Application of a baseline subtraction routine greatly improved the spectral quality. The advantages of these relay methods over INADEQUATE are independence from variation of J_{CC} values and no sensitivity loss caused by double-quantum filtration (*20*).

Correlations between proton and carbon via more than three bonds could be obtained by the DEPT C-C relay methods, tuning the C-C relay part for long-range C-C couplings. That made it possible to observe the CH correlations through 4 bonds (^{1}H-^{13}C-X-X-^{13}C).

3. Discrimination of C-H connectivities via two and three bonds.

Heteronuclear long-range CH correlation spectroscopies, such as COLOC and HMBC detect long-range CH couplings existing between carbon and proton via two (^{13}C-X-H) and three (^{13}C-X-X-H) bonds, where X represents carbon or other heteroatom. The small differences in absolute values between $^{2}J_{CH}$ and $^{3}J_{CH}$, however, result in the difficulty in distinguishing C-H couplings via two and three bonds, which might be in some cases critical in structure elucidation of natural products.

The discrimination of CH connectivities via two and three bonds was achieved by detection of two-bond connectivities selectively by the application of heteronuclear $^{13}C\{^{1}H\}$ NOE experiments. The spatial distance of a proton to a carbon via two and that via three bonds are quite different, in contrast to the small difference in values of $^{2}J_{CH}$ and $^{3}J_{CH}$. The $^{13}C\{^{1}H\}$ NOE experiments are, however, not recognized as a routine measurement compared to homonuclear $^{1}H\{^{1}H\}$ NOE experiments because of its inherent low sensitivity. There are two methods for $^{13}C\{^{1}H\}$ NOE experiments as in the case for the $^{1}H\{^{1}H\}$ NOE; saturation of proton transitions (steady-state NOE) (*21*) and inversion of proton transitions (transient NOE) (*22*). Two methylenes (g and h) of shizukaols F (**3**) and B (**4**) had not been assigned by conventional $^{LR}J_{CH}$ detection methods, COLOC or HMBC, because both methylenes showed correlation to both carbonyl carbons of C-f and C-i. Heteronuclear $^{13}C\{^{1}H\}$ NOE experiments reveal the assignment by NOEs from H-g to C-f and from H-h to C-i (*23*, *24*). In the transient NOE experiments, double DANTE pulse train (*25*) was used for simultaneous inversion of two non-equivalent protons whose chemical shifts were far from each other.



	R_1	R_2
3	Me	H
4	H	Me

shizukaol F (**3**) and B (**4**)

1.2 General experimental conditions

NMR spectra were recorded on a Bruker AM500 spectrometer operating at 500.13 MHz for ^{1}H and 125.77 MHz for ^{13}C with a 5-mm tube using a $^{13}C/^{1}H$ dual probe for ^{13}C detecting methods or an $^{1}H/^{13}C$ inverse probe for ^{1}H detecting methods. The temperature was maintained at 297° K. Chemical shifts (δ) in ppm were determined relative to tetramethylsilane (TMS) or residual proton and carbon signals of solvents as follows.

	δ_H(ppm)	δ_C(ppm)	
TMS	0	0	
acetone-d_6	2.04	29.8	(Me)
pyridine-d_5	7.19	123.4	(C-3)
chloroform-d	7.26	77.0	
DMSO-d_6	2.49	39.7	

Typical experimental conditions are as follows. For 1D ^{1}H spectra, FIDs were accumulated in 32K data points for a spectral width of 8,064 Hz at 500.135 MHz. Exponential multiplication (line broadening (LB) factor = 0.2) was performed prior to Fourier transformation. For proton-decoupled ^{13}C spectra, FIDs were accumulated in 64K data points for a spectral width of 31,250 Hz at 125.759 MHz. Exponential weighting with a LB factor of 1 Hz were applied before Fourier transformation.

In pulse sequence schemes, narrow and wide bars represent 90° and 180° pulses, respectively. ^{1}H pulses were derived from the high-power output of the decoupler channel attenuated by 1 dB (90° pulse duration was 10 - 15 μs) except for ^{1}H normal spectra in which the pulse was derived from the high-power output of the transmitter (90° pulse duration was 17 μs). ^{13}C pulses were derived from the high-power output

of the transmitter (90° pulse duration was 5-9 μs), and selective ^{13}C rectangular pulse was derived by attenuation of transmitter pulse through BFX-5 amplifier (90° pulse duration was 2.1 ms, the calculated field strength, $\gamma B_1/2\pi$, is 120 Hz) (*26*) unless otherwise stated. RD and BD represent a repetition delay and a BIRD delay for eliminating ^{12}C-bonded proton signals, respectively. Other pulses and delays are mentioned in each Chart's legend.

The following acronyms are used in the text.

BIRD: bilinear rotation decoupling

CW: continuous wave

COLOC: ^{1}H-^{13}C shift correlation via long-range coupling

COSY: correlated spectroscopy

DANTE: delays alternating with nutations for tailored excitation

DEPT: distortionless enhancement by polarization transfer

DQF-COSY: double quantum filtered-COSY

INADEQUATE: incredible natural abundance double quantum transfer experiment

INEPT: insensitive nuclei enhanced by polarization transfer

HETLOC: determination of heteronuclear long-range couplings

HMBC: heteronuclear multiple-bond correlation

HMQC: heteronuclear multiple-quantum coherence

LSPD: long-range selective proton decoupling

MLEV: Malcom Levitt

NOESY: nuclear Overhauser enhancement spectroscopy

ROESY: rotating-frame Overhauser enhancement spectroscopy

TOCSY: total correlation spectroscopy

TPPI: time proportional phase increment

2 Structure elucidation of C_2 symmetric molecules

2.1 Introduction

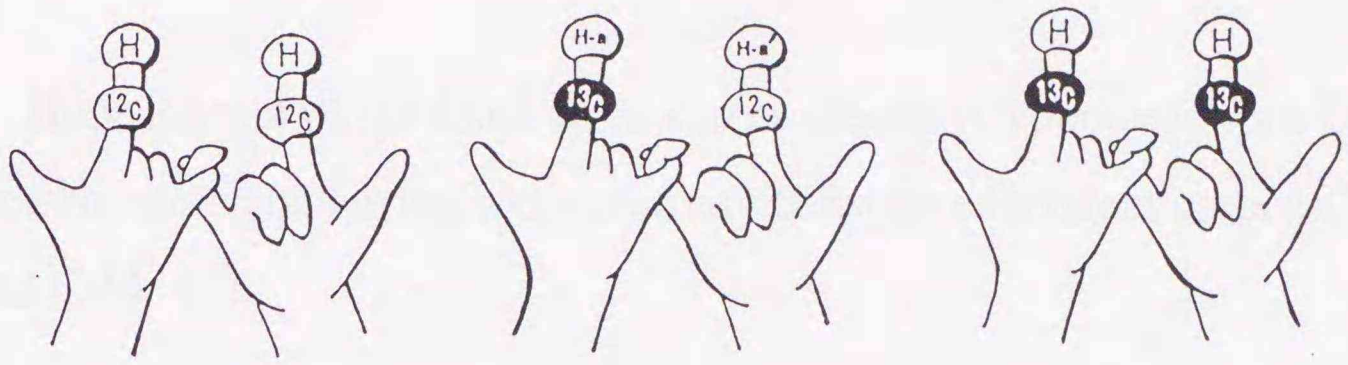
A number of biologically active natural products having C_2 symmetry have been isolated over the last few years (*27 - 29*). A C_2 symmetric molecule has a symmetry axis of second order and two equivalent units. The structure elucidation of such symmetric compounds by NMR methods is problematic because of the presence of two equivalent units in the molecule. Each pair of equivalent nuclei gives same signals in ^{1}H and ^{13}C NMR. Thus, it is almost impossible to distinguish between equivalent nuclei in the conventional NMR methods.

This inherent problem of symmetric molecules has been overcome from the isotopomeric point of view which utilizes low natural abundance of ^{13}C, an NMR active isotope in contrast to inactive abundant ^{12}C.

2.2 The non-equivalency of equivalent nuclei in NMR

A C_2 symmetric molecule has two equivalent units. In Fig. 2.1, each of two equivalent units is exhibited as one right hand. The natural abundance of NMR detectable carbon nucleus, ^{13}C, is 1.11%. It usually causes a trouble of low sensitivity of NMR methods concerned ^{13}C. This low natural abundance of ^{13}C, however, fortunately gives a breakthrough in NMR analysis of symmetric molecules. Regarding one pair of equivalent carbons in a C_2 symmetric molecule, an isotopomer consisted of $\{^{12}C, ^{12}C\}$ is predominant (97.8%), whereas $\{^{13}C, ^{12}C\}$ (2.20%) and $\{^{13}C, ^{13}C\}$ (0.01%) isotopomers are minor. In ^{13}C NMR the major $\{^{12}C, ^{12}C\}$ isotopomer is undetectable, and is therefore excluded.

Further, in the detectable two minor isotopomers, the $\{^{13}C, ^{13}C\}$ species can also be neglected because of its low natural abundance. Hence, the only isotopomer to be considered is the $\{^{13}C, ^{12}C\}$ species. Obviously, this molecule is not symmetrical and, therefore, the two units are now distinguishable.



97.8% 2.20% 0.01%

Fig. 2.1. Three isotopomers of a C_2 symmetric molecule. Each of two equivalent units is exhibited as one right hand. Regarding one pair of equivalent carbons in a C_2 symmetric molecule, an isotopomer consisted of $\{^{12}C, ^{12}C\}$ is predominant (97.8%), whereas $\{^{13}C, ^{12}C\}$ (2.20%) and $\{^{13}C, ^{13}C\}$ (0.01%) isotopomers are minor.

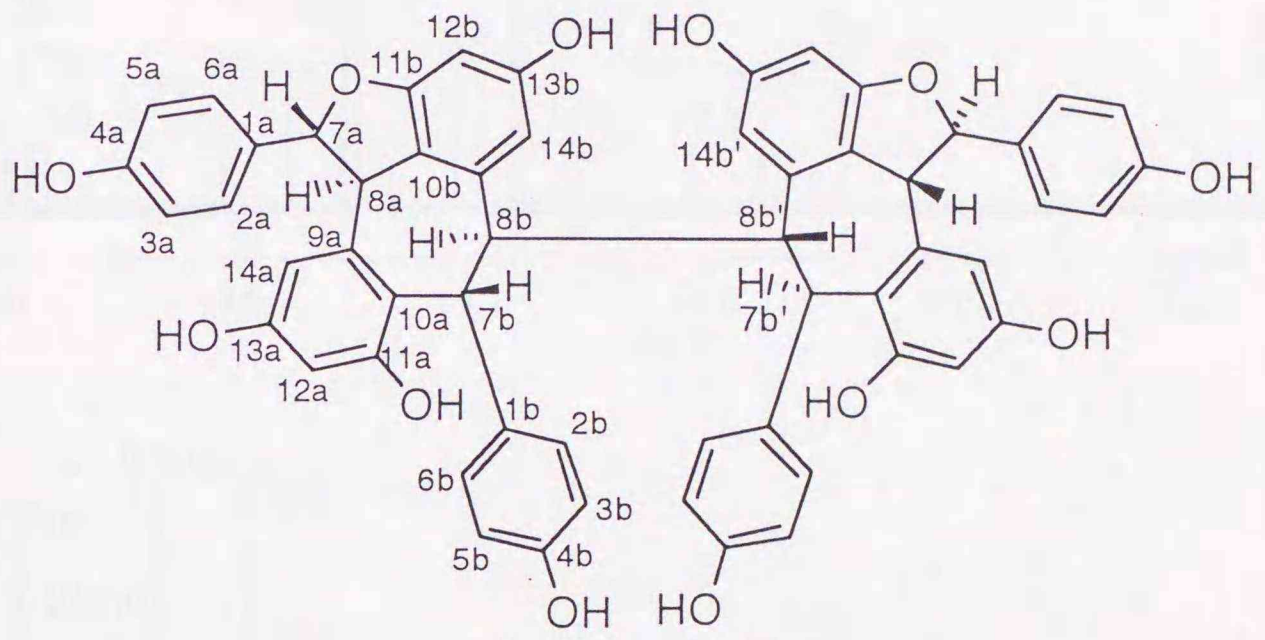
In the case of ^1H NMR, the circumstances are the same and a proton attached to the ^{13}C is evidently non-equivalent to that attached to the ^{12}C. Concerning the heteronuclear coupling, the former proton splits into a remarkable large doublet by $^1J_{CH}$ (> 120 Hz) whereas the latter proton is a singlet or a doublet by small long range coupling ($^{LR}J_{CH}$ < 15 Hz). These heteronuclear couplings are decoupled in most of the conventional NMR methods. Novel or modified pulse sequences without heteronuclear decoupling enabled the structure elucidation of C_2 symmetric molecules from the viewpoint of this isotopomeric asymmetry (*4*).

The large doublet split by $^1J_{CH}$ is represented as a satellite signal. To present the symmetric structures or structural fragments in this thesis,

when the two units should be distinguished, the numbering without prime is given to the unit bearing a ^{13}C, and that with prime to the ^{12}C counterpart.

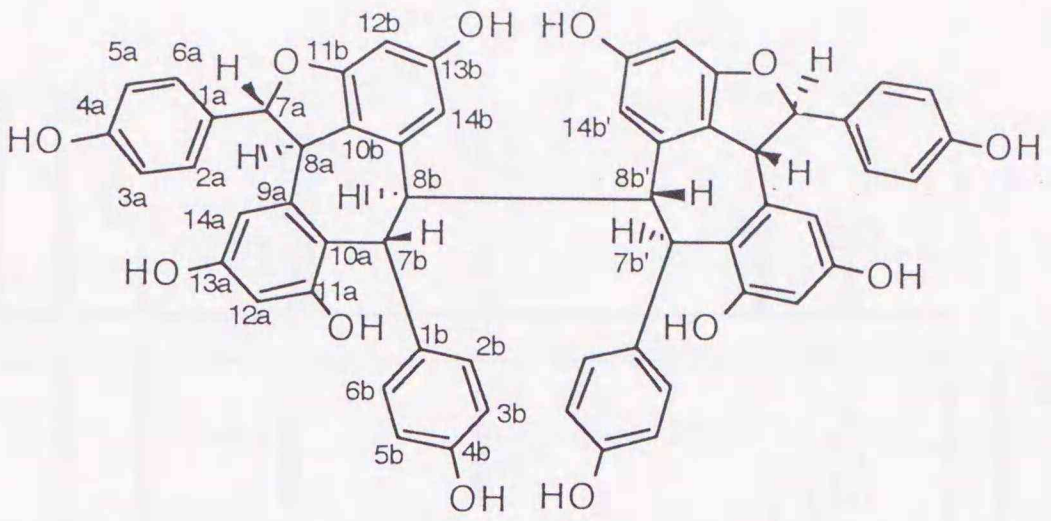
2.3 Connectivity between equivalent carbons

Hopeaphenol (**1**) isolated from *Carex* species (Cyperaceae) is a C_2 symmetric molecule having a connectivity between equivalent carbons, C-8b and C-8b' (*4*).

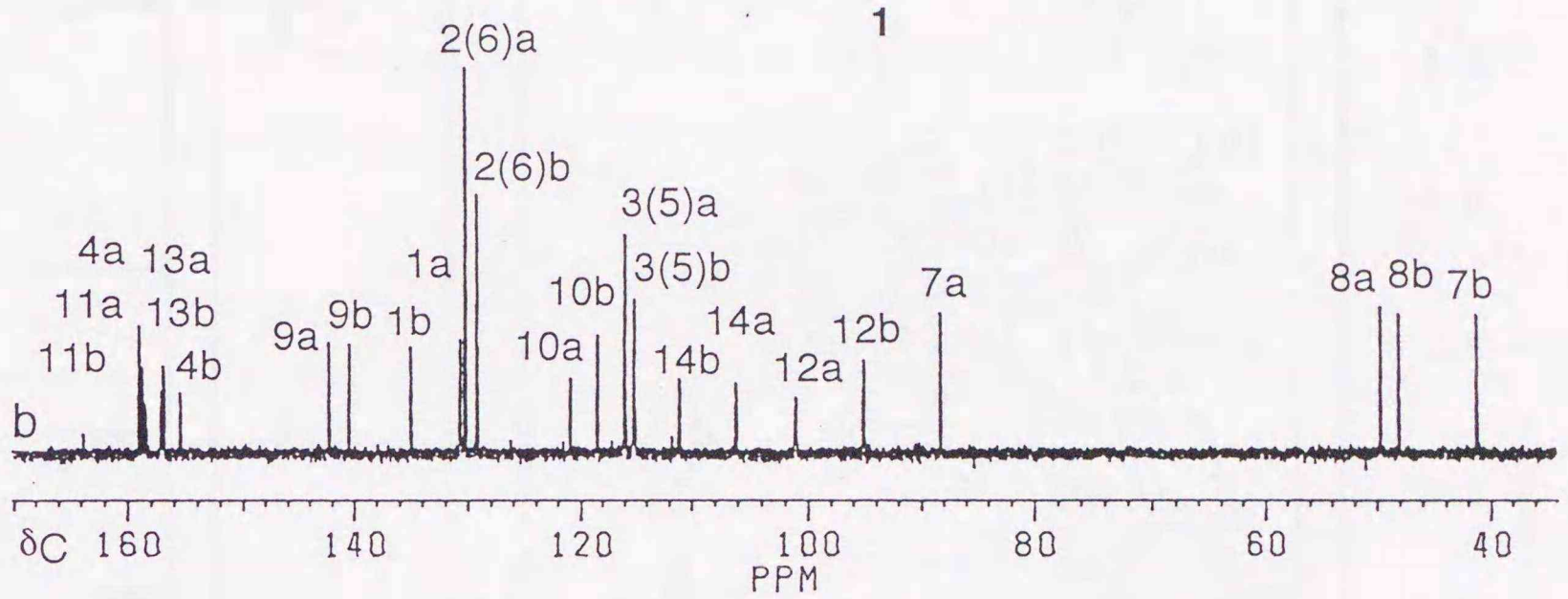


hopeaphenol (**1**)

The ^{1}H and ^{13}C NMR spectra (Chart 2.1) were relatively simple in contrast to the molecular formula, $C_{56}H_{42}O_{12}$. Conventional 2D NMR measurements involving ^{1}H-^{1}H and ^{13}C-^{1}H COSY and COLOC disclosed the carbon-carbon connectivities of one unit of the molecule. The C-8b carbon of one unit should be bonded to the corresponding carbon (C-8b') in another unit. The relative stereochemistry of the unit was established by ROESY (*30*, *31*). As shown in Chart 2.2, ROEs between H-2a/H-8a, H-14a/H-7a, H-8a/H-2b and H-8b/H-2b indicated the relative



1



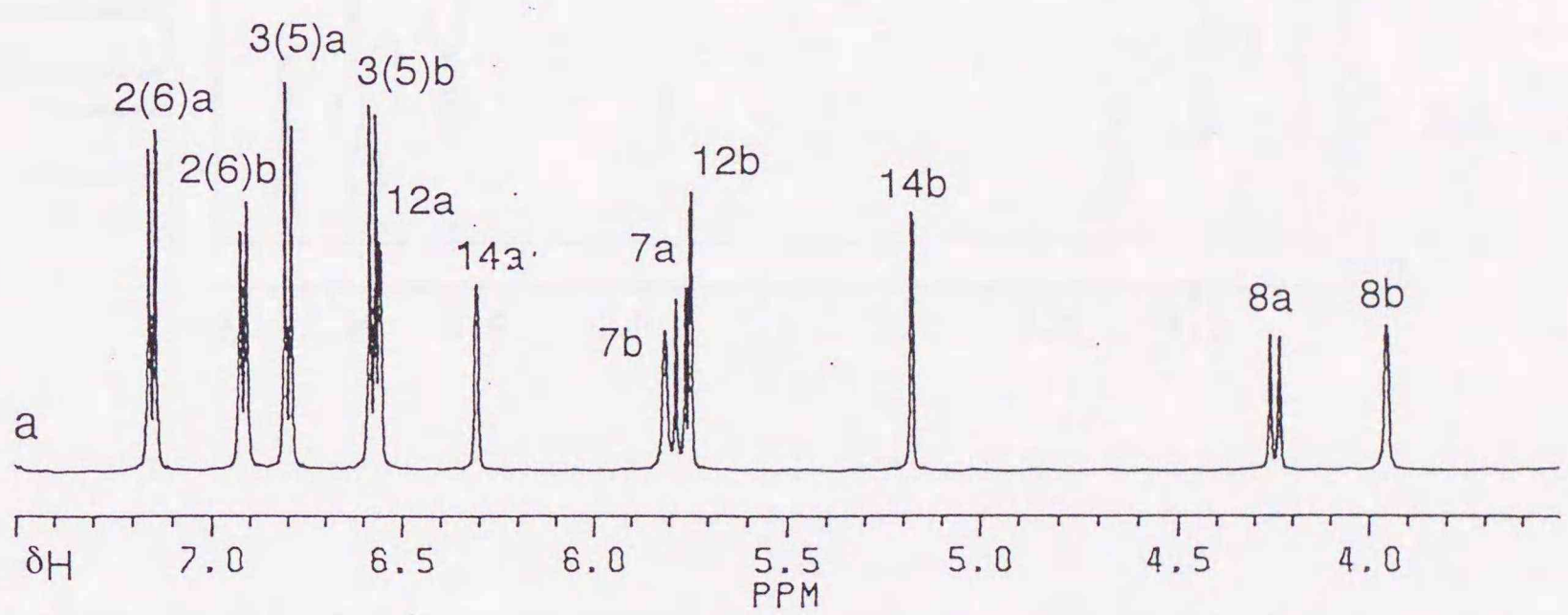


Chart 2.1. ^{1}H (a) and ^{13}C (b) NMR spectra of **1** (*ca.* 40 mg in 0.5 ml of acetone-d_6).

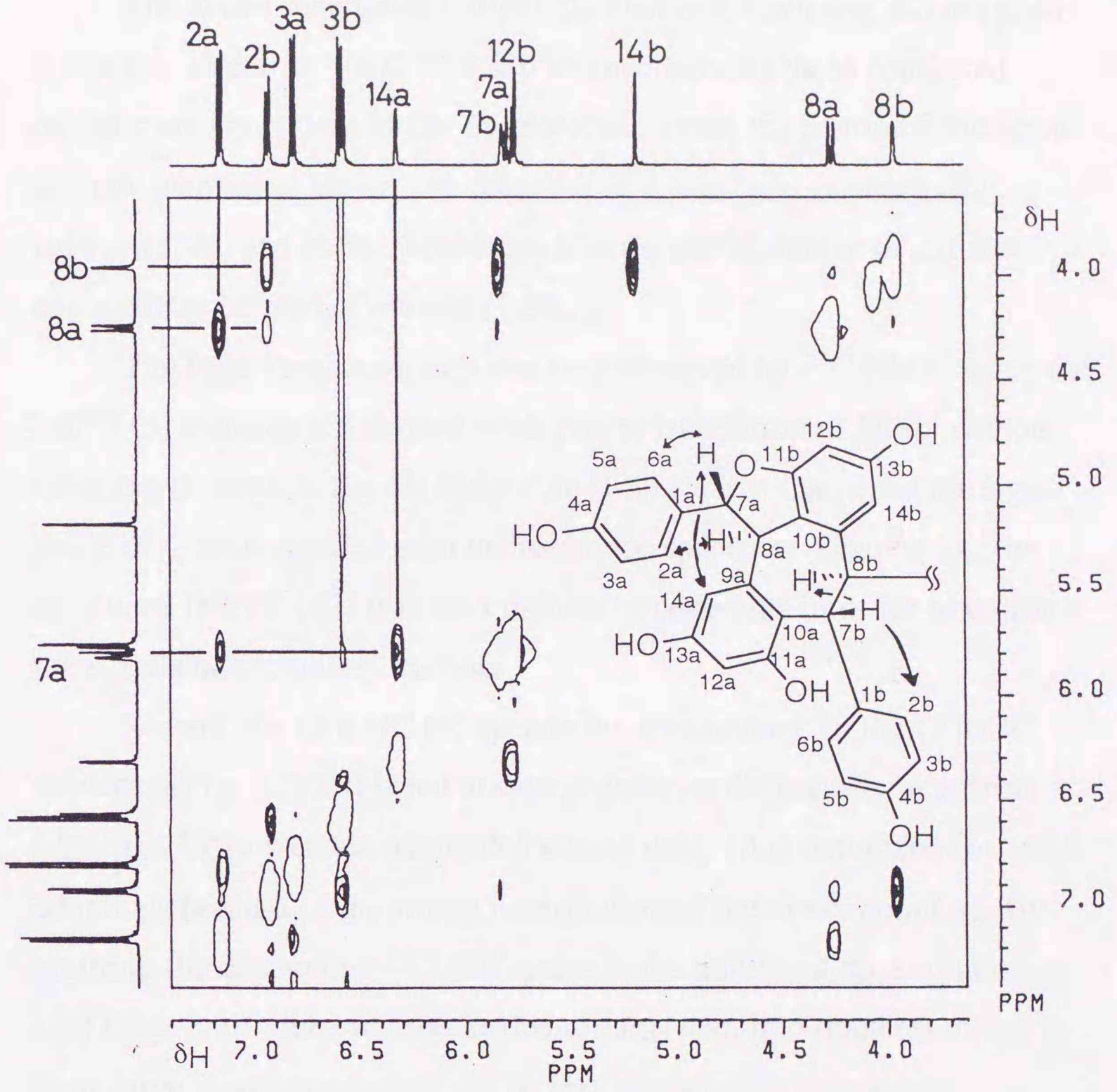


Chart 2.2. The phase-sensitive ROESY spectrum of **1** (*ca.* 40 mg in 0.5 ml of acetone-d_6). All pulses were derived from the high-power output of the decoupler attenuated by 18 dB (90° pulse duration was 100 μs). The offset for spin locking was placed at 3.2 ppm. The spin-lock time was set to 0.4 s. Diagonal peaks are negative, whereas all other cross-peaks are positive owing to ROE correlation. Each of the 128 t_1 increments was accumulated using 64 transients. The total measuring time was *ca.* 6 h.

stereochemistry within the unit. No inter-unit NOE interaction could be observed at this stage.

The above-mentioned normal 2D methods, however, did not make it possible to clarify the C-8b/C-8b' connectivity, as those connected carbons are equivalent in this C_2 molecule. From the isotopomeric point of view mentioned above, the detection of a two-bond connectivity between C-8b and H-8b' should result in the establishment of a direct connectivity between C-8b and C-8b'.

The long-range coupling was first observed by ^{13}C NMR, using the LSPD (*5*) technique. Selective weak power irradiation of H-8b' without affecting its satellite signals assignable H-8b clearly sharpened the signal shape of C-8b compared with the reference spectrum (Chart 2.3). The refocused INEPT (*32*) was used in these experiments in order to enhance the signals of protonated carbons.

Second, the COLOC (*6*) spectra were examined. In the COLOC sequence (Fig. 2.2a), it is not always possible to distinguish $^1J_{CH}$ from $^2J_{CH}$ and $^3J_{CH}$ even via a long defocusing delay (Δ_1) optimized for small couplings because of the strong contribution of the direct coupling. By omitting the decoupling ^{13}C 180° pulse in the middle of the evolution (*33*) (Fig. 2.2b), the cross peaks due to $^1J_{CH}$ split into doublets owing to their large coupling constant (>120 Hz), whereas the long-range correlations ($^{2,3}J_{CH} < 15$ Hz) are still singlets because of the low resolution in F_1 dimension. Therefore, direct and long-range correlations are separately detectable in this modified sequence.

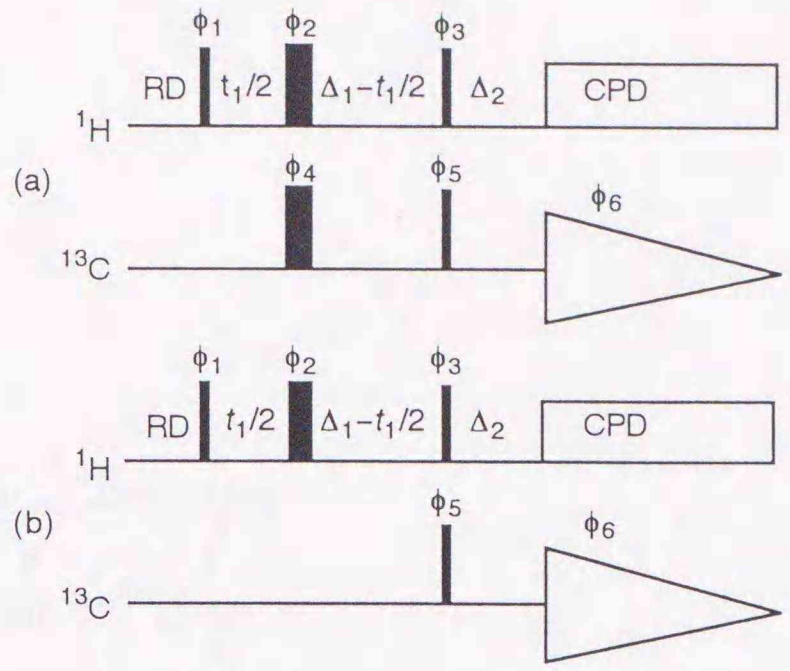
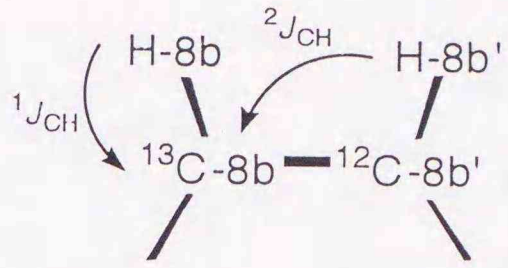


Fig. 2.2. Pulse sequences for 2D COLOC (*6*) (a) and the modified COLOC (*33*) (b) experiment. The delays, Δ_1 and Δ_2 are $1/2^{LR}J_{CH}$ and $1/4^{LR}J_{CH}$, respectively. Phase cycling used is as follows: $\phi_1 = x$; $\phi_2 = x^4,-x^4$; $\phi_3 = x, -x,y,-y$;
$\phi_4 = x^4,-x^4,y^4,-y^4$; $\phi_5 = x^8,y^8,-x^8,-y^8$; $\phi_6 = x,-x,y,-y, x, -x,y,-y,y,-y,-x, x,y,-y,-x,x,-x,x,-y,y, -x,x,-y,y,-y,y,x, -x,-y,y,x,-x.$

In the case of **1**, only a strong doublet for ^{13}C-8b/H-8b was observed using relatively short delays (Δ_1 = 55 ms and Δ_2 = 27.5 ms) (Chart 2.4a). Using longer delays (Δ_1 = 90 ms and Δ_2 = 45 ms) (Chart 2.4b), however, the doublet arising from the direct coupling disappeared and a singlet due to the long-range coupling (^{13}C-8b/H-8b') appeared. In contrast, the correlation for H-8a and C-8a appeared as a doublet from a large coupling, regardless of the duration of the delays (Chart 2.4).

The next choice for distinguishing between one- and multiple-bond correlation is HMBC (*7*, *8*). This method does not involve any carbon decoupling and, consequently, it seems to be suitable for this purpose. Actually, the HMBC spectrum of **1** (Chart 2.5) showed the triplet for the correlation between H-8b and C-8b, which was interpreted by the overlap of the singlet from the long-range correlation and the doublet from the direct correlation. Since the HMBC sequence involved the low-pass *J*



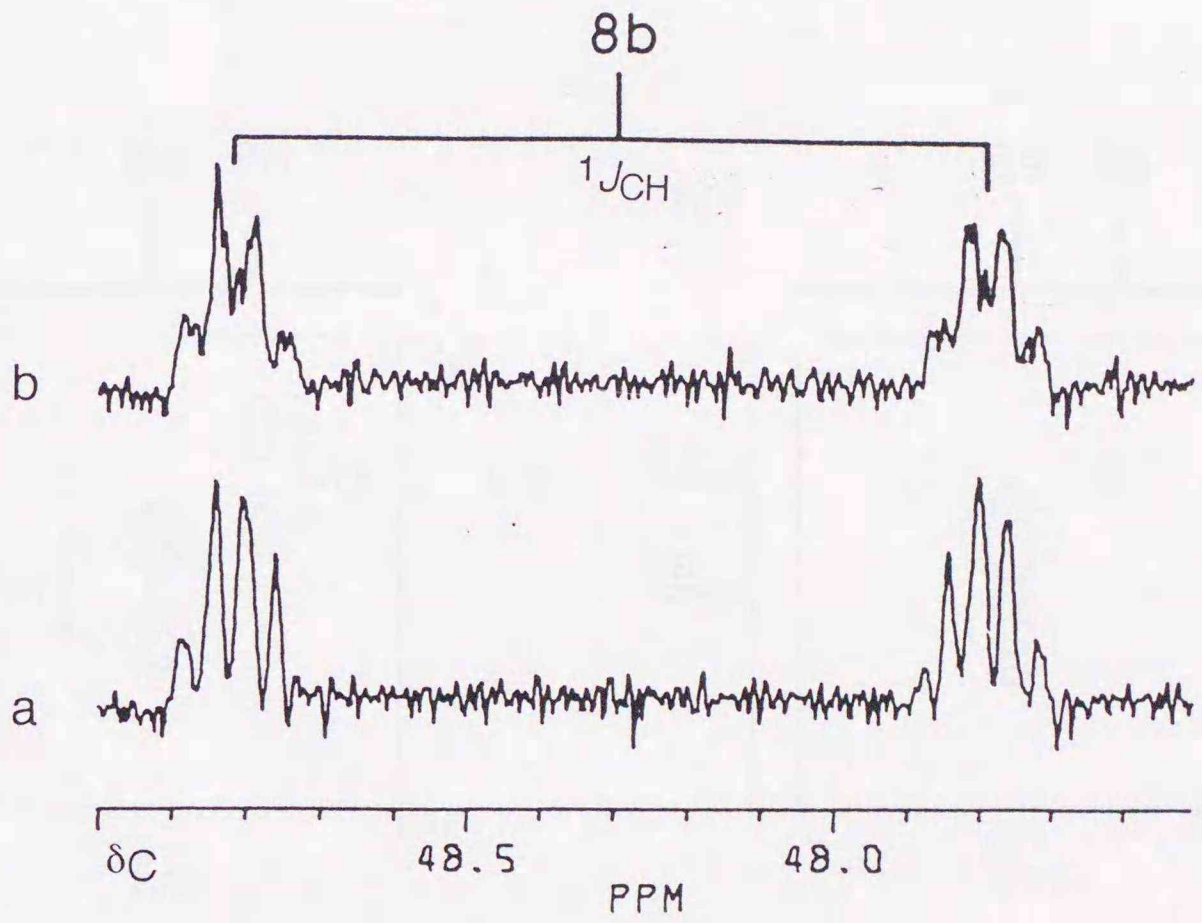
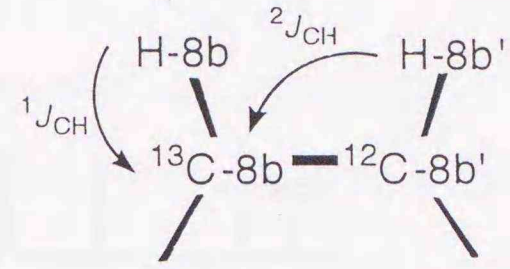


Chart 2.3. The INEPT-LSPD spectra of C-8b of **1** (*ca.* 40 mg in 0.5 ml of acetone-d_6) obtained by irradiation at the center peak of H-8b (a) and at the spectral extremity for reference (b). Selective proton irradiation was carried out using a low-power output of the decoupler channel (0.2 W) attenuated by 60 dB. Both defocusing and refocusing delays were 1.7 ms ($^{1}J_{CH}$ = 147 Hz). The large coupling was due to ^{1}J(C-8b/H-8b). Each spectrum was accumulated using 15,000 transients. The total measuring time was *ca.* 17 h each.



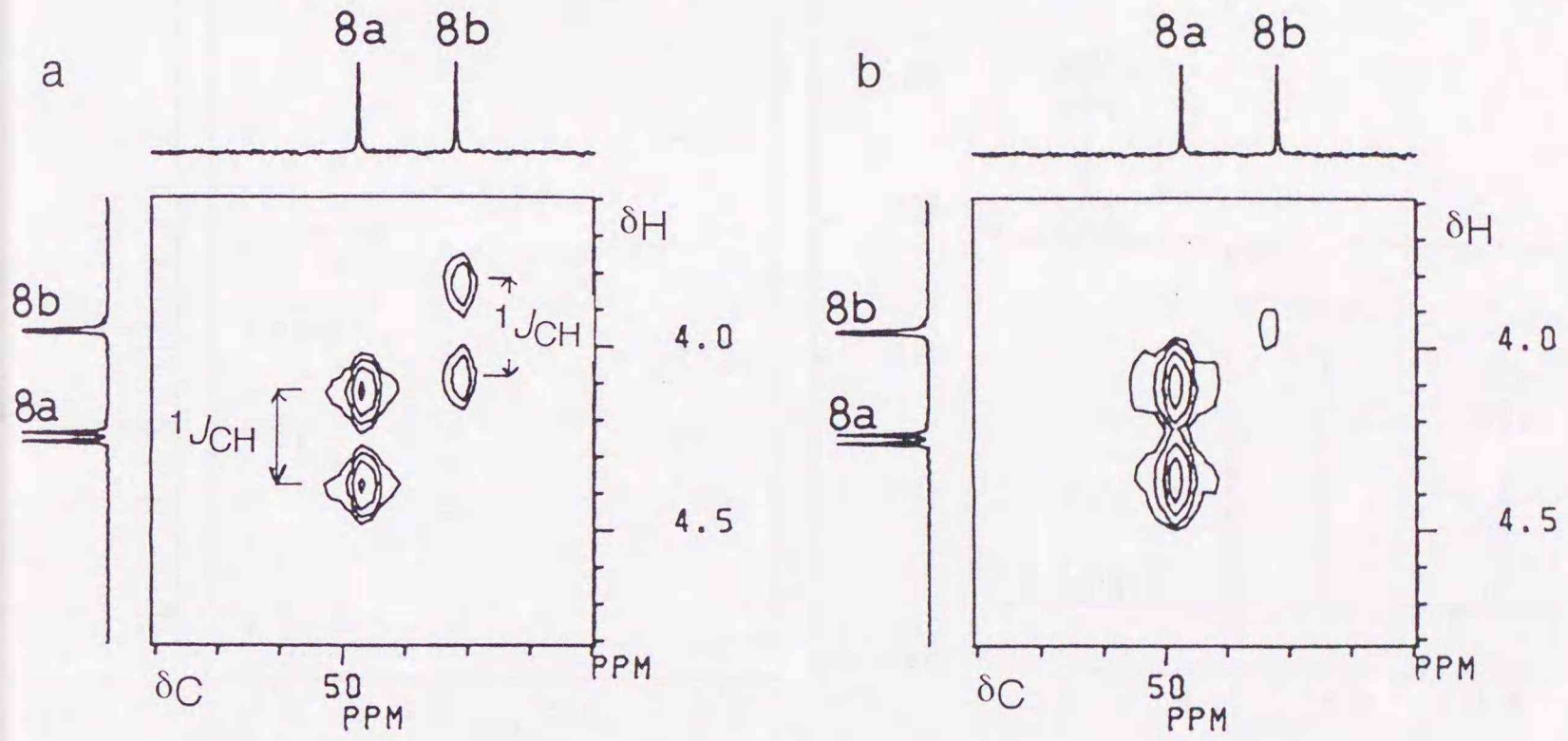
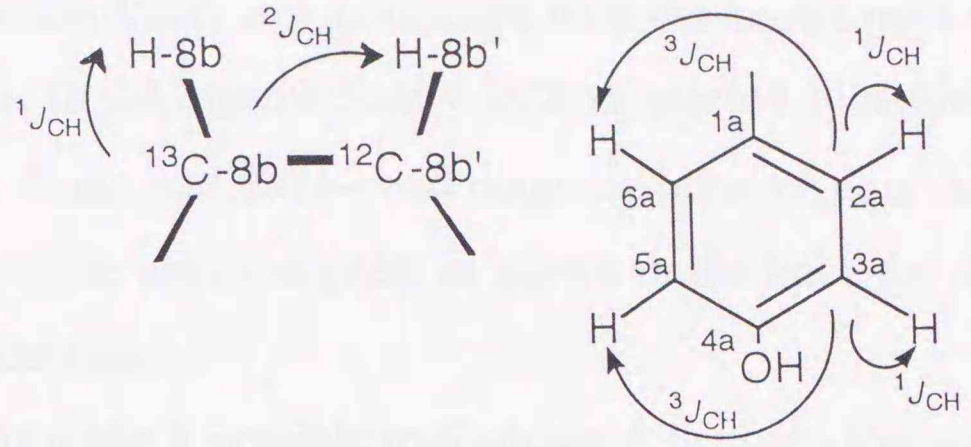


Chart 2.4. Part of the modified COLOC spectra of **1** (*ca.* 40 mg in 0.5 ml of acetone-d_6). Only the spectral region for the cross-peaks of H-8b/C-8b and H-8a/C-8a is shown. The spectra were obtained with the pulse sequence shown in Fig. 2.2b. The delays: (a) Δ_1=55 ms and Δ_2=27.5 ms ($^{LR}J_{CH}$ = 9Hz) and (b) Δ_1=90 ms and Δ_2=45 ms ($^{LR}J_{CH}$ = 5.5 Hz). Each of the 126 (a) and 128 (b) t_1 increments was accumulated using 192 transients. The total measuring time were *ca.* 14 (a) and 15 (b) h.



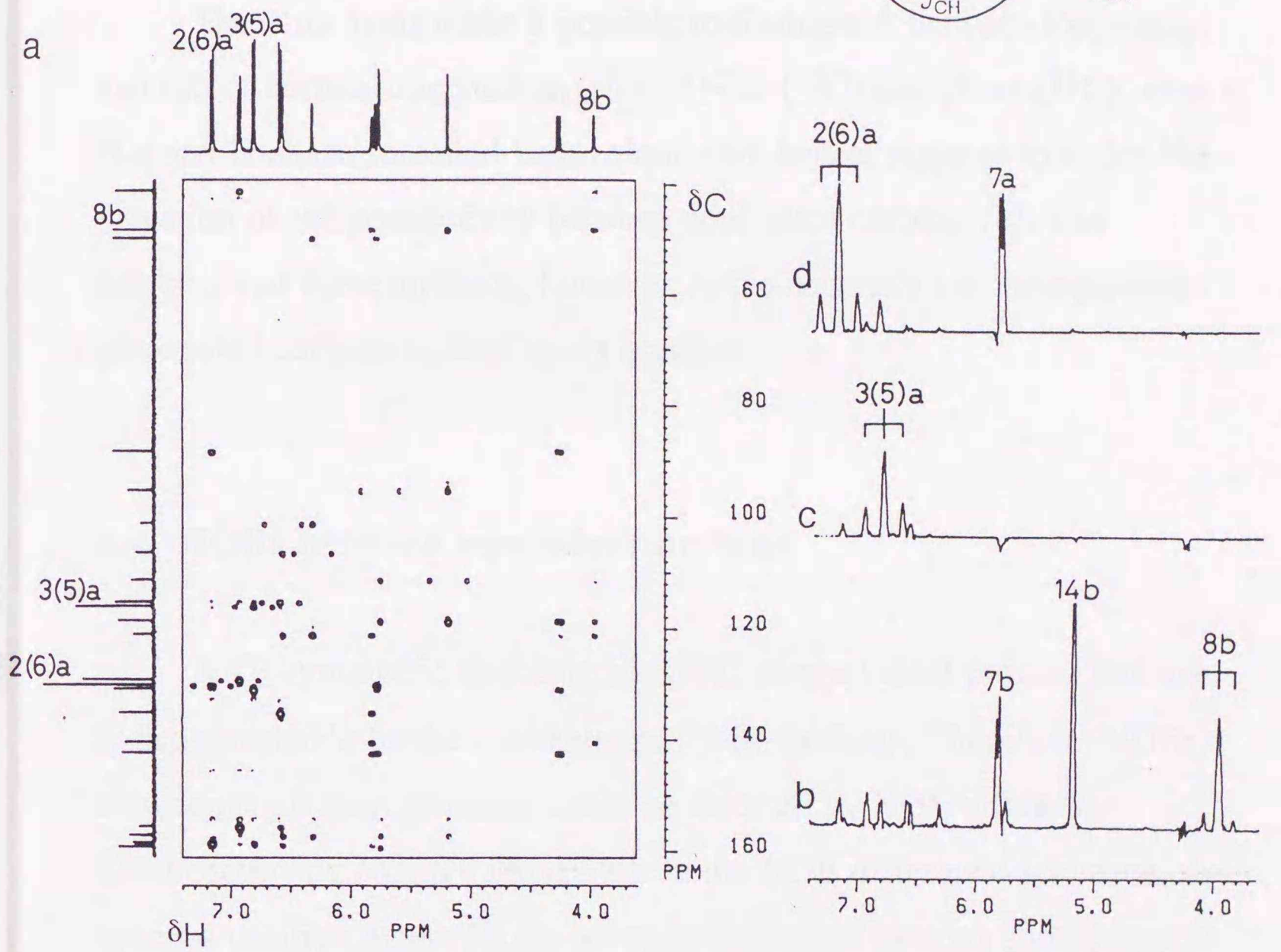


Chart 2.5. The HMBC spectrum of **1** (*ca.* 40 mg in 0.5 ml of acetone-d_6)(a) and rows at the positions of C-8b (b), C-3(5)a (c), and C-2(6)a (d). The deforcusing delay was set to 55 ms ($^{LR}J_{CH}$ = 9.1 Hz). The vertical scale for the rows is arbitrary. Each of the 472 t_1 increments was accumulated using 48 transients. The total measuring time was *ca.* 15 h.

filter for the suppression of direct coupling, the intensity of the doublet of the satellite was remarkably low compared with the center peak shown in F_1 trace for C-8b. In the symmetrical 4-hydroxyphenyl substructures the coexistence of a direct and three-bond coupling between equivalent protons and a carbon was also observed, as shown in the trace for the C-2(6)a and C-3(5)a resonances.

These methods make it possible to distinguish between long-range and direct correlation, such as (H-a')-(^{12}C)-(^{13}C) and (H-a)-(^{13}C), even if H-a and H-a' are so-called 'equivalent' and, hence, serve as tools for the detection of the connectivity between equivalent carbons (*4*). The limitation of these methods, however, is the necessity for the equivalent protonated carbons to be directly bonded.

2.4 NOEs between equivalent protons

A C_2 symmetric molecule has pairs of equivalent protons that are indistinguishable by the conventional NMR methods. Therefore, NOEs between equivalent protons cannot be detected by NOE difference spectroscopy or NOESY (ROESY). In the NOE difference spectrum, the spectral position where NOEs between equivalent protons should appear is completely superimposed on irradiation point. In the case of NOESY (ROESY) spectrum, correlation peaks appear right on the diagonal line (Chart 2.2).

As mentioned in section 2.2, discrimination of equivalent protons is accomplished, as ^{13}C-H and ^{12}C-H, since the former proton splits into a doublet at the satellite position whereas the latter proton is observed as a singlet in the middle of the satellite signals. Recently, observation of TOCSY cross-peaks between overlapped protons by a similar idea using a

2D ^{13}C-coupled HMQC-TOCSY sequence was reported (*9*), and the possibility of utilizing HMQC-NOESY (Fig.2.3) for the detection of NOE cross-peaks between overlapped protons was indicated (*9*, *10*).

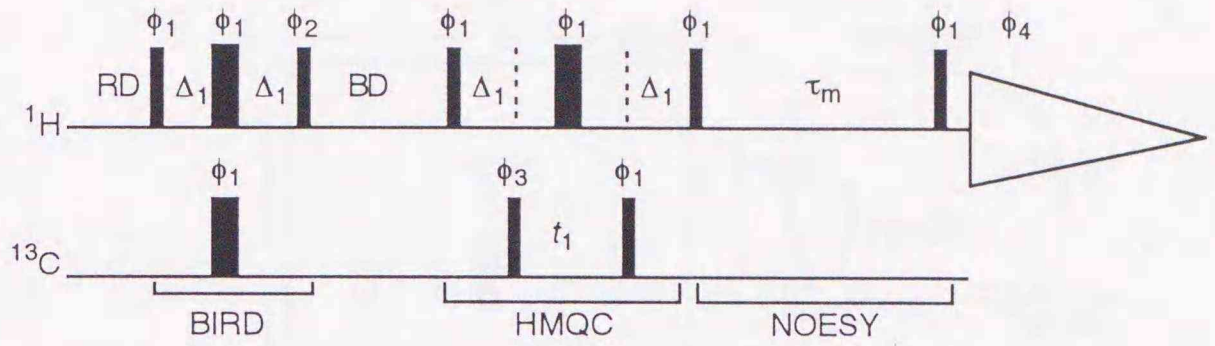


Fig. 2.3. Pulse sequence for the 2D ^{13}C-coupled HMQC-NOESY experiment (*9*). The delays Δ_1 and τ_m are $1/2^1J_{CH}$ and a mixing time, respectively. TPPI was applied to phase ϕ_3 for quadrature detection in F_1. Phase cycling used is as follows: ϕ_1 = x,x,y,y,-x,-x,-y,-y; ϕ_2 = -x,-x, -y, -y,x,x,y,y; ϕ_3 = x,-x,y,-y,-x,x,-y,y; ϕ_4 = x,-x, y,-y, -x,x, -y,y.

This strategy was thought to be useful for the detection of cross-peaks between equivalent protons. In this spectrum (Fig.2.4) of a structural fragment (H-a)-(C-a)...(C-a')-(H-a'), the signals appearing in {F_1 = C-a} region are derived from an isotopomer of (H-a)-(^{13}C-a)...(C-a')-(H-a'). The HMQC peaks (H-a) appear as doublet by ^1J(C-a/H-a). If an NOE between H-a and H-a' is present, an NOE peak (H-a') should appear as a negative singlet at the center of the HMQC signals.

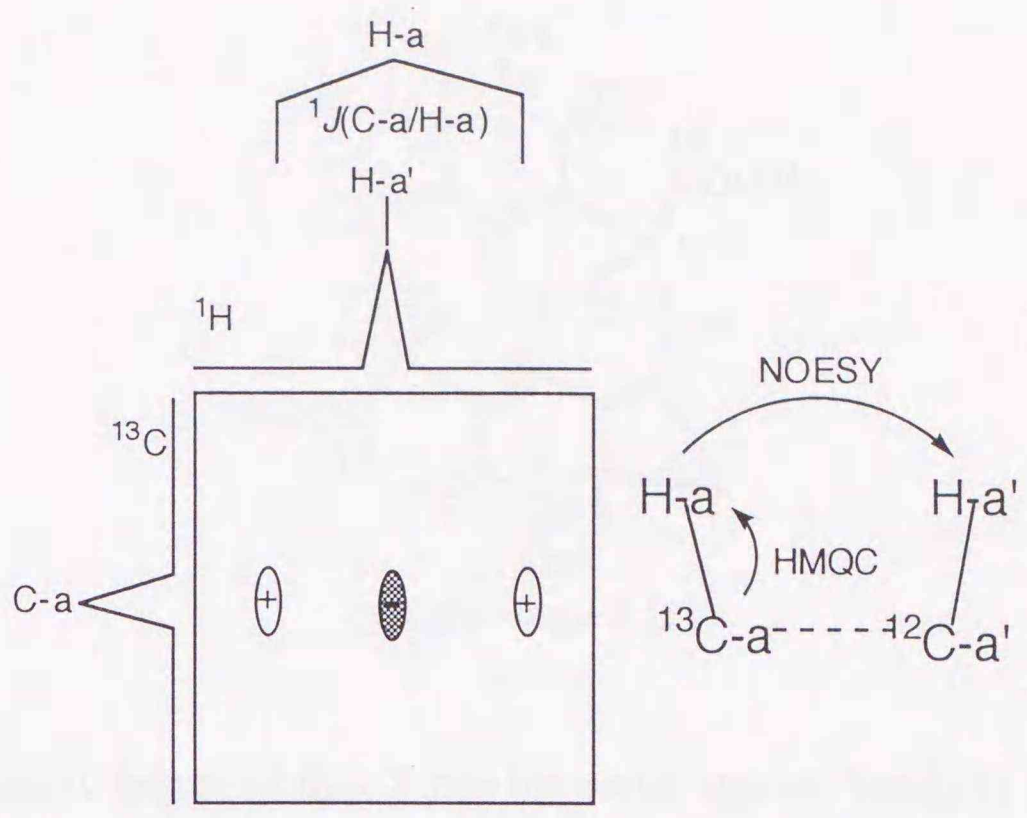
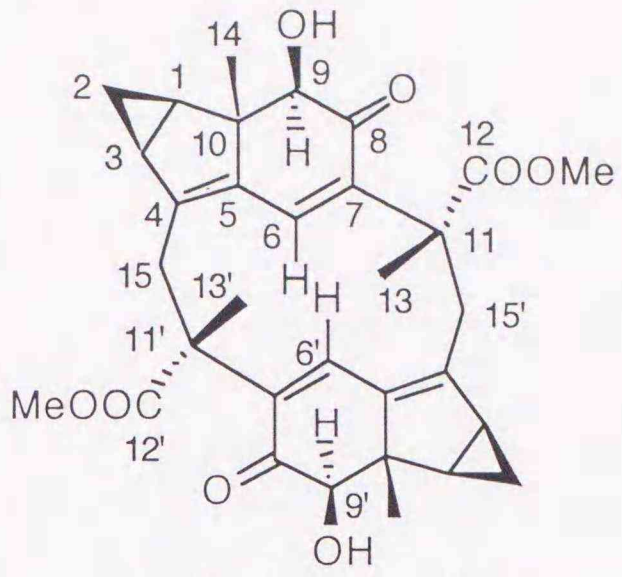


Fig. 2.4. Schematic HMQC-NOESY spectrum of a symmetric structural fragment. The HMQC peaks (H-a) appear as a doublet by ^{1}J(C-a/H-a). The NOE peak (H-a') appears as a negative singlet at the center of the HMQC signals.

At first, I applied this 2D ^{13}C-coupled HMQC-NOESY sequence (Fig. 2.3) (*9*) to a symmetric sesquiterpene dimer, cycloshizukaol A (**2**), isolated from the ether extracts of the roots of *Chloranthus serratus*. (*11*). The plane structure was deduced by the results of 2D ^{1}H-^{1}H COSY, ^{13}C-^{1}H COSY and COLOC experiments. This cyclic structure is comprised of two identical lindenane ester units. The connectivity of the two units in **2** was unambiguously determined by COLOC as follows. The non-equivalent methylene protons at δ 2.60 (H-15β) and 2.97 (H-15α) showed cross-peaks with one of the tertiary methyl carbons (C-13', δ 28.6) and the ester carbonyl (C-12', δ 175.5), respectively. These cross-peaks are evidently due to the three-bond inter-unit correlations.



cycloshizukaol A (**2**)

It is easily assumed that **2** has the same stereochemistry as that of the other *Chloranthus* lindenanes (*34*) and the results of NOE difference experiments supported this estimation, *i. e.* NOEs between H-2β and H-14, and H-1 and H-9. Determination of the stereochemistry on C-11 seems somewhat difficult because this chiral center is included in a 12-membered ring. The methyl protons (H-13) exhibited NOEs with methylene proton (H-15') and with methyne proton (H-6). The flexibility of the medium-sized ring made it impossible to determine the stereochemistry by these results, even with the presence of additional NOEs between H-15β and H-6, and H-15α and H-3. The conformation of the ring should therefore be demonstrated by the other NOE results.

The ^{13}C-coupled HMQC-NOESY (Fig. 2.3) was applied to **2** to get information concerning the conformation of the central ring. The spectrum (Chart 2.6) clearly showed the existence of NOEs between H-6 and H-6', and H-9 and H-9' by the presence of the negative cross-peaks at the center of the split HMQC correlations.(*11*) These results strongly indicated the conformation of the central 12-membered ring as shown in Fig. 2.5, and in consequence the configuration at C-11 was deduced to be *R* on the basis of results of the above NOE results.

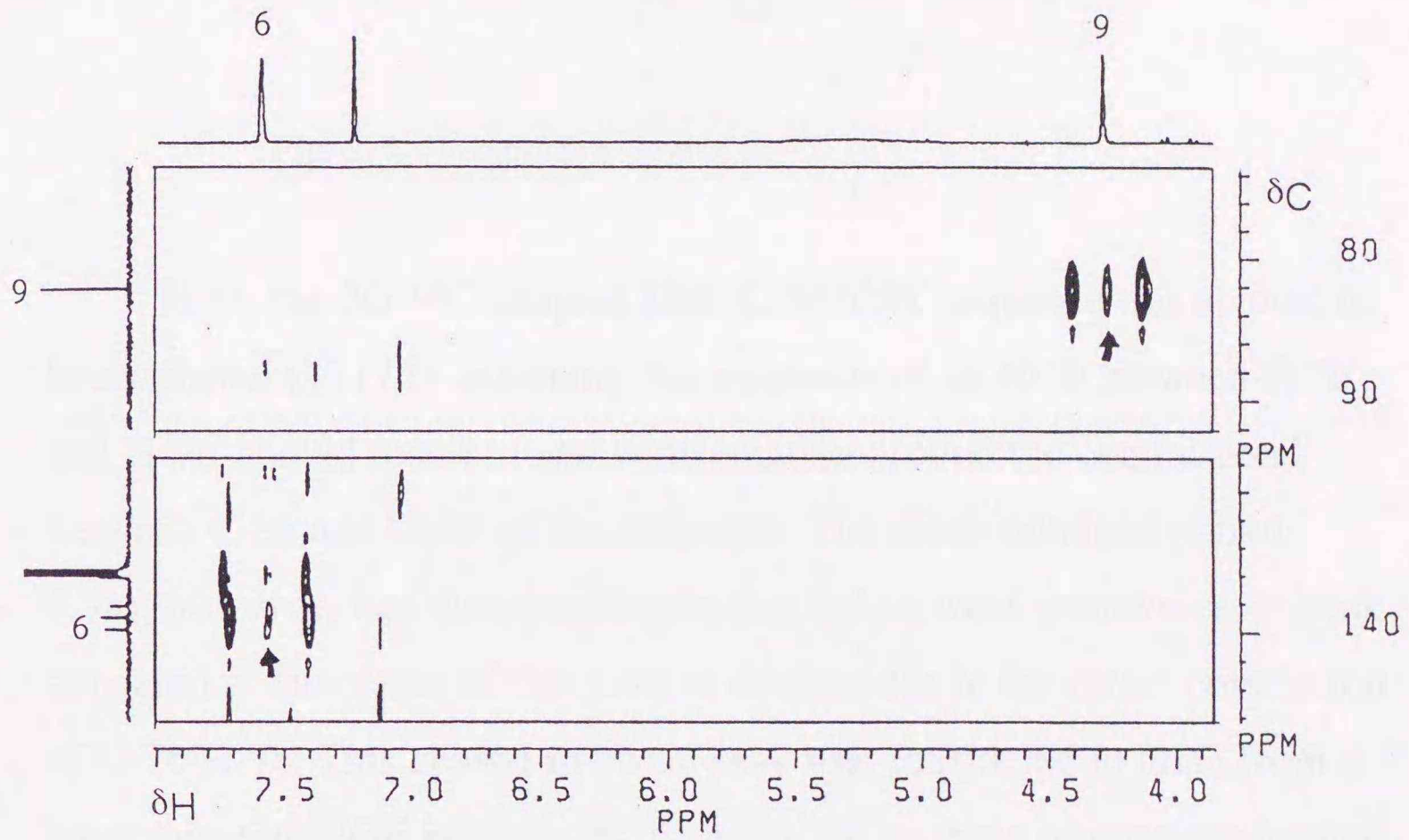


Chart 2.6. Parts of the ^{13}C-coupled HMQC-NOESY spectrum of **2** (21 mg in pyridine-d_5) determined by the sequence shown in Fig.2.3 . The delays, RD, BD, Δ_1 and τ_m were set to 2.0 s, 0.4 s, 3.6 ms ($^1J_{CH}$ = 140 Hz), and 0.4 s, respectively. Negative cross-peaks are marked by arrows. Each of the 128 t_1 increments was accumulated using 192 transients. The total measuring time was *ca.* 21 h.

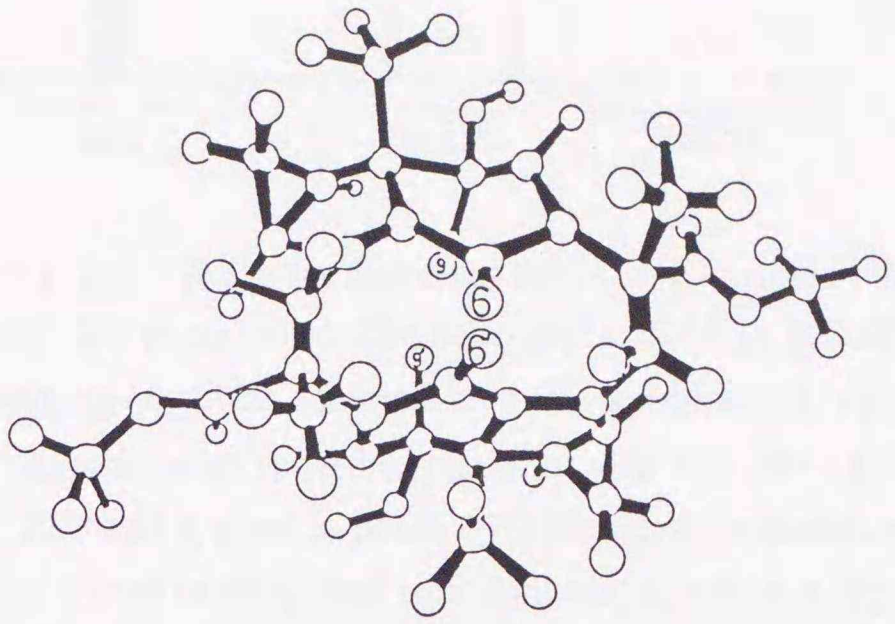


Fig. 2.5. Perspective view of **2**.

Next, the 2D ^{13}C-coupled HMQC-NOESY sequence was applied to hopeaphenol (**1**) (*12*), assuming that existance of an NOE between H-7b and H-7b' should result in *anti* conformation around the central bond between C-8b and C-8b' of the molecule. The result obtained (Chart 2.7a), however, was disappointing in that only a weak positive cross-peak appeared at the center of the positive doublet due to the direct correlation of C-7b/H-7b. This central in-phase peak was considered to arise from a weak negative NOE between H-7b and H-7b', as these protons are located at the less mobile inner part of this molecule of intermediate size (*35*). Thus the spatial proximity of these protons will be detected more efficiently by using ROE (*30*, *31*). The 2D ^{13}C-coupled HMQC-ROESY sequence (Fig. 2.6) was then constructed, and the resultant spectrum of the same region is shown in Chart 2.7b.

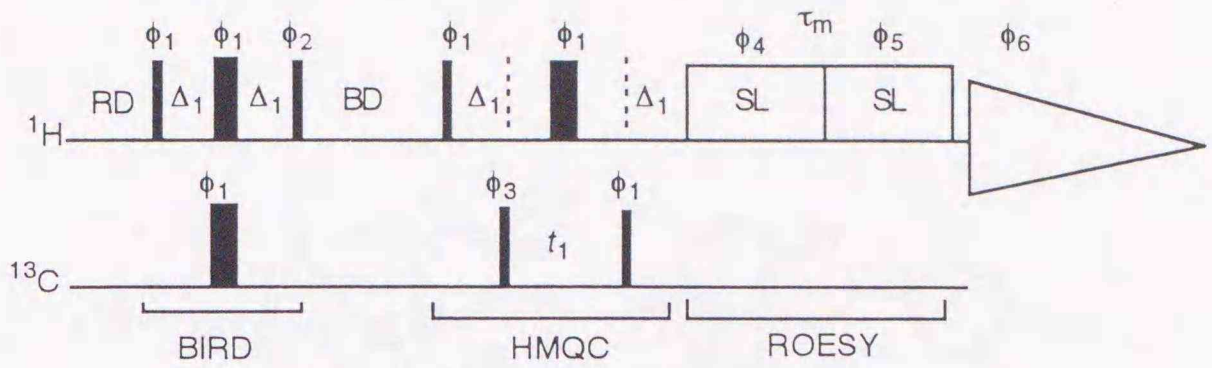


Fig. 2.6. Pulse sequence for the 2D ^{13}C-coupled HMQC-ROESY experiment. The delay Δ_1 is $1/2^1J_{CH}$. ROESY mixing (τ_m) was achieved by a CW spin-lock (SL) divided into two parts (shifted in phase by +90° and -90°) (*36*). TPPI was applied to phase ϕ_3 for quadrature detection in F_1. Phase cycling used is as follows: ϕ_1 = x,-x,y,-y; ϕ_2 = -x,x,-y,y; ϕ_3 = x,x,y,y,-x, -x,-y,-y; ϕ_4 = y,-y,x,-x; ϕ_5 = -y,y,-x,x; ϕ_6 = x,x,y,y,-x, -x,-y,-y.

A strong ROE-relayed negative cross-peak clearly appeared between the C-7b/H-7b doublet. Additional ROE correlations for H-8b/H-7b and H-8b/H-14b were also detected in this region. This result strongly supported the anti conformation of **1** in which H-7b is located in close proximity to H-7b', as shown in Fig. 2.7 (*12*).

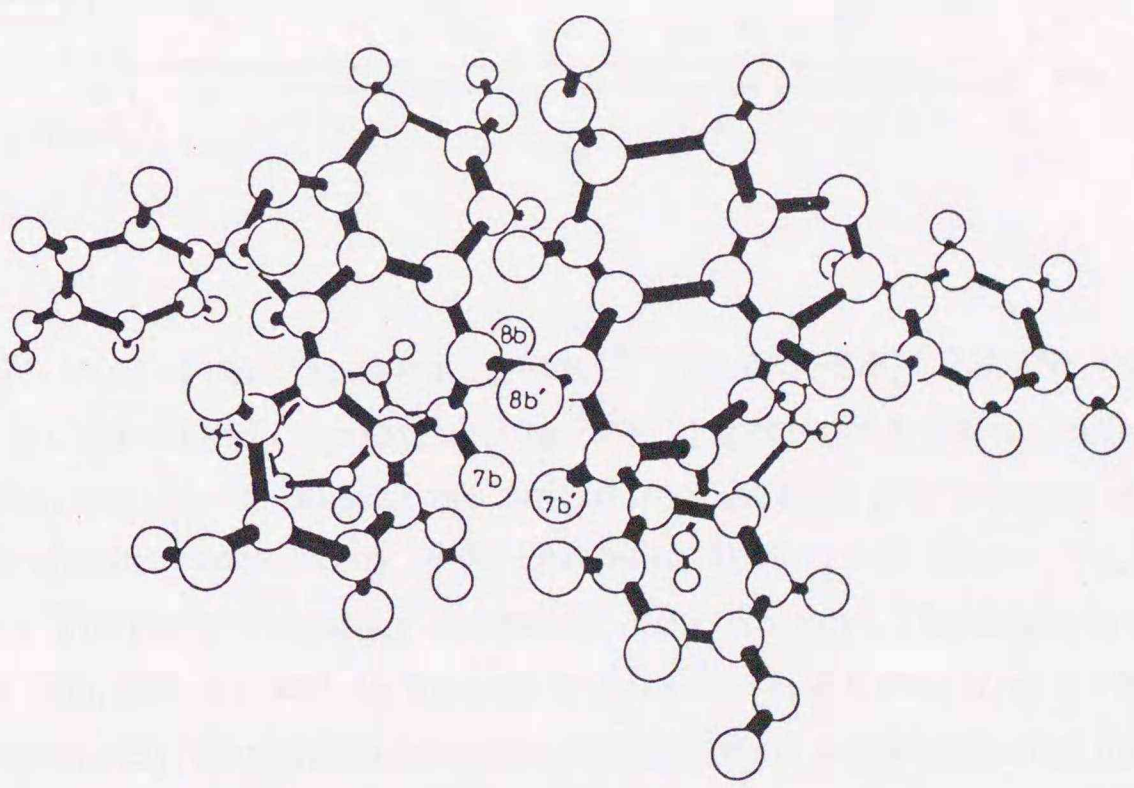
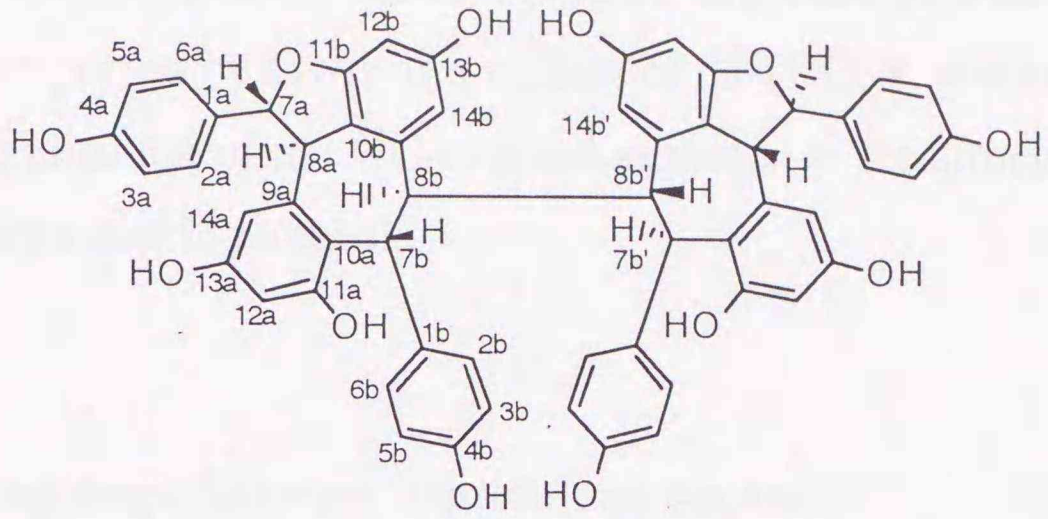


Fig. 2.7. Perspective view of **1**.



1

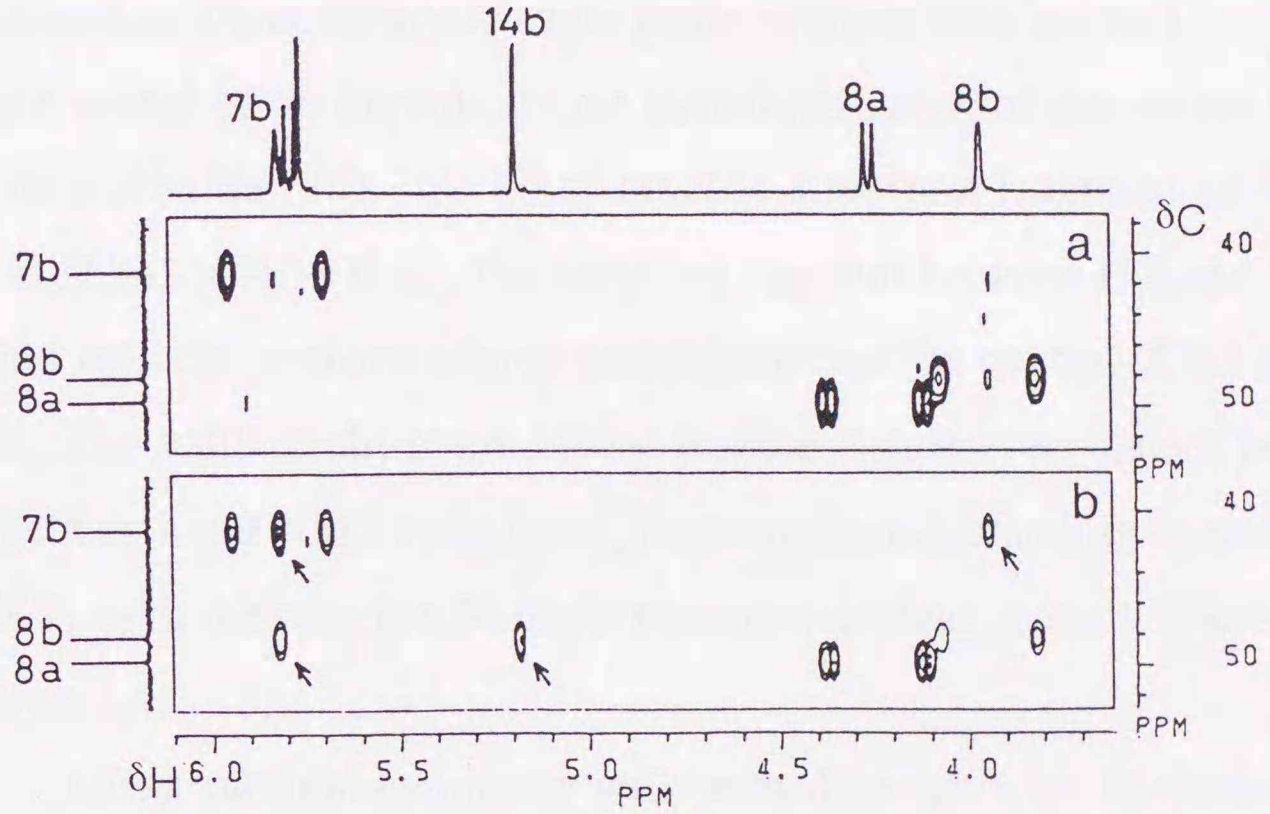


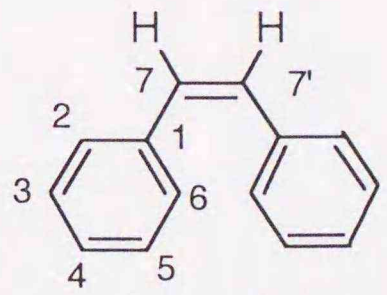
Chart 2.7. Parts of the 2D phase sensitive ^{13}C-coupled HMQC-NOESY (sequence : Fig.2.3) (a) and -ROESY (sequence : Fig.2.6) (b) spectra of **1** (50 mg in 0.5 ml of acetone-d_6). For (b), ^1H pulses were derived from the high-power output of the decoupler channel attenuated by 18 dB (90° pulse duration was 100 μs, a 2,500 Hz spin-lock field). The carrier frequency was positioned at 6.7 ppm. The delays in each spectrum, RD, BD, Δ_1, and τ_m were set to 2.0 s, 0.4 s, 3.6 ms ($^1J_{CH}$ = 140 Hz), and 0.4 s, respectively. Negative cross-peaks are marked by arrows. Each of the 116 t_1 increments was accumulated using 224 transients. The total measuring time was *ca.* 21 h each.

The detection of the NOE between equivalent protons by the 2D ^{13}C-coupled HMQC-ROESY sequence at natural abundance has thus been achieved. Although the 2D HMQC-ROESY sequence with carbon decoupling was reported by Davis as a variant of its TOCSY analog (*37*), this is the first application of the ^{13}C-coupled sequence to the structural analysis of the C_2 symmetric molecule.

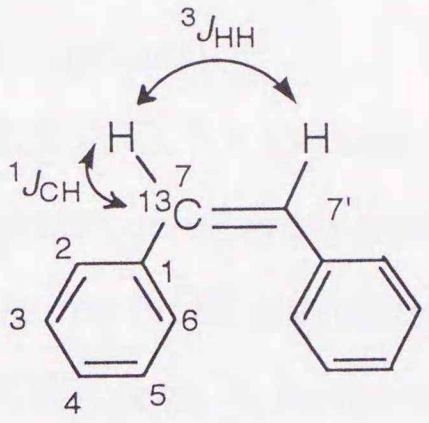
2.5 *J* couplings between equivalent protons

A vicinal ^{1}H-^{1}H coupling constant for ^{1}H-C-C-^{1}H system gives an information about torsional angle made of those four nuclei (*38*, *39*), which would be an important clue to determination of the stereochemistry of the molecules (*40*). In a C_2 symmetric structural fragment such as (H-a)-(C-a)-(C-a')-(H-a'), the coupling constant between H-a and H-a' would help the conformational analysis around the central (C-a)-(C-a') bond. The value in the symmetrical fragment, however, cannot be given by conventional NMR techniques, homonuclear decoupling spectrum or COSY, as in the case for NOEs between equivalent protons discussed in section 2.4.

This structural symmetry will be broken again by detecting (H-a)-(^{13}C-a)-(^{12}C-a')-(H-a') isotopomer. In the ^{1}H-NMR spectrum of *Z*-stilbene (**5**) (Chart 2.8), for example, a main signal of H-7 is derived from the (H-7)-(^{12}C-7)-(^{12}C-7')-(H-7') isotopomer.



Z-stilbene (**5**)



5

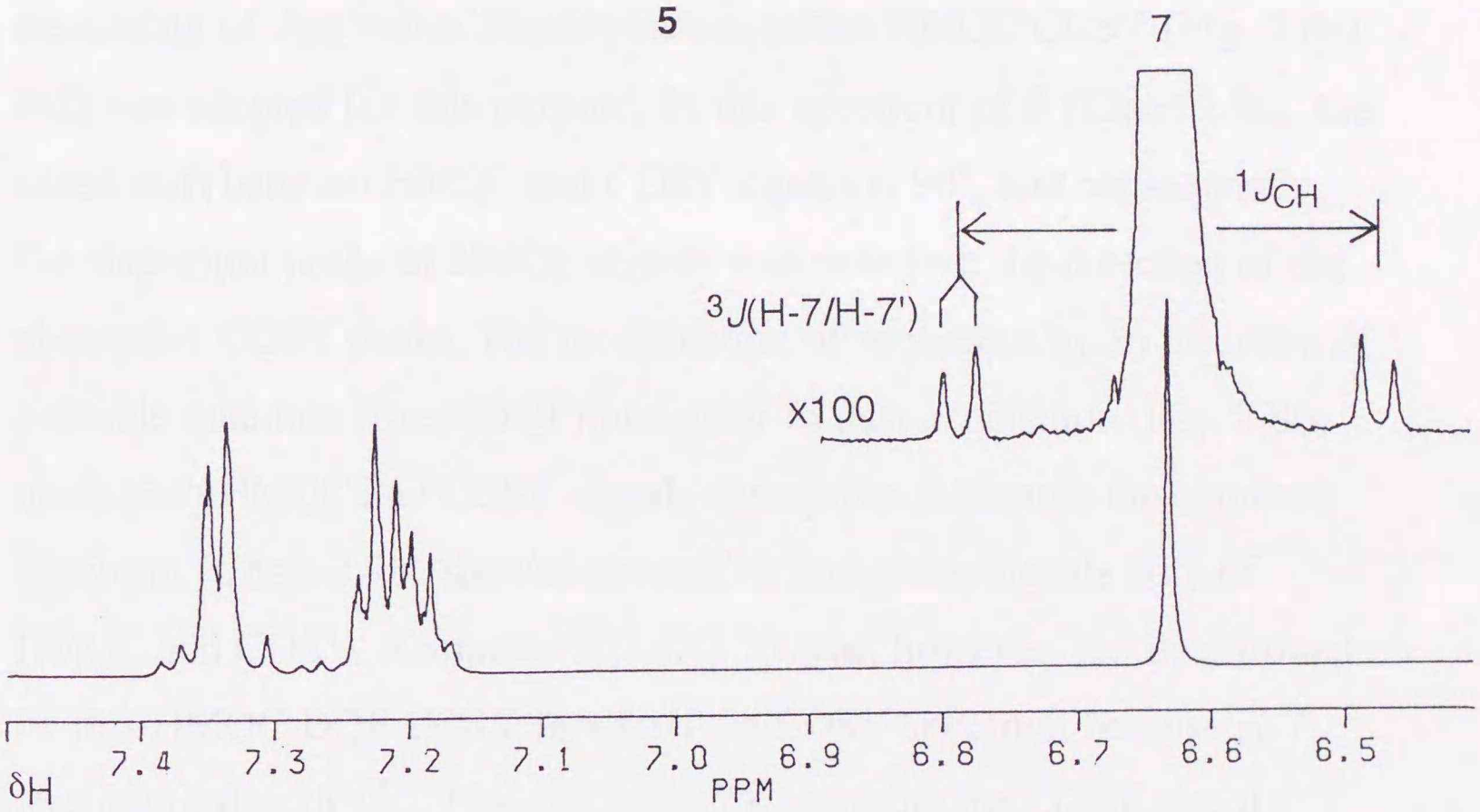


Chart 2.8. ^{1}H NMR spectrum of **5** (33 mg in pyridine-$d5$)

As for the (H-7)-(^{13}C-7)-(^{12}C-7')-(H-7') isotopomer existing about 2%, a signal of H-7 splits into large doublet by ^{1}J(C-7/H-7) and the signal of H-7' appears in the center of the doublet. Each of satellite signals further split into small doublet, which is caused by additional homonuclear coupling between H-7 and H-7'. The signal of H-7b' must also be split, although it is invisible because of being buried under large peak of (H-7)-(^{12}C-7)-(^{12}C-7')-(H-7') isotopomer.

2D ^{13}C-coupled HMQC-TOCSY (*9*) can detect *J* couplings between equivalent protons by the presence of cross-peaks at the center of the split HMQC signals as in the case for NOE correlation peaks in the HMQC-NOESY. The in-phase TOCSY peak is, however, unsuitable for accurate measuring of J_{HH} value. Hence phase-sensitive HMQC-COSY (Fig. 2.8a) (*41*) was adopted for this purpose. In this spectrum of **5** (Chart 2.9a), the phase shift between HMQC and COSY signals is 90°, and consequently, the dispersion peaks of HMQC signals may interfere the detection of the absorptive COSY peaks. The modification of sequences by an insertion of a double quantum filter (DQF) just prior to data acquisition (Fig. 2.8b) made both HMQC and COSY signals absorptive. Although the obtained spectrum (Chart 2.9b) showed absorptive anti-phase signals both of HMQC and COSY. Accurate ^{3}J(H-7/H-7') was, however, not determined by this HMQC-DQF-COSY in which the COSY spectrum because H-7' also coupled with ^{13}C-7 by ^{2}J(C-7/H-7'), resulting the COSY signal contained both ^{3}J(H-7,H-7') and ^{2}J(C-7/H-7').

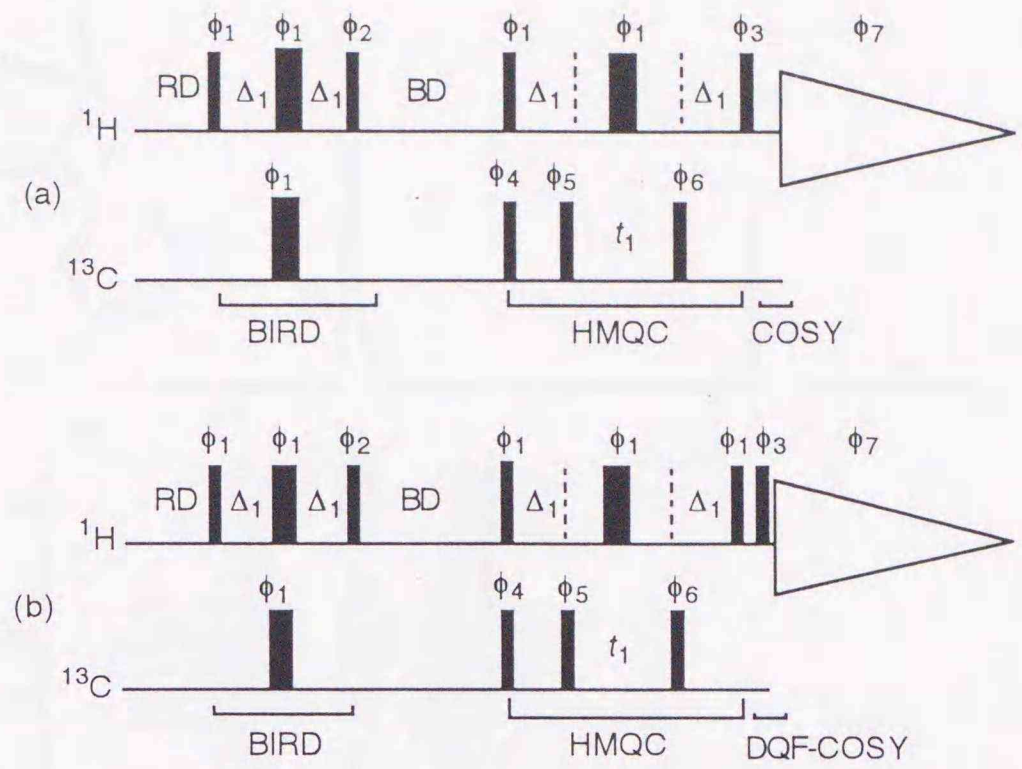
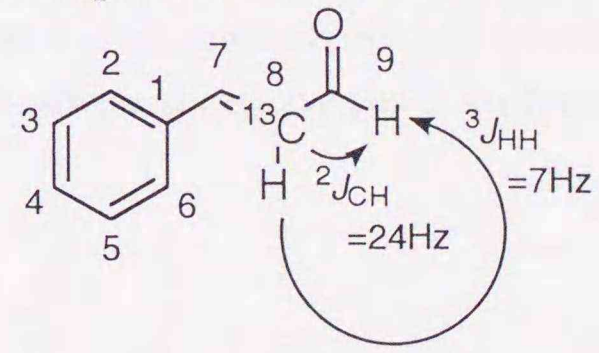


Fig. 2.8. Pulse sequences for the 2D ^{13}C-coupled HMQC-COSY (a) and the 2D ^{13}C-coupled HMQC-DQF-COSY (b) experiments. The delay Δ_1 is $1/2^1J_{CH}$. TPPI was applied to phase ϕ_5 for quadrature detection in F_1. Phase cycling used is as follows: ϕ_1 = x; ϕ_2 = -x; ϕ_3 = y; ϕ_4 = x^4,$-x^4$; ϕ_5 = x,-x; ϕ_6 = x,x,-x,-x; ϕ_7 = x,-x,-x,x.

This overlapping of $^3J_{HH}$ and $^2J_{CH}$ is demonstrated in the ^{13}C-coupled HMQC-DQF-COSY spectrum of cinnamaldehyde (**6**) (Chart 2.10). The value of $^2J_{CH}$ between aldehydic proton and α-carbon is known to be exceptionally large (20-25 Hz). In the case of **6**, the C-8/H-9 correlation peak in Chart 2.10 appeared as doublet of doublet in F_2 dimension. The large (24 Hz) passive doublet is due to ^2J(C-8/H-9), whereas the small (7 Hz) active doublet is due to ^3J(H-8/H-9). The $^2J_{CH}$ values are, however, as small as those of J_{HH} in most compounds. Therefore separate measurement of each value of $^3J_{HH}$ and $^2J_{CH}$ is impossible from the cross-peak in this method.



cinnamaldehyde (**6**)

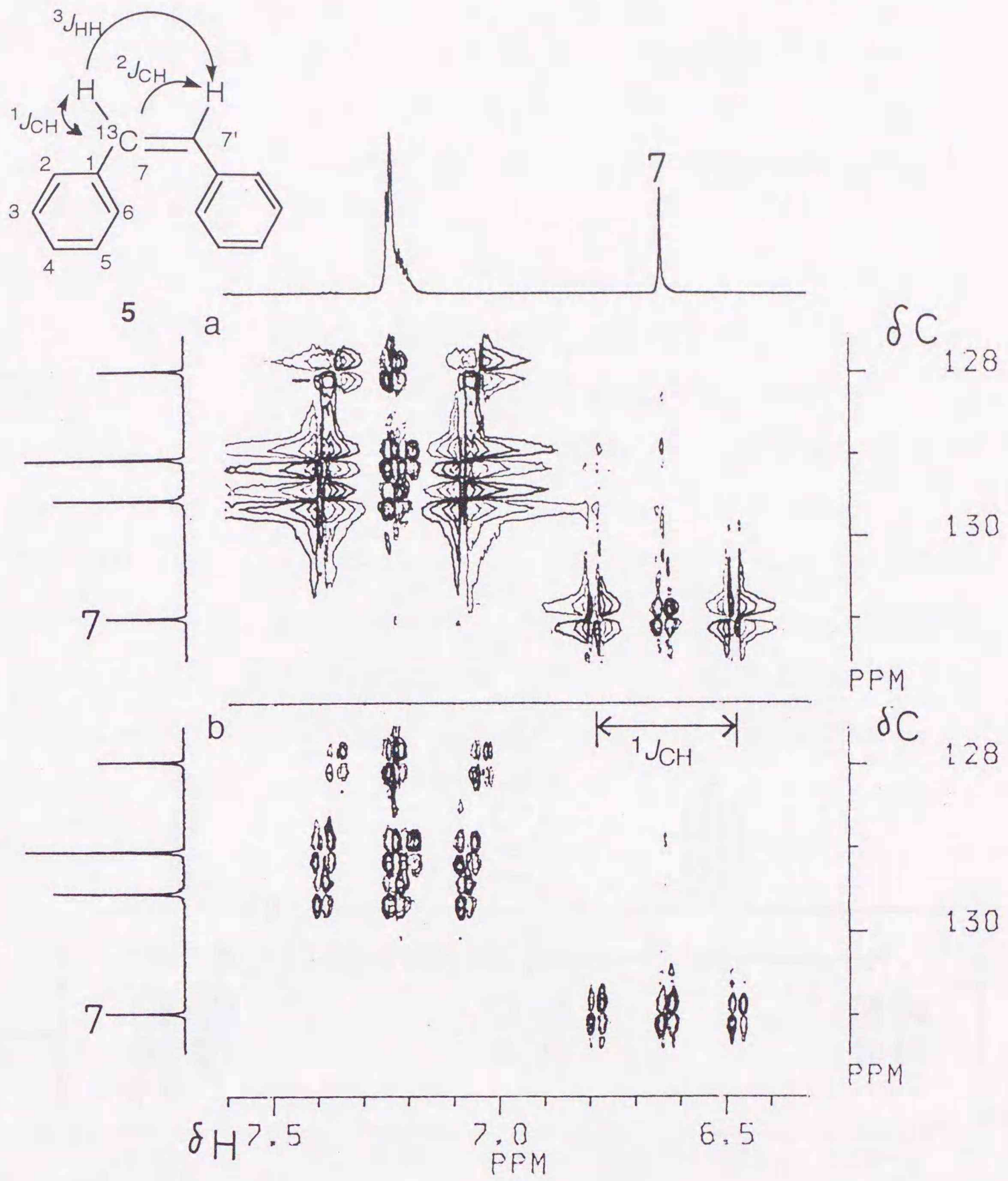


Chart 2.9. The 2D phase sensitive ^{13}C-coupled HMQC-COSY spectrum (a) and ^{13}C-coupled HMQC DQF-COSY spectrum (b) of **5** (20 mg in acetone-d_6). The spectra were obtained with the pulse sequences shown in Fig. 2.8a and b, respectively. The delays, RD, BD, and Δ_1 were set to 3.0 s, 2.3 s, and 3.6 ms ($^1J_{CH}$ = 140 Hz), respectively. Each of the 50 t_1 increments was accumulated using 16 transients. The total measuring time was *ca.* 1.5 h each. Positive and negative peaks are drawn without distinction.

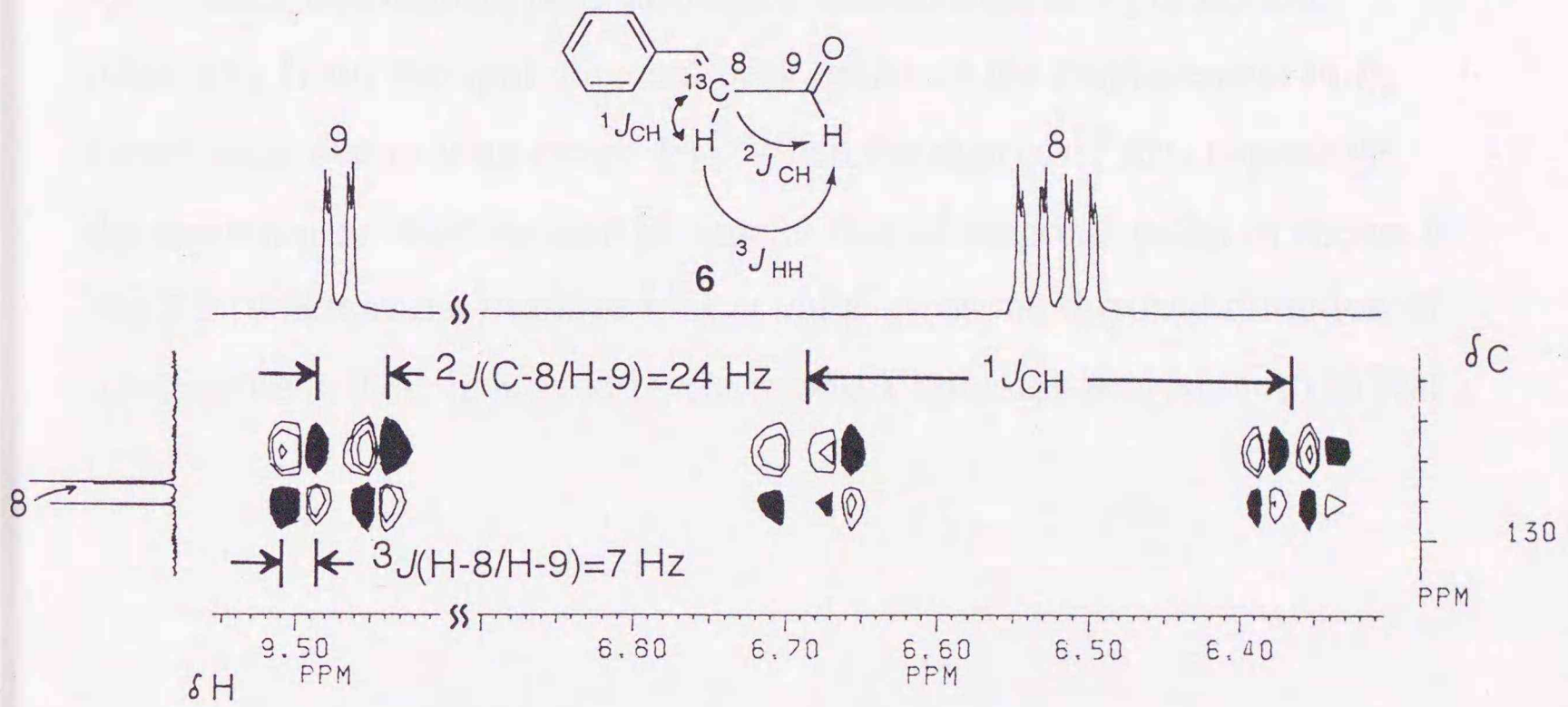


Chart 2.10. The 2D phase sensitive ^{13}C-coupled HMQC-COSY spectrum of **6** (30 mg in chloroform-*d*). The spectra were obtained with the pulse sequences shown in Fig. 2.8b. The delays, RD, BD, and Δ_1, were set to 5.3 s, 3.22 s, and 3.6 ms ($^1J_{CH}$ = 140 Hz), respectively. Each of the 32 t_1 increments was accumulated using 160 transients. The total measuring time was *ca.* 13 h. Positive and negative peaks are drawn with open-center and completely black peaks, respectively.

Kurtz *et al.* reported (*14*) that the homo- and heteronuclear couplings could be separated in 2D ω_1 hetero half-filtered TOCSY (HETLOC, Fig. 2.9). In this spectrum (Fig.2.10) of a structural fragment (H-a)-(C-a)-(C-b)-(H-b), both F_1 (vertical) and F_2 (horizontal) dimensions are ^{1}H axes. In the F_1 dimension (=ω_1), only protons attached to ^{13}C are selected by the hetero half filter. The signals appearing in $\{F_1$ = H-a$\}$ region are therefore derived from an isotopomer of (H-a)-(^{13}C-a)-(^{12}C-b)-(H-b), whereas those along $\{F_1$ = H-b$\}$ region are from an isotopomer of (H-a)-(^{12}C-a)-(^{13}C-b)-(H-b). The correlation peak H-b/H-a represents F_1=H-b and F_2=H-a. Each diagonal peak appears as doublet along the diagonal line because of splitting in both dimension by $^1J_{CH}$. Each correlation peak also splits into doublet in F_1 direction, inheriting from the split diagonal peak, whereas the displacement in F_2 direction is due to long-range J_{CH}. When the sign of $^{LR}J_{CH}$ is positive, the direction of displacement is same as that of diagonal peaks as shown in Fig.2.9, whereas the negative $^{LR}J_{CH}$ value gives the opposite direction of displacement. This is proved by the product operator analysis (*42*) in Ref (*15*).

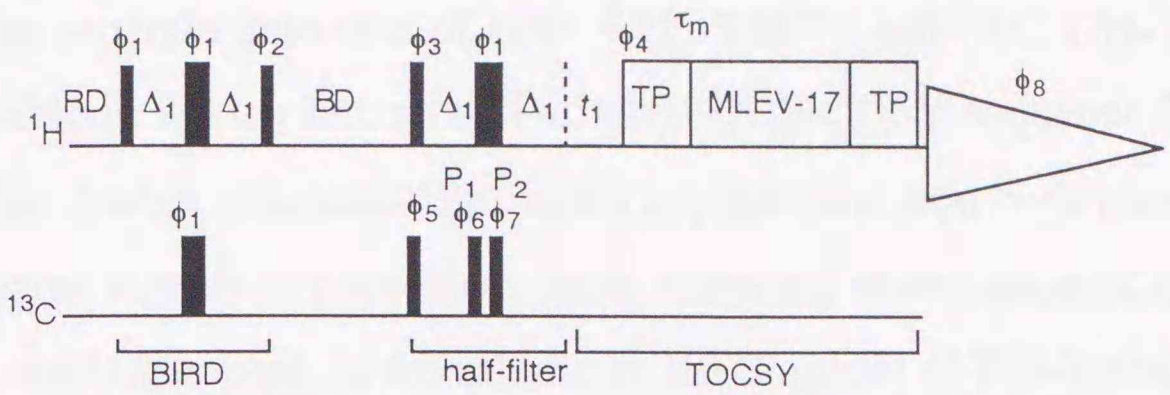


Fig. 2.9. Pulse sequence for the 2D ω_1 hetero half-filtered TOCSY experiment (*14*). P1 and P2 are composite pulses consisting of (58° -140° 172°) and (24° -152° 346° -152° 24°), respectively (*43*). The delay Δ_1 is $1/2^1J_{CH}$. TP and MLEV-17 represent a trim pulse and a composite pulse for TOCSY, respectively. TPPI was applied to phase ϕ_3 for quadrature detection in F_1. Phase cycling used is as follows: ϕ_1 = y; ϕ_2 = -y; ϕ_3 = -y; ϕ_4 = y; ϕ_5 = x^4,$-x^4$; ϕ_6 = x,-x; ϕ_7 = x,x,-x,-x.

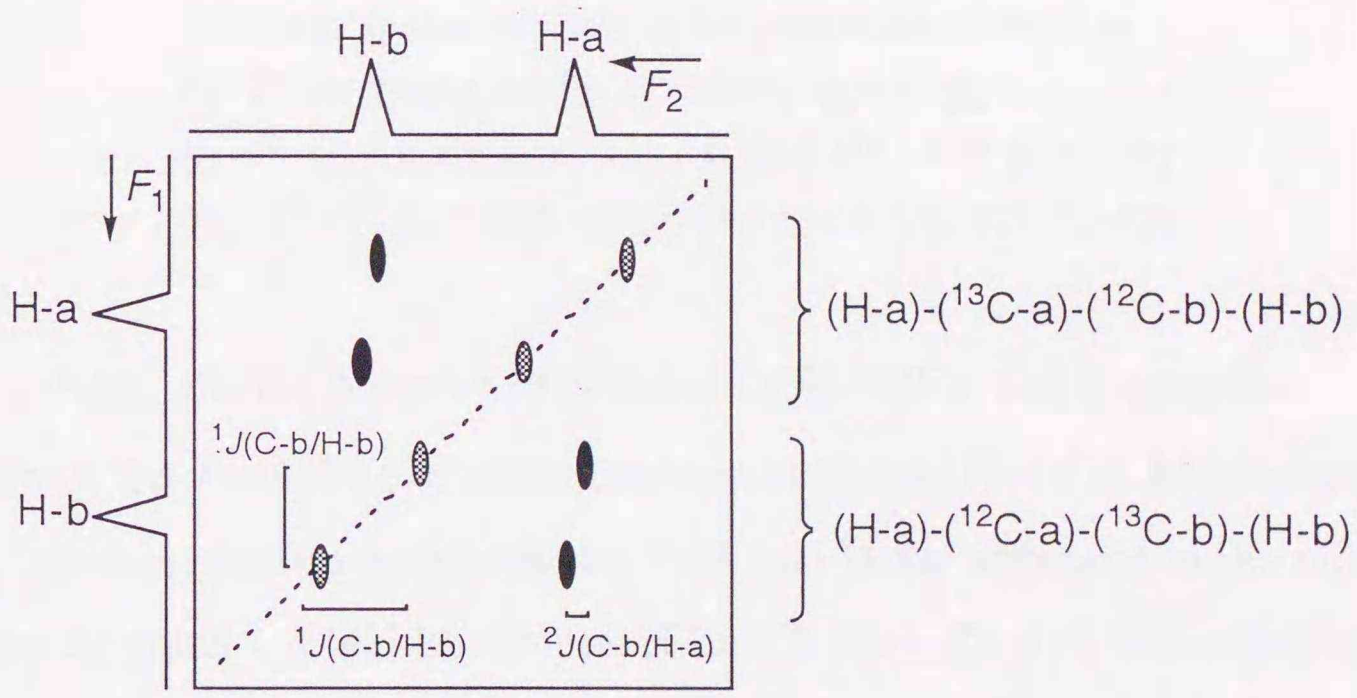


Fig.2.10. Schematic spectrum of the 2D ω_1 hetero half-filtered TOCSY. The magnetization transfers from H-b to H-a in the isotopomer of (H-a)-(^{12}C-a)-(^{13}C-b)-(H-b).

The separate detection of both ^3J(H-7/H-7') and ^2J(C-7/H-7') in **5**, was possible in 2D ω_1 hetero half-filtered DQF-COSY sequence (Fig. 2.11). The double quantum filter again applied to obtain both correlation and diagonal signals in pure absorption, allowing observation of the H-7/H-7' correlation peak in the middle of the diagonal C-7/H-7 doublet (Chart 2.11). The spin-spin coupling between C-7 and H-7' appeared as displacement of two signals of H-7/H-7' correlation peak.

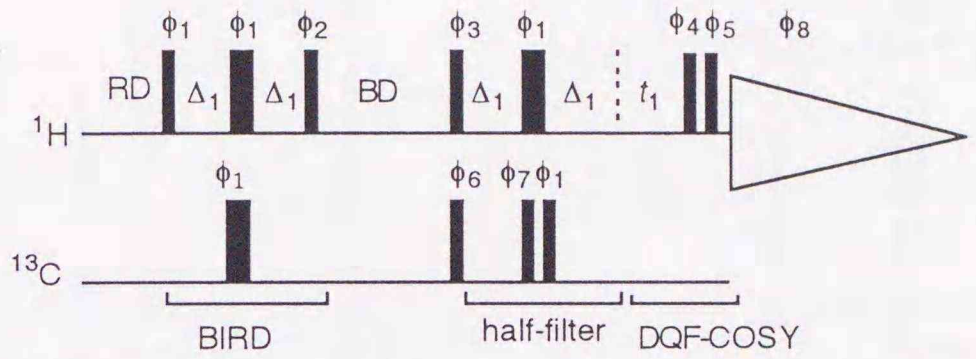


Fig. 2.11. Pulse sequence for the 2D ω_1 hetero half-filtered DQF-COSY experiment. The delay Δ_1 is $1/2^1J_{CH}$. TPPI was applied to phase ϕ_3 for quadrature detection in F_1. Phase cycling used is as follows: ϕ_1 = x; ϕ_2 = -x; ϕ_3 = x; ϕ_4 = x,x,y,y,-x,-x,-y,-y; $\phi_5 = x^{16}, -x^{16}$; ϕ_6 = x,-x; $\phi_7 = x^8,-x^8$; ϕ_8 =.x,-x,-y ,y,-x,x,y,-y,-x,x,y,-y,x,-x, -y,y.

Next, the ω_1 hetero half-filtered DQF-COSY was applied to measure the *J* coupling constant between H-8b and H-8b' of hopeaphenol (**1**). The correlation peak between H-8b and H-8b' appeared in the middle of the diagonal C-8b/H-8b doublet (Chart 2.12a). Two F_1 slices through the high- and low-frequency signals of the diagonal peak of H-8b (arrow b and c) were inverse Fourier transformed, zero-filled 64th times, and Fourier transformed again (Chart 2.12b and 2.12c, respectively) for resolution enhancement. Three different couplings were separated in the resultant 1D spectra as follows: The coupling between equivalent protons H-8b/H-8b' was measured from anti-phase active splitting in each of the slices ($^3J_{HH}$=7.4 Hz), whereas the in-phase passive doublet was due to

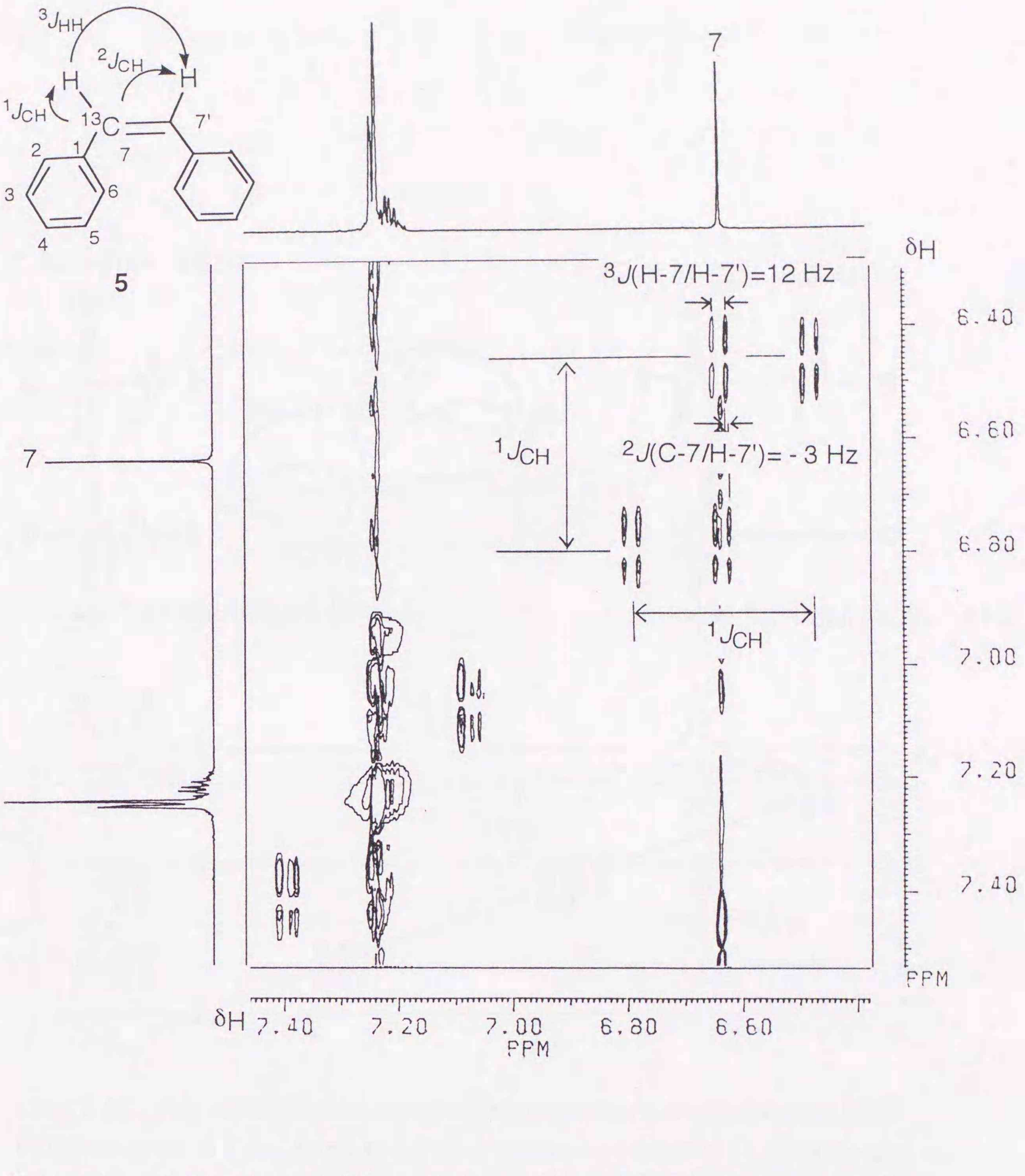


Chart 2.11. The 2D phase sensitive ω_1 hetero half-filtered DQF-COSY spectrum of **5** (20 mg in acetone-d_6). The spectrum was obtained with the pulse sequences shown in Fig. 2.10. The delays, RD, BD, and Δ_1 were set to 2.0 s, 2.3 s, and 3.6 ms ($^1J_{CH}$ = 140 Hz), respectively. Eight transients were accumulated for each of the 64 t_1 increments. The total measuring time was *ca.* 1 hr. Positive and negative peaks are drawn without distinction.

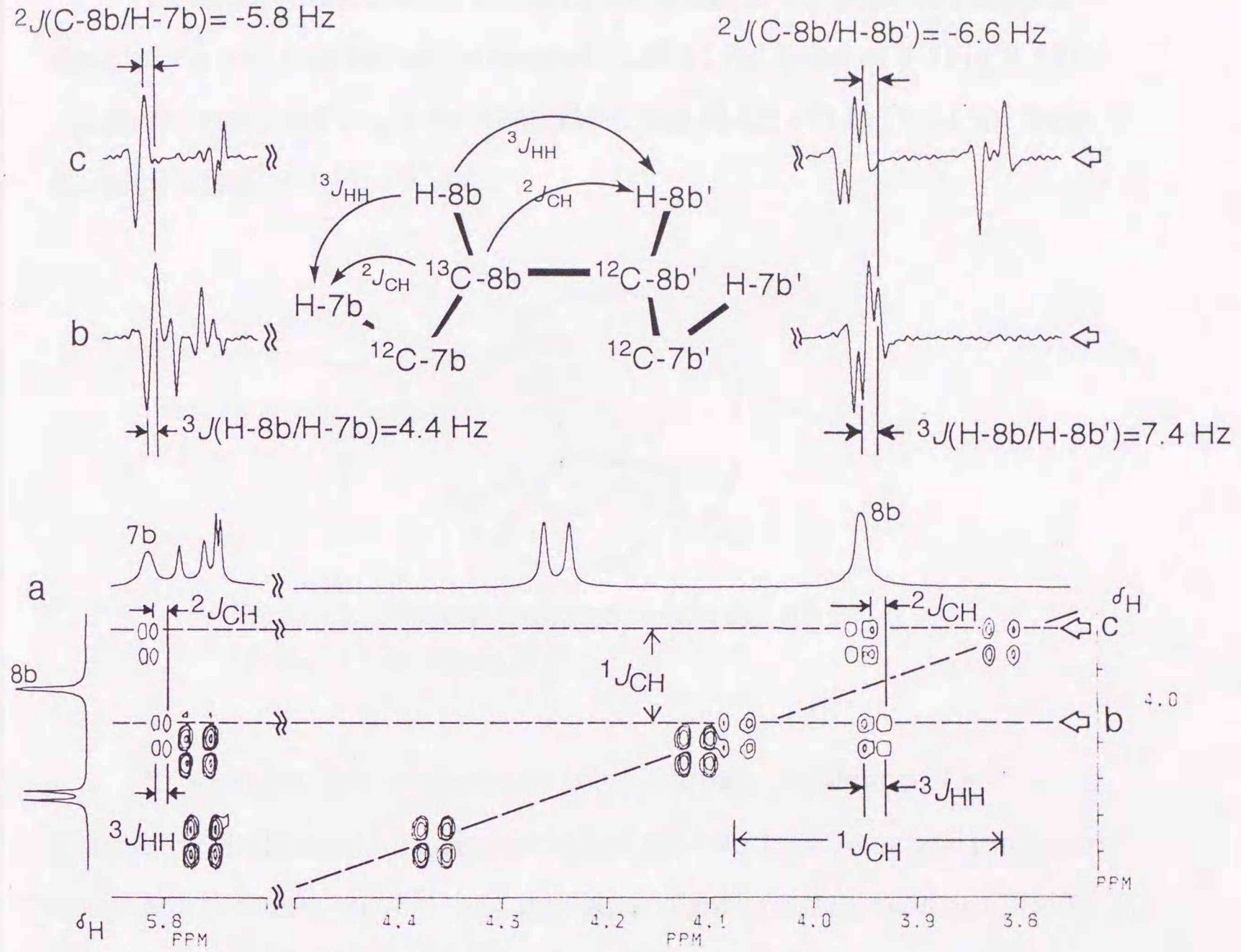


Chart 2.12. Part of the 2D phase sensitive ^{13}C-coupled ω_1 hetero half-filtered DQF-COSY spectrum of **1** (*ca.* 50 mg in 0.5 ml of acetone-d_6) (a) and its F_1 slices through the higher (b) and lower (c) frequency signals of diagonal peak of H-8b. The spectra were obtained with the pulse sequences shown in Fig. 2.11. The delays, RD, BD, and Δ_1 were set to 2.0 s, 0.4 s, and 3.6 ms ($^1J_{CH}$ = 140 Hz), respectively. Each of the 112 t_1 increments was accumulated using 512 transients. The total measuring time was *ca.* 48 h each. Positive and negative peaks are drawn without distinction. The two slices were inverse Fourier transformed, zero-filled 64th times, and Fourier transformed again for resolution enhancement.

H-8b/H-7b coupling ($^3J_{HH}$=4.4 Hz). On the other hand, the heteronuclear C-8b/H-8b' coupling separately appeared as displacement of the signals in two slices ($^2J_{CH}$=-6.6 Hz), which enabled accurate measurements of the H/H couplings free from the contribution of $^{LR}J_{CH}$.

The coupling constant between H-8b and H-8b' obtained supported the *pseudo-anti* conformation around C-8b/C-8b' bond of **1** (Fig.2.12), in which the torsional angle between H-8b and H-8b' (θ) is 140-150° from Karplus equation (*38*, *39*, *44*).

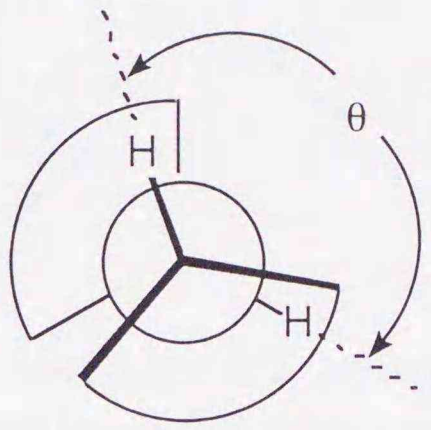


Fig. 2.12. Newman projection looking through the (C-8b) - (C-8b') bond of **1**.

In addition, this method can solve another problem of C_2 symmetric molecules, discrimination of the two heteronuclear long-range couplings between one ^{13}C and two equivalent protons, such as C-8b/H-7b ($^2J_{CH}$), and C-8b/H-7b' ($^3J_{CH}$) in **1**, which can not be measured separately by conventional NMR methods. Since the H-8b/H-7b cross peak (F_1=H-8b and F_2=H-7b; from an isotopomer of {(^{12}C-7b)-(^{13}C-8b)-(^{12}C-8b')-(^{12}C-7b')} in the ω_1 hetero half-filtered DQF-COSY spectrum is arising from H-8b/H-7b ($^3J_{HH}$) coupling, but is little contributed by H-8b/H-7b' coupling ($^4J_{HH}$) (Fig.2.13a), the displacement of these signals showed only C-8b/H-7b coupling ($^2J_{CH}$=-5.8 Hz). In the same manner, as for the isotopomer of {(^{13}C-7b)-(^{12}C-8b)-(^{12}C-8b')-(^{12}C-7b')} (Fig.2.13b), there exists C-7b/H-8b ($^2J_{CH}$) coupling and C-7b/H-8b'

($^3J_{CH}$) to be separately measured. The former is measured selectively from the cross-peaks of H-7b/H-8b in this spectrum ($^2J_{CH}$= -0.9 Hz) since no magnetization transfer between H-7b/H-8b' was contributed because H-7b and H-8b' are 4-bond away.

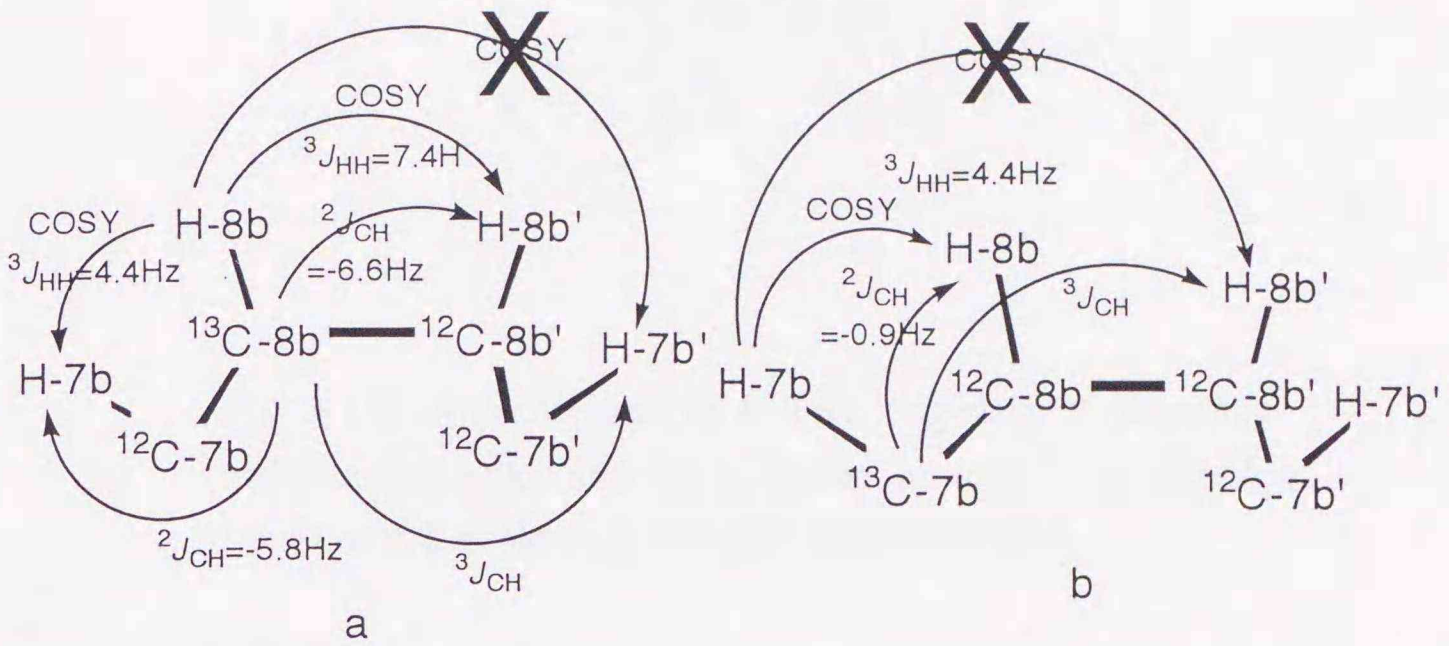


Fig. 2.13. Two isotopomers of **1**. Among the long-range *J* couplings between one carbon and two equivalent protons, $^2J_{CH}$ and $^3J_{CH}$, the former is measured selectively in the ω_1 hetero half-filtered DQF-COSY.

2.6 Introduction of paired satellite selection (PASS) and its product operator analysis

In the previous section, selective measurement of one of the two long-range J_{CH} values between one carbon and two equivalent protons was achieved. Next, I demonstrate simultaneous measurements of both couplings separately. The fact that the cross-peak between H-8b and H-7b in the ω_1 hetero half-filtered DQF-COSY spectrum of **1** is little contributed from H-8b/H-7b' coupling ($^4J_{HH}$) demonstrates displacement of these signals to be C-8b/H-7b coupling (Fig.2.13a). On the other hand, the H-8b/H-7b correlation peak in the 2D ω_1 hetero half-filtered TOCSY (HETLOC) (Fig. 2.9) (*14*, *15*) spectrum contains both ^2J(C-8b/H-7b) and

^{3}J(C-8b/H-7b') (Fig.2.14) since magnetization of H-8b is transferred to H-7b' via H-8b' during the mixing time.

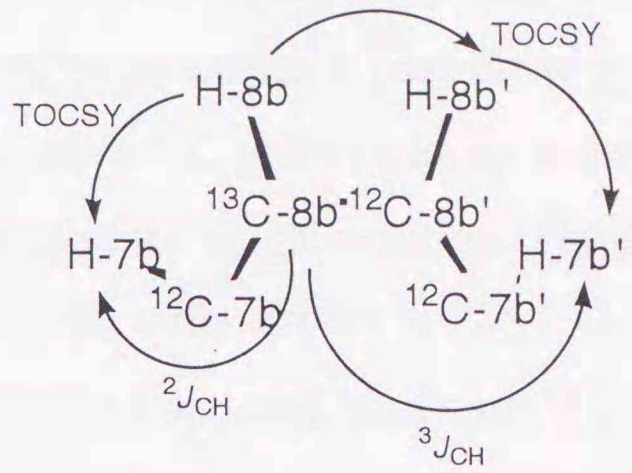


Fig. 2.14. An isotopomer of **1**. Two long-range J couplings between one carbon and two equivalent protons, $^{2}J_{CH}$ and $^{3}J_{CH}$, are contained in the ω_1 hetero half-filtered TOCSY.

It is almost impossible, however, to measure each of their values separately from the displacement of two cross-peaks in the 2D spectrum because of inherent low resolution even if resolution enhancement for the slices could be applied. Thus the separate observation of these two couplings must be performed by a high-resolution 1D variant of the ω_1 hetero half-filtered TOCSY, which should give two 1D subspectra corresponding to the two slices used for measurement of $^{LR}J_{CH}$ in the 2D experiment.

The ordinary method to convert 2D sequences into their 1D variants is use of selective pulse to excite only one nucleus and fixation of the variable t_1 evolution time. In this case, however, the required pair of 1D spectra to be separately measured must be derived from the "single" selective excitation experiment since the two 1D spectra are derived from two satellite signals arising from a certain ^{13}C-H connectivity. Hence, it is impossible to obtain these two 1D spectra separately by the conventional strategy.

I propose the *PA*ired *S*atellite *S*election (PASS) technique (*13*) that enables separate excitation of each signal of the satellite peak. In this method, the combination of an appropriate delay and ^{1}H pulse offset in addition to selective ^{13}C pulse makes it possible to get the requisite pair of 1D spectra. The selective ^{13}C pulse picks up a certain isotopomer that contains one ^{13}C nucleus at the single position. The directly bonded proton appears as a doublet with respect to $^{1}J_{CH}$. Generally, the output of ^{13}C selective pulses needs an optional hardware, *e.g.* a selective excitation unit. Unfortunately the instrument used in this study, however, is not equipped with any such options. Therefore the selective pulses in these experiment were delivered by attenuation of the transmitter pulse through a BFX-5 amplifier (*26*) which caused an inevitable problem of insufficient selectivity.

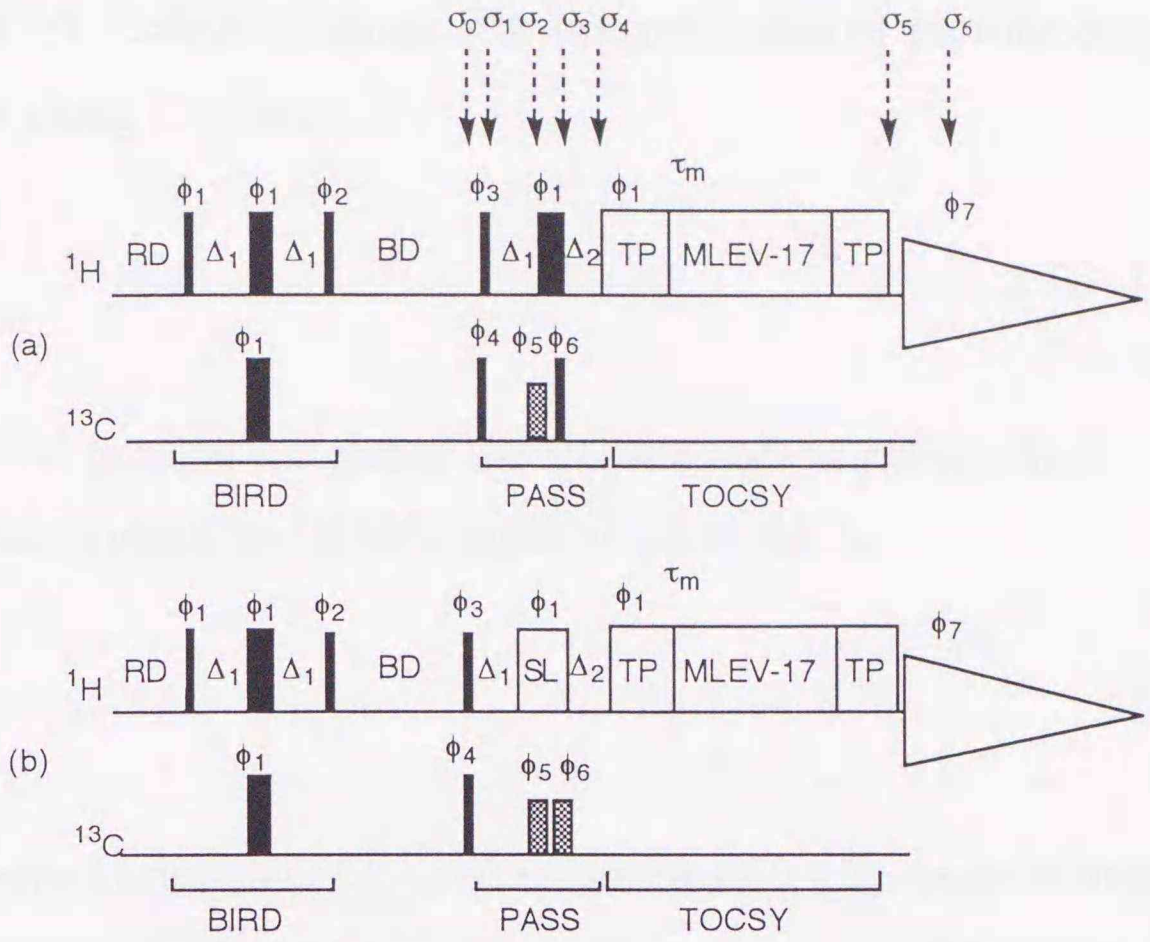


Fig. 2.15. Pulse sequence for the 1D PASS-TOCSY experiment (a) and its slightly modified version (b). SL, TP, MLEV-17, and hatched bar represent a CW spin-locking pulse, a trim pulse, a composite pulse for TOCSY, and selective 90° pulse, respectively. The delays, Δ_1 and Δ_2 is $1/2^1J_{CH}$ and $1/4^1J_{CH}$, respectively. ^{1}H pulse offset should be positioned at each satellite signal or $\pm 2n^1J_{CH}$ (n = 1,2,3$\cdots$) shifted point. See the text for σ_0 - σ_6. Phase cycling used is as follows:. ϕ_1 = y, -y, y, -y, x,-x, x, -x; ϕ_2 = -y, y, -y, y, -x, x, -x, x; $\phi_3 = x^4, y^4, -x^4, -y^4$; $\phi_4 = x^8, -x^8$; ϕ_5 = x, -x; ϕ_6 = x, x, -x, -x; ϕ_7 = x, -x, -x, x, y, -y, -y, y, -x, x, x, -x, -y, y, y, -y.

The product operator analysis (*42*) of the PASS-TOCSY sequence (Fig. 2.15 σ_0 - σ_6) is examined dealing with a structural fragment represented as (H-I)-(C-S)-(X)-(Y)-(H-K), where X and Y are heteroatoms without magnetic moment. To avoid confusion in numeric formulae, the delays, Δ_1 and Δ_2 in Fig. 2.15 are represented as Δ and τ, respectively. For simplicity, only terms that contribute to the final spectrum (observable terms) are retained. The BIRD pulse and BD suppress the

signals of ^{12}C-bonded protons. The magnetization of protons bound to ^{13}C (I) is along the z-axis.

$$\sigma_0 = I_Z \qquad \text{.....[1]}$$

The 90° ^{13}C pulse at the end of the BD does not affect the final observable terms. The $^{1}H\ 90°_{X}$ pulse affect to the I_Z.

$$\sigma_1 = -\ I_Y \qquad \text{.....[2]}$$

Heteronuclear coupling ($^{1}J_{IS}$) and chemical shift (Ω_I) evolves during Δ, whereas the evolution of homonuclear coupling ($J_{IK} < 20$ Hz) is negligible.

$$\begin{aligned}\sigma_2 = &-\ I_Y \cos(\pi J_{IS}\Delta)\ \cos(\Omega_I\Delta) \\ &+\ I_X \cos(\pi J_{IS}\Delta)\ \sin(\Omega_I\Delta) \\ &+\ 2I_X\ S_Z \sin(\pi J_{IS}\Delta)\ \cos(\Omega_I\Delta) \\ &+\ 2I_Y\ S_Z \sin(\pi J_{IS}\Delta)\ \sin(\Omega_I\Delta) \quad \text{.....[3]}\end{aligned}$$

The phase cycling of $\phi 5$ and $\phi 6$ in Fig.2.15 corresponds to 180° and 0° ^{13}C pulses. The first and second terms in eqn.[3] are canceled out by the phase cycling of $\phi 5$, $\phi 6$, and $\phi 7$.

$$\begin{aligned}\sigma_3 = &\ 2I_X\ S_Z \sin(\pi J_{IS}\Delta)\ \cos(\Omega_I\Delta) \\ &-\ 2I_Y\ S_Z \sin(\pi J_{IS}\Delta)\ \sin(\Omega_I\Delta) \quad \text{.....[4]}\end{aligned}$$

Heteronuclear coupling ($^{1}J_{IS}$) and chemical shift (Ω_I) evolves during τ.

$$\sigma_4 = 2I_x S_z \sin(\pi J_{IS}\Delta) \cos[\Omega_I(\Delta-\tau)] \cos(\pi J_{IS}\tau)$$
$$+ 2I_y \sin(\pi J_{IS}\Delta) \cos[\Omega_I(\Delta-\tau)] \sin(\pi J_{IS}\tau)$$
$$- 2I_y S_z \sin(\pi J_{IS}\Delta) \sin[\Omega_I(\Delta-\tau)] \cos(\pi J_{IS}\tau)$$
$$+ 2I_x \sin(\pi J_{IS}\Delta) \sin[\Omega_I(\Delta-\tau)] \sin(\pi J_{IS}\tau) \quad \ldots\ldots\ldots[5]$$

The spin-locking y-pulse purged the first and fourth terms, and then it causes inphase magnetization transfer from I_y to K_y.

$$\sigma_5 = + 2I_y \sin(\pi J_{IS}\Delta) \cos[\Omega_I(\Delta-\tau)] \sin(\pi J_{IS}\tau)$$
$$- 2I_y S_z \sin(\pi J_{IS}\Delta) \sin[\Omega_I(\Delta-\tau)] \cos(\pi J_{IS}\tau)$$
$$+ 2K_y \sin(\pi J_{IS}\Delta) \cos[\Omega_I(\Delta-\tau)] \sin(\pi J_{IS}\tau)$$
$$- 2K_y S_z \sin(\pi J_{IS}\Delta) \sin[\Omega_I(\Delta-\tau)] \cos(\pi J_{IS}\tau) \quad \ldots\ldots\ldots[6]$$

The first and second terms correspond to an diagonal peak of the 2D spectrum during acquisition time, and the third and fourth terms to an off-diagonal one. These terms evolve during acquisition time (t) as follows:

$$\sigma_6 = + 2I_y \sin(\pi J_{IS}\Delta) \cos[\Omega_I(\Delta-\tau)] \sin(\pi J_{IS}\tau) \cos(\Omega_I t)\cos(\pi J_{IK} t)\cos(\pi J_{IS} t)$$
$$- 2I_y S_z \sin(\pi J_{IS}\Delta) \sin[\Omega_I(\Delta-\tau)] \cos(\pi J_{IS}\tau) \cos(\Omega_I t)\cos(\pi J_{IK} t)\cos(\pi J_{IS} t)$$
$$+ 2K_y \sin(\pi J_{IS}\Delta) \cos[\Omega_I(\Delta-\tau)] \sin(\pi J_{IS}\tau) \cos(\Omega_K t)\cos(\pi J_{IK} t)\cos(\pi J_{KS} t)$$
$$- 2K_y S_z \sin(\pi J_{IS}\Delta) \sin[\Omega_I(\Delta-\tau)] \cos(\pi J_{IS}\tau) \cos(\Omega_K t)\cos(\pi J_{IK} t)\cos(\pi J_{KS} t)$$
$\ldots\ldots\ldots[7]$

These terms show that the phase difference between two signals of S satellite is $\pi/2$ when the delay τ is set to $1/(4^1 J_{IS})$. Setting the I pulse offset to the high frequency satellite signal, namely $\Omega_I = -\pi J_{IS}$, the relevant terms are;

$$\sigma_6' = +\ 1/2\{I_y\ \cos(\Omega_I t)\ \cos(\pi J_{IK} t)\ \cos(\pi J_{IS} t)$$
$$-I_y \cos(\Omega_I t)\ \cos(\pi J_{IK} t)\ \sin(\pi J_{IS} t)\}$$
$$+\ K_y \cos(\Omega_K t)\ \cos(\pi J_{IK} t)\ \cos(\pi J_{IS} t)$$
$$-K_y \cos(\Omega_K t)\ \cos(\pi J_{IK} t)\ \sin(\pi J_{IS} t)\} \quad \ldots\ldots\ldots [8]$$

Each term is in-phase with respect to homonuclear J_{IK} coupling. As for the heteronuclear coupling, the first and third terms are in-phase while the second and fourth ones are antiphase. Hence, the superposition of all terms gives the 1D spectrum corresponding to the F_1 slice through the high-frequency satellite signal of the diagonal peak (Fig.2.16 right bottom). In the same way, when the I pulse is offset onto the low frequency satellite signal, namely, $\Omega_I = \pi J_{IS}$, the relevant terms of σ_6 under this condition are as follows:

$$\sigma_6'' = +\ 1/2\{I_y \cos(\Omega_I t)\ \cos(\pi J_{IK} t)\ \cos(\pi J_{IS} t)$$
$$+I_y \cos(\Omega_I t)\ \cos(\pi J_{IK} t)\ \sin(\pi J_{IS} t)\}$$
$$+\ K_y \cos(\Omega_K t)\ \cos(\pi J_{IK} t)\ \cos(\pi J_{IS} t)$$
$$+K_y \cos(\Omega_K t)\ \cos(\pi J_{IK} t)\ \sin(\pi J_{IS} t)\} \quad \ldots\ldots\ldots [9]$$

The resulting spectrum, then, corresponds to the F_1 slice through the low-frequency satellite signal of diagonal peak (Fig.2.16 right top). In addition, these calculated results reveal that I pulse offset can be shifted by $\pm 2n^1 J_{IS}$ and the delay τ can be varied by $+n/(2^1 J_{IS})$ (n=1,2,3.....), though longer τ intervals allow undesired J_{IK} evolution.

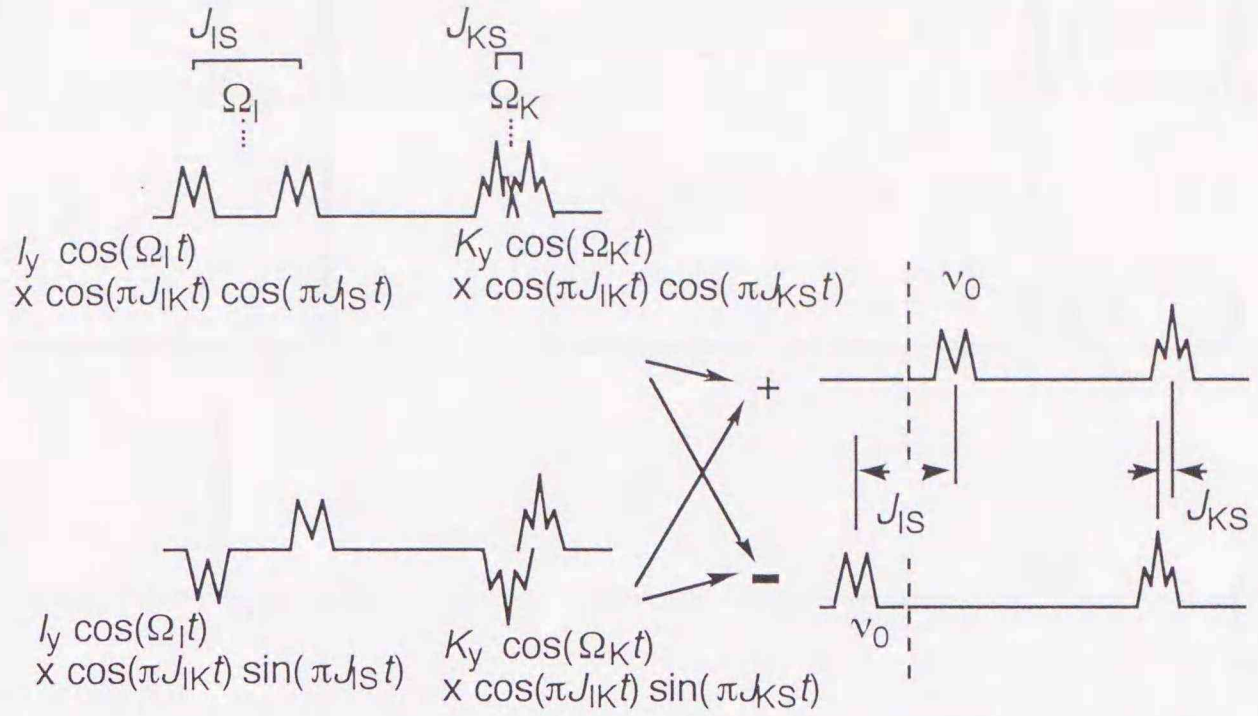
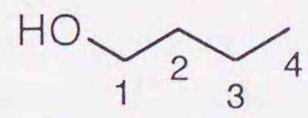


Fig.2.16. Schematic spectrum of 1D PASS-TOCSY from the product operator calculation. The first and third terms of the σ_6' and σ_6'' are in-phase with respect to both homo- and heteronuclear couplings (left top), whereas the second and fourth terms are in-phase with respect to homonuclear coupling and antiphase with respect to heteronuclear coupling (left bottom). The σ_6' is the subtraction of the second and fourth terms from the first and third terms, whereas the σ_6'' is the sum of all terms.

The conventional 2D ω_1 hetero half-filtered TOCSY spectrum of 1-butanol (**7**) (Chart 2.13a) and F_1 slices through H-1 (Chart 2.13b and c) are shown. The resolution of the slices is insufficient to show their multiplet pattern, although it has been enhanced by the sequence of inverse Fourier transformation, zero filling to 8K, and re-transformation.



1-butanol (**7**)

In contrast, the selective one-dimensional PASS-TOCSY spectra of **7** (Chart 2.13d and e) show the higher resolution inherent to the selective one-dimensional experiment. These 1D subspectra were obtained by

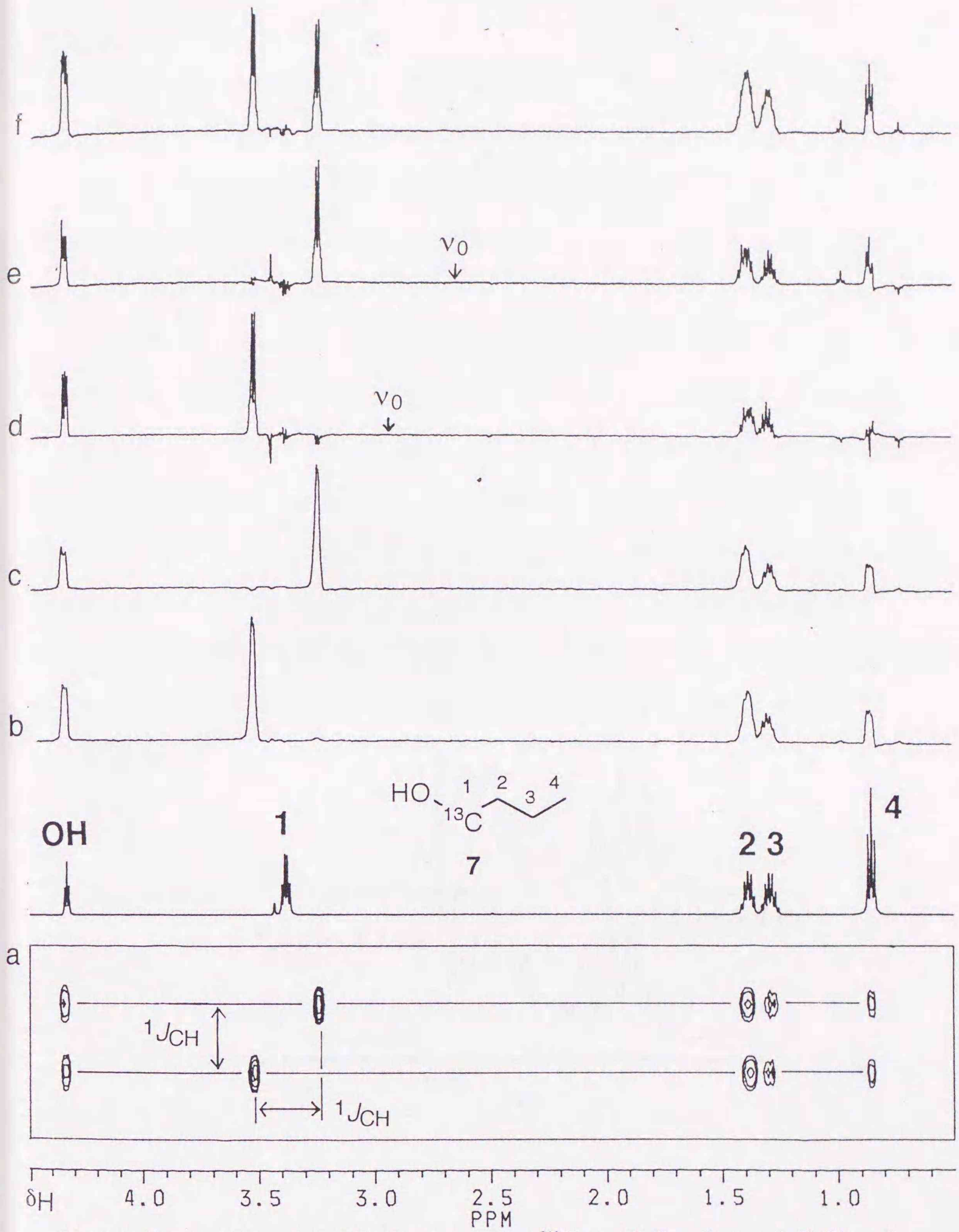


Chart 2.13. (a) Part of the 2D phase sensitive ^{13}C-coupled ω_1 hetero half-filtered TOCSY spectrum of **7** (30 mg in 0.5 ml DMSO-d_6) (sequence in Fig.2.9). Each of the 128 t_1 increments was accumulated using 32 transients. The total measuring time was *ca.* 4.5 h. (b) and (c): F_1 slices through the higher (b) and lower (c) frequency signals of diagonal peak of H-1. (d) and (e): PASS-TOCSY spectra (sequence in Fig.2.15a). The delays, RD, BD, Δ_1, Δ_2, and τ_m were 2.0 s, 1.7 s, 3.6 ms, 1.8 ms ($^1J_{CH}$ = 140 Hz), and 43 ms, respectively. ^{1}H pulse offset (ν_0) was shifted to +2^1J (C-1, H-1), 276 Hz, upfield point of higher (d) and lower (e) frequency signal of ^{13}C satellite of H-1. Each spectrum was accumulated using 128 transients. The total measuring time was 9 min each. (f) The 1D HMQC-TOCSY spectrum. Both the defocusing and refocusing delays were 3.6 ms. The other measurement conditions were the same as (d). For each spectrum, ^{1}H pulses were derived from the high-power output of the decoupler channel attenuated by 11 dB (90° pulse duration was 39 μs).

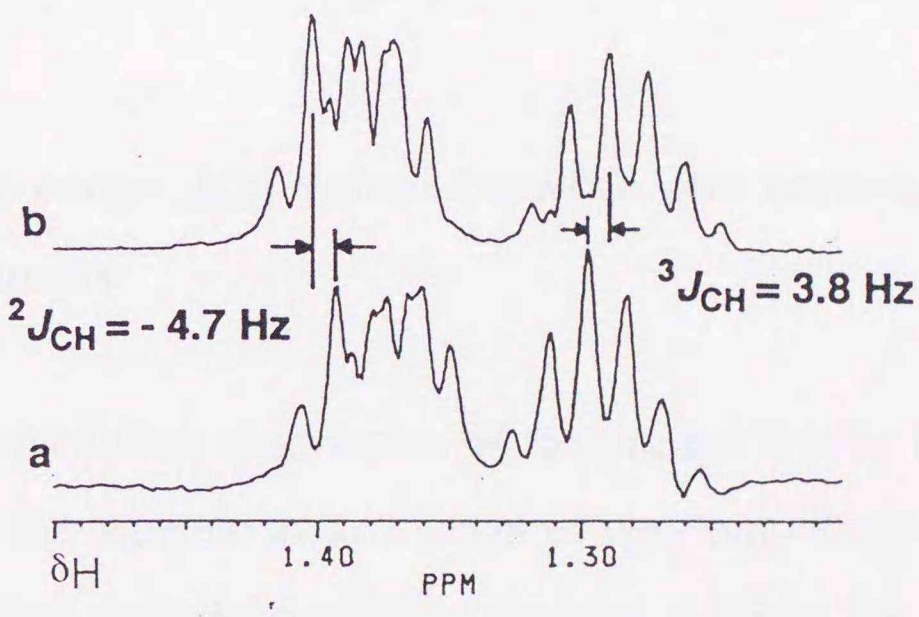


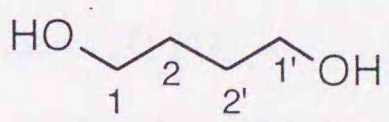
Chart 2.14. Partial expanded spectra for Charts 2.13d (a) and 2.13e (b).

paired satellite selection for H-1, setting the ^{1}H pulse offset $+^2J$ (C-1, H-1), 276 Hz, upfield of each satellite signal in order to attain an efficient Hartman-Hahn match between the H-1 and the higher-field protons, H-2 and H-3. Each subspectrum originates from one of the satellite peaks of H-1 in the ^{1}H spectrum.

The conventional 1D HMQC-TOCSY (*45*) gave only a single 1D spectrum corresponding to superposition of two subspectra (Chart 2.13f). The PASS achieved the selective excitation of each signals of one doublet peak. The resolution of each 1D subspectrum of the PASS-TOCSY is as high as the normal ^{1}H spectrum. Since the same multiplet pattern can be seen in each signal in two subspectra, the displacement of signals is unequivocally clear (Chart. 2.14). From those spectra, ^2J (C-1, H-2) and ^3J (C-1, H-3) can be accurately measured as -4.7 Hz and 3.8 Hz, respectively.

2.7 Two long-range J_{CH} values between one carbon and two equivalent protons

The high-resolution observation of long-range J_{CH} by PASS-TOCSY enables the separate measurement of two long-range J_{CH} values between one carbon and two equivalent protons. At first, the validity of the PASS-TOCSY for a symmetric molelcule is demonstrated by using 1,4-butanediol (**8**) as a model compound.



1,4-butanediol (**8**)

Each satellite signal of H-2 was selectively excited by PASS. Two sets of the spectra were obtained with different TOCSY mixing time. The

each spectrum with shorter (31 ms) (Chart 2.15a, higher H-2 satellite selection, and 2.15b, lower H-2 satellite selection) and longer (88 ms) mixing time (Chart 2.15c, higher H-2 satellite selection, and 2.15d, lower H-2 satellite selection) are shown. Their expansion plots of the region of H-1 (and its equivalent proton H-1') are shown in Chart 2.16a-d, respectively. Each signal is composed of overlapping of two triplets. Intensity of each triplet marked with + became relatively larger in the longer mixing time experiment, whereas the triplet marked with - became smaller. Then the former was concluded to be the TOCSY signal of H-2/H-1' and the latter was that of H-2/H-1. Consequently, the ^{3}J(C-2/H-1') was obtained to be +4.0 Hz, and ^{2}J(C-2/H-1) to be -2.1 Hz.

Next, this method was applied to hopeaphenol (**1**) to measure long-range couplings between one ^{13}C and two equivalent protons, namely C-8b and H-7b ($^{2}J_{CH}$) and C-8b and H-7b' ($^{3}J_{CH}$). Although the former was already determined as -5.8 Hz in the section 2.5, the latter has not yet been determined. In the case of **1**, the selective pulse for C-8b also excited C-8a incompletely, which is distant only 1.5 ppm from C-8b. Furthermore, the high-frequency satellite signal of H-8b and low frequency H-8a satellite signals are in the almost same position in the ^{1}H spectrum. Then, even partial excitation of C-8a caused appearance of lower-frequency signal of H-8a satellite (marked with * in Chart 2.17a). From H-8a satellite, TOCSY magnetization may transfer to H-7b, which would overlap the H-7a signals. Sufficient improvement was given by heightening the selectivity of ^{13}C selective pulse (90° pulse duration was changed from 2.1 ms ($\gamma B_1/2\pi$=120 Hz) to 3.4 ms ($\gamma B_1/2\pi$=74 Hz)) and some modification to the portion of selective excitation of the sequence (Fig. 2.15b), in which the second carbon pulse was changed to a selective pulse, and proton 180° pulse was replaced with spin locking (*46*) (Chart 2.17b).

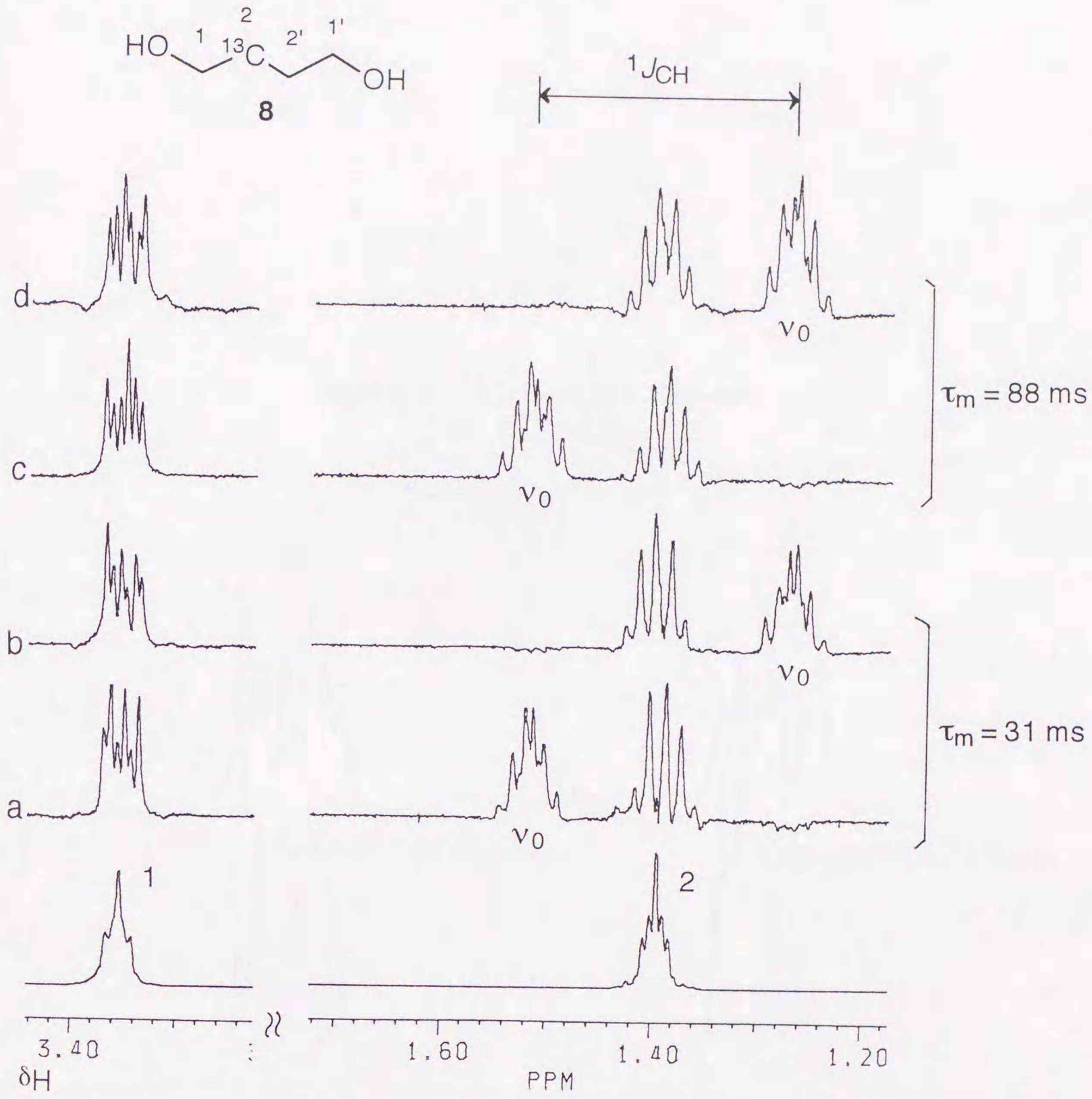
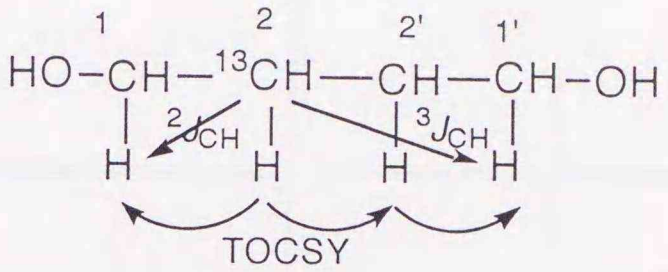
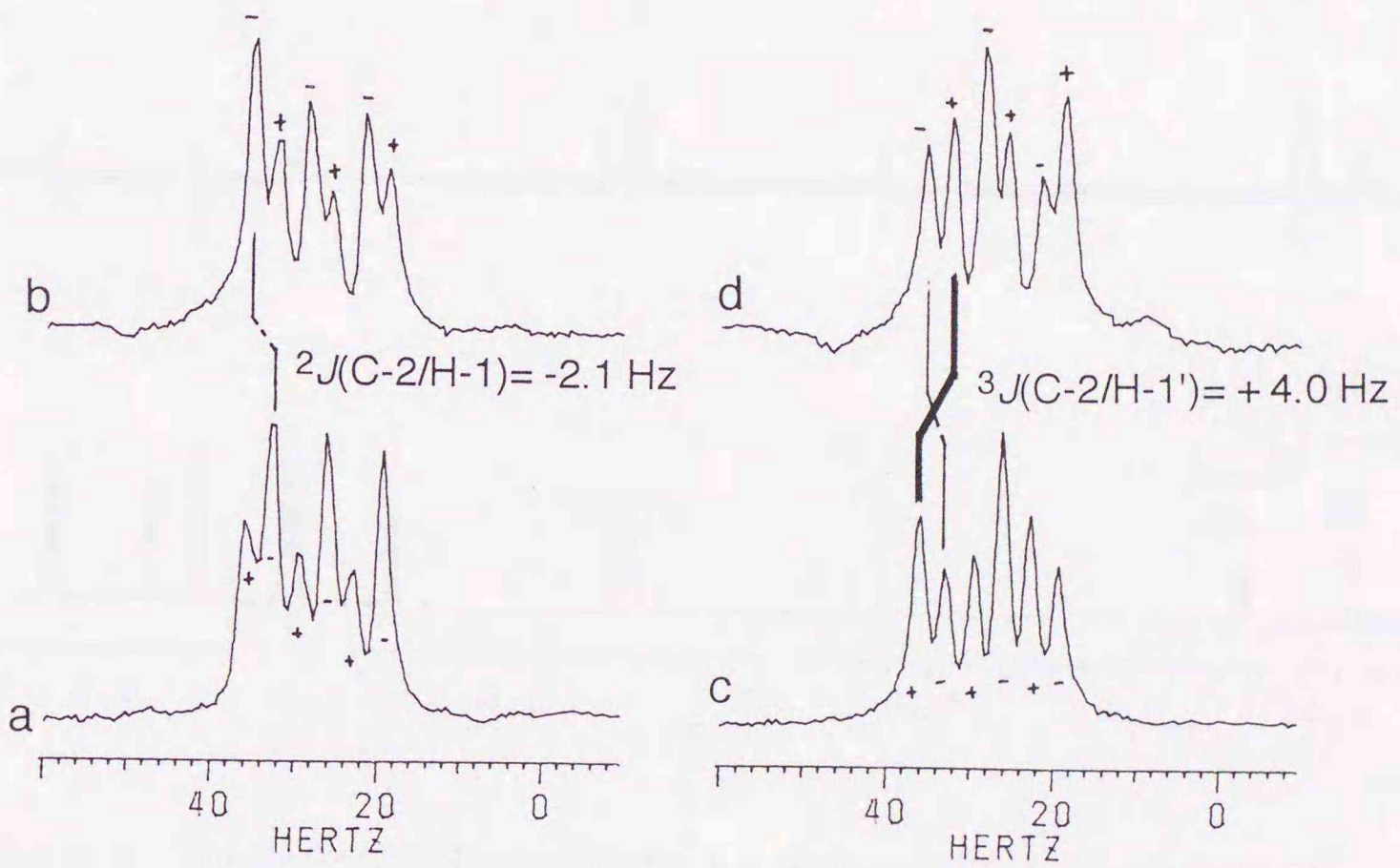


Chart 2.15. The PASS-TOCSY spectra (sequence in Fig.2.15a) of **8** (30 mg in 0.5 ml DMSO-d_6. A few drops of D_2O was added to suppress the -OH signal). The delays, RD, BD, Δ_1, and Δ_2 were 4.0 s, 0.86 s, 3.94 ms, and 1.97 ms ($^1J_{CH}$ = 127 Hz), respectively. ^1H pulse offset (ν_0) was set on higher (a and c) and lower (b and d) frequency signal of ^{13}C satellite of H-2. τ_m were 31 ms (a and b) and 88 ms (c and d). Each spectrum was accumulated using 512 transients. The total measuring time was *ca.* 1 h each. The other measuring conditions were the same as those of Chart 2.13d.



8



$\tau_m = 31$ ms ⇨ $\tau_m = 88$ ms

Chart 2.16. Partial expanded spectra (H-1 region) for Charts 2.15a-d.

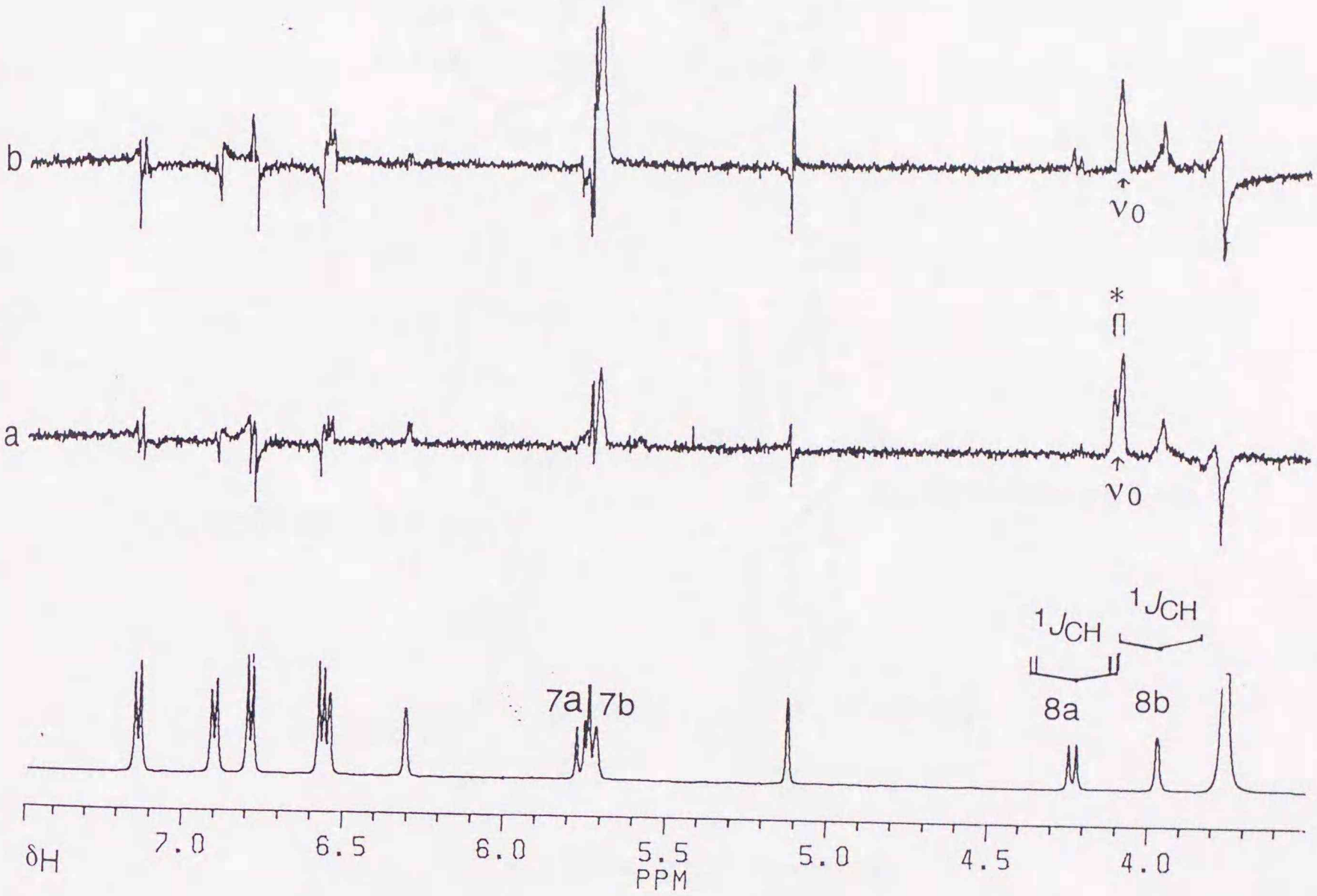


Chart 2.17. The PASS-TOCSY spectra of **1** (*ca.* 50 mg in 0.5 ml of acetone-d_6) The spectra were obtained with the pulse sequences shown in Fig.2.15a. The delays, RD, BD, Δ_1, Δ_2, and τ_m were 0.1s, 0.4 s, 3.88 ms, 1.94 ms ($^1J_{CH}$ = 129 Hz), and 18 ms, respectively. ^{1}H pulse offset (ν_0) was set on the higher frequency signal of ^{13}C satellite of H-8b. Pulse sequence used was Fig. 2.15a (a) and b (b). Duration of selective ^{13}C pulses are 2.1 ms (a), and 3.4 ms (b). Each spectrum was accumulated using 4480 transients. The total measuring time was *ca.* 1 h each. The other measuring conditions were the same as those of Chart 2.13d. *: Unwanted doublet of lower frequency signal of H-8a satellite.

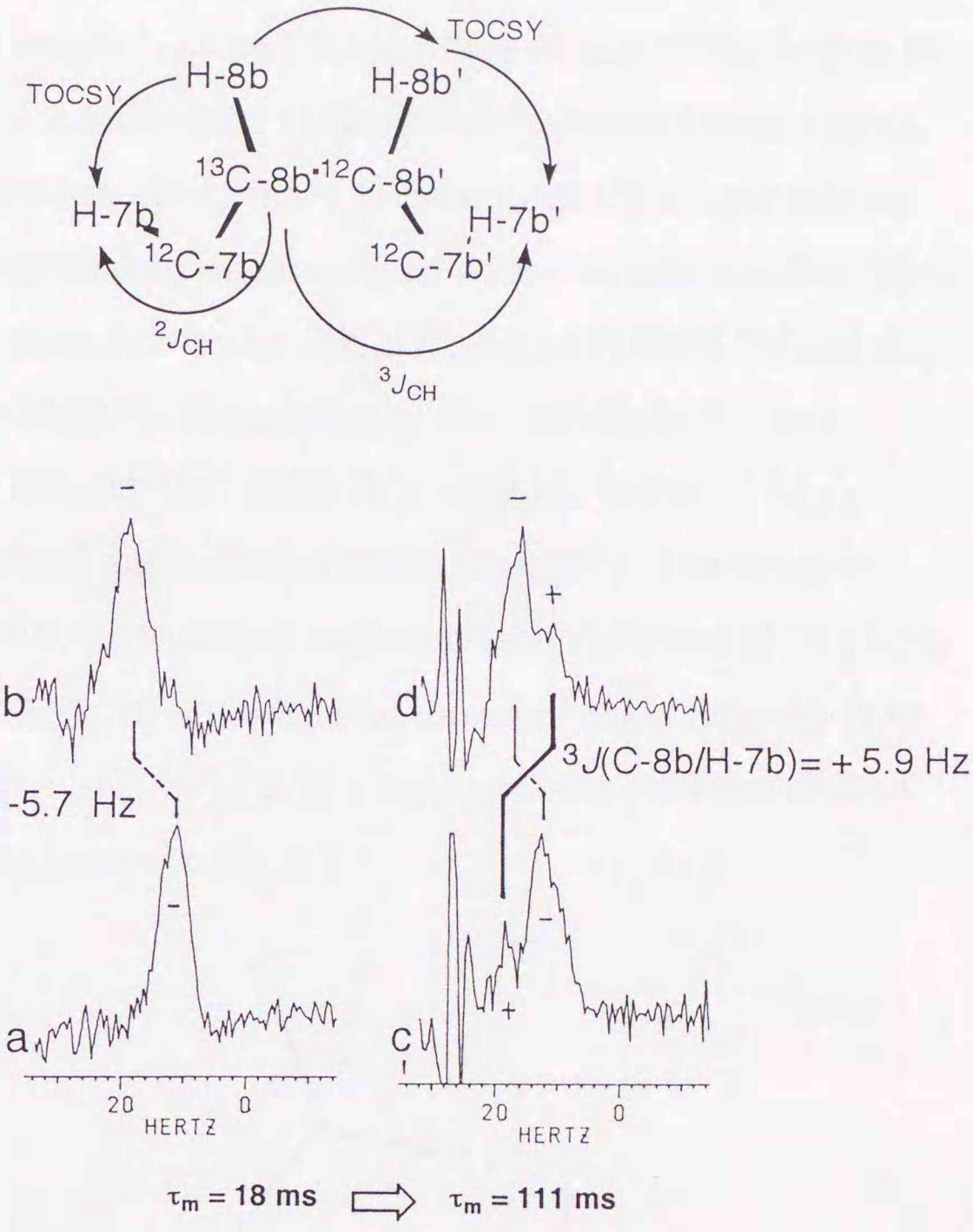


Chart 2.18. H-7b region of PASS-TOCSY spectra of **1** (*ca.* 50 mg in 0.5 ml of acetone-d_6). Pulse sequence used was Fig. 2.15b. ^{1}H pulse offset (ν_0) was set on higher (a and c) and lower (b and d) frequency signal of ^{13}C satellite of H-8b. τ_m were 18 ms (a and b), and 111 ms (c and d). The other measuring conditions were the same as those of Chart 2.17b.

Each satellite signal of H-8b was selectively excited by the modified PASS. Two sets of the spectra were obtained with different TOCSY mixing time (Chart 2.18). The each spectrum with shorter (18 ms) (Chart 2.18a, higher H-8b satellite selection, and 2.17b, lower H-8b satellite selection) and with longer (111 ms) mixing time (Chart 2.18c, higher H-8b satellite selection, 2.18d, lower H-8b satellite selection) were shown. Intensity of each signal marked with + became larger in longer mixing time experiment, whereas the signal marked with - became smaller. Then the former was concluded to be the TOCSY peak of H-8b/H-7b' and the latter was that of H-8b/H-7b. Consequently, the ^{2}J(C-8b/H-7b) was obtained to be -5.7 Hz, and ^{3}J(C-8b/H-7b'), +5.9 Hz. Value of $^{3}J_{CH}$ depends on the torsional angle similar to the $^{3}J_{HH}$ (*47*). The value of ^{3}J(C-8b/H-7b') = +5.9 Hz (torsional angle between C-8b and H-7b (θ_1) is 20 - 40°) and ^{3}J(H-8b/H-7b) = 4.4 Hz (the torsional angle between H-8b and H-7b (θ_2) is 120 - 140°) (Fig.2.17) suppoeted the conformation of seven-menbered ring shown in Fig.2.7.

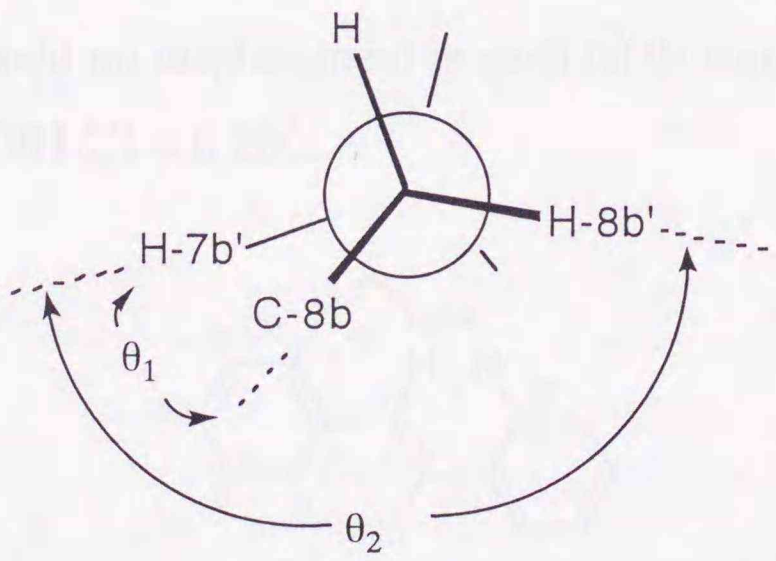
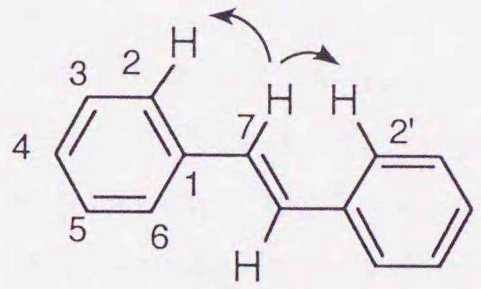


Fig.2.17. Newman projection looking through the (C-8b')-(C-7b') bond of **1**.

2.8 Discrimination of intra- and inter-unit NOEs

The separate detection of two long-range J_{CH} values between one carbon and two equivalent protons should enable the partial discrimination of intra- (Ha/Hb) and inter- (Ha/Hb') unit NOEs in a C_2 symmetric molecule containing a (CaHa)--(CbHb)--(Cb'Hb')--(Ca'Ha') system as a structural fragment. It will be performed by PASS-NOESY (ROESY) (Fig. 2.17). Since the value of the long-range J_{CH} must appear as the displacement of signals in two 1D subspectra of PASS-NOESY (ROESY), the intra- or inter-unit NOE could be discriminated in the case that long-range J(C-b/H-a) and J(C-b/H-a') are different.

At first, the PASS-NOESY spectra of a symmetric model compound, *E*-stilbene (**9**), were measured with the sequence shown in Fig.2.16a to demonstrate the discrimination of intra- (H-7/H-2) and inter- (H-7/H-2') unit NOEs. If an intra-unit NOE (H-7/H-2) appears, each NOE signal in the two subspectra must be displaced by ^3J(C-7/H-2) ,whereas an existence of an inter-unit NOE (H-7/H-2') must yield no displacement in each NOE signal in the two subspectra (^4J(C-7/H-2') ≈ 0 Hz).



E-stilbene (**9**)

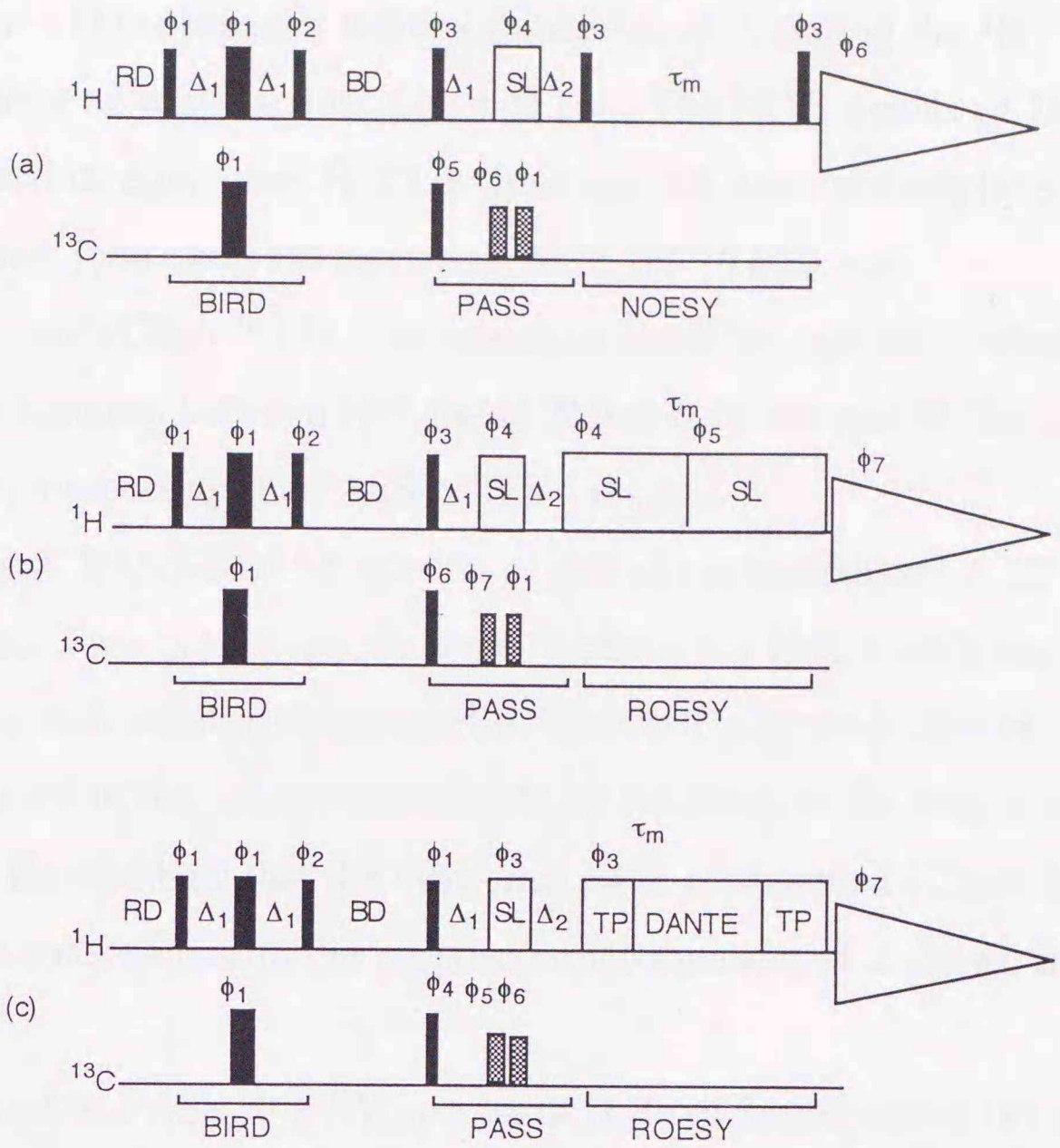


Fig. 2.17. Pulse sequence for the 1D PASS-NOESY (a) and -ROESY (b and c) experiment. SL, TP, and hatched bar represent a CW spin-locking pulse, a trim pulse, and a selective 90° pulse respectively. Δ_1 and Δ_2 is $1/2^1J_{CH}$ and $1/4^1J_{CH}$. ^{1}H pulse offset should be positioned at each satellite signal or $\pm 2n\,^1J_{CH}$ (n = 1,2,3 $\cdots$). Phase cycling used is as follows: (a): ϕ_1 = x, -x, y, -y; ϕ_2 = -x, x, -y, y; ϕ_3 = y, -y, -x, x; ϕ_4 = x, x, y, y; ϕ_5 = x^8,$-x^8$; ϕ_6 = x,x,y,y,-x,-x,-y,-y (b): ϕ_1 = x, -x, y, -y; ϕ_2 = -x, x, -y, y; ϕ_3 = y, -y, -x, x; ϕ_4 = x, x, y, y; ϕ_5 = -x, -x, -y, -y; ϕ_6 = x^8,$-x^8$; ϕ_7 = x,x,y,y,-x,-x,-y,-y (c): ϕ_1 = x^4,y^4, $-x^4$,$-y^4$; ϕ_2 = $-x^4$,$-y^4$,x^4, y^4; ϕ_3 = y,-y,y,-y,-x,x,-x,x; ϕ_4 = x^{16},$-x^{16}$; ϕ_5 = x,-x; ϕ_6 = x,x,-x, -x; ϕ_7 = x,-x,-x,x,y,-y,-y,y, -x,x,x,-x,-y,y,y,-y.

Two 1D subspectra were obtained for H-7, setting the ^{1}H pulse offset on each satellite signal of H-7. The NOE signals of H-7/H-2 (and its equivalent H-2') in those spectra were not displaced each other, indicating the inter-unit NOE (H-7/H-2') was predominant (Chart 2.19). The examination of the molecular model gave the distance between H-7 and H-2' was 0.18 nm and H-7/H-2 0.25 nm, supporting the PASS-NOESY results.

Next, PASS-NOESY spectra at H-9 of cycloshizukaol A (**2**) were examined. Two 1D subspectra were obtained for H-9, setting the ^{1}H pulse offset on each satellite signal of H-9. The NOE signals of H-9/H-1 (or H-1') obtained in the subspectra indicate an existence of the long-range J_{CH} of +6.0 Hz, showing that the intra-unit NOE is observed (Chart 2.20), which is consistent with the proposed conformation of **2** shown in Fig.2.4.

Finally, PASS-ROESY spectra at H-8b of hopeaphenol (**1**) were examined to discriminate the intra-unit ROE (H-8b/H-14b) and inter-unit one (H-8b/H-14b'). In the two 1D subspectra obtained with sequence shown in Fig.2.17b (Chart 2.22) for H-8b, setting the ^{1}H pulse offset on each satellite signal of H-8b , strong TOCSY peak between H-8 and H-8b' appeared. The TOCSY transfer in the ROESY spectrum may cause a TOCSY-ROESY false peak, which is not discriminated from a ROESY peak because they appear in the same phase (*36*). If the expected ROE is the intra-unit one (H-8b/H-14b) (Fig.2.18a), the TOCSY magnetization transfer from H-8b to H-8b' leads the TOCSY-ROESY false peak to H-14b' since the intra-unit ROE should also exist between H-8b' and H-14b'. Both real (H-8b/H-14b) ROESY and false (H-8b→H-8b'→H-14b') TOCSY-ROESY peaks are overlapped. On the contrary, if the expected ROE is the inter-unit one (H-8b/H-14b') (Fig.2.18b), the TOCSY magnetization transfer from H-8b to H-8b' then leads the TOCSY-

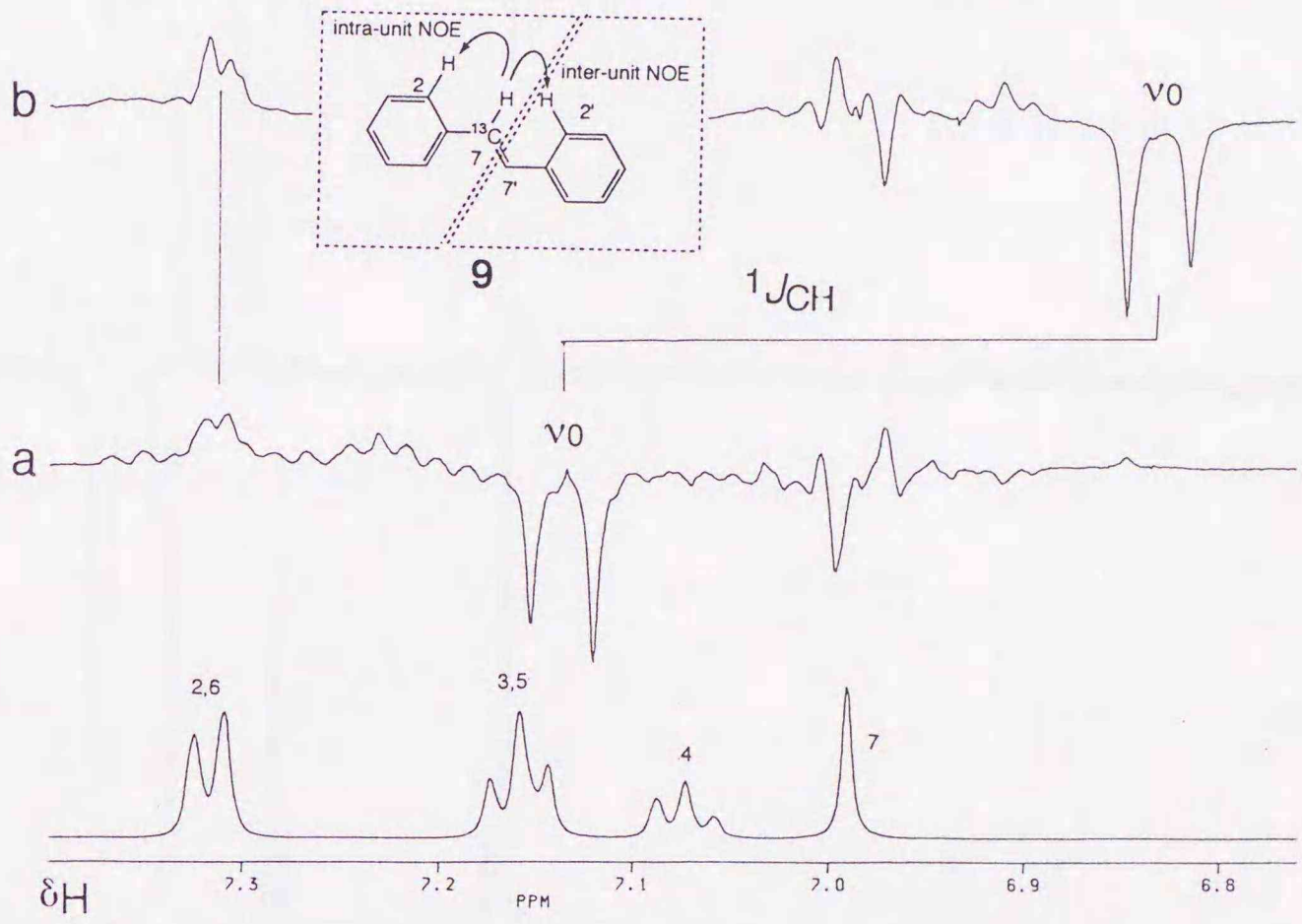


Chart 2.19. Parts of the PASS-NOESY spectra of **9** (35 mg in 0.5 ml of benzene-d_6). Pulse sequence used was Fig. 2.17a. The delays, RD, BD, Δ_1, Δ_2, and τ_m were 5.0 s, 1.24s, 3.2 ms, 1.66 ms ($^1J_{CH}$ = 156 Hz), and 2.5 s, respectively. ^{1}H pulse offset (ν_0) was set on higher (a) and lower (b) frequency signal of ^{13}C satellite of H-7. Each spectrum was accumulated using 3200 transients. The total measuring time was *ca.* 9 h each.

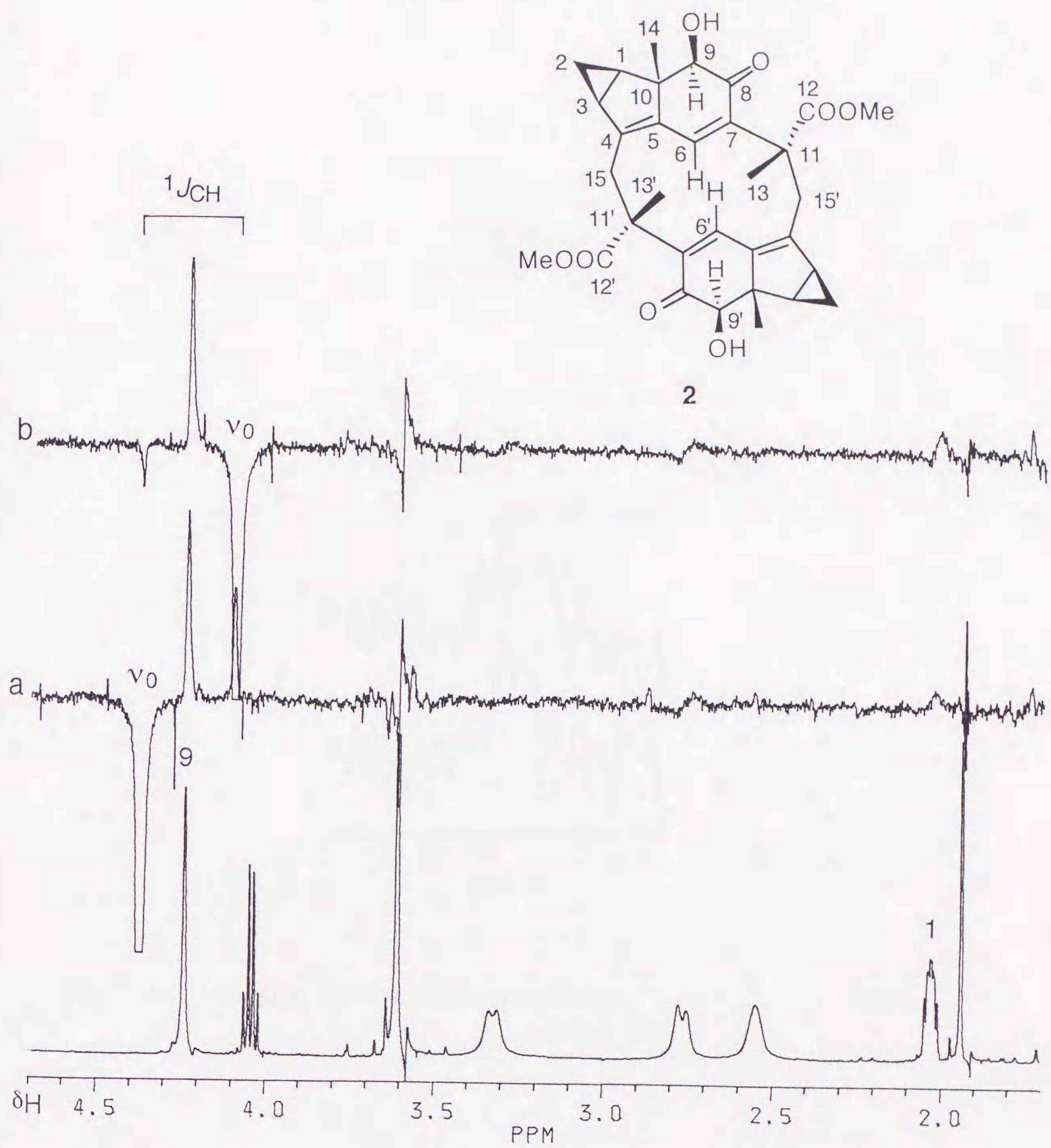


Chart 2.20. Parts of the PASS-NOESY spectra of **2** (40 mg in 0.5 ml of pyridine-d_5). Pulse sequence used was Fig. 2.17a. The delays, RD, BD, Δ_1, Δ_2, and τ_m were 1.2 s, 0.4 s, 3.62 ms, 1.81 ms ($^1J_{CH}$ = 138 Hz), and 0.4 s, respectively. ^{1}H pulse offset (ν_0) was set on higher (a) and lower (b) frequency signal of ^{13}C satellite of H-7. Each spectrum was accumulated using 20 992 transients. The total measuring time was *ca.* 22 h each.

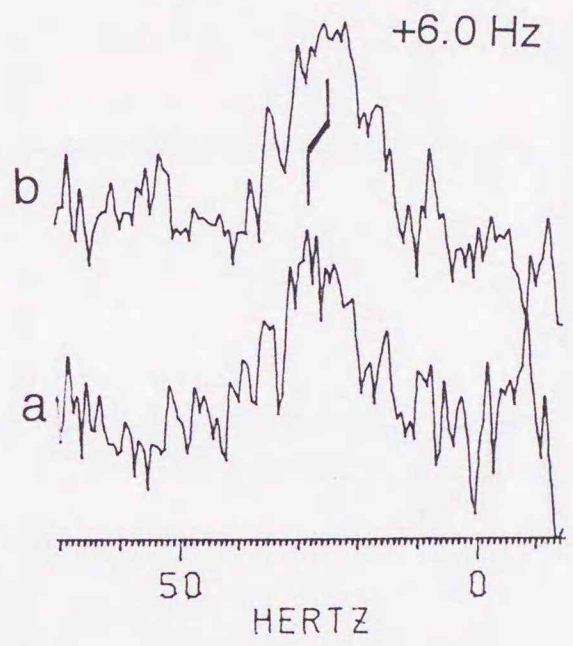


Chart 2.21. H-1 region for Chart 2.20a (a) and b (b).

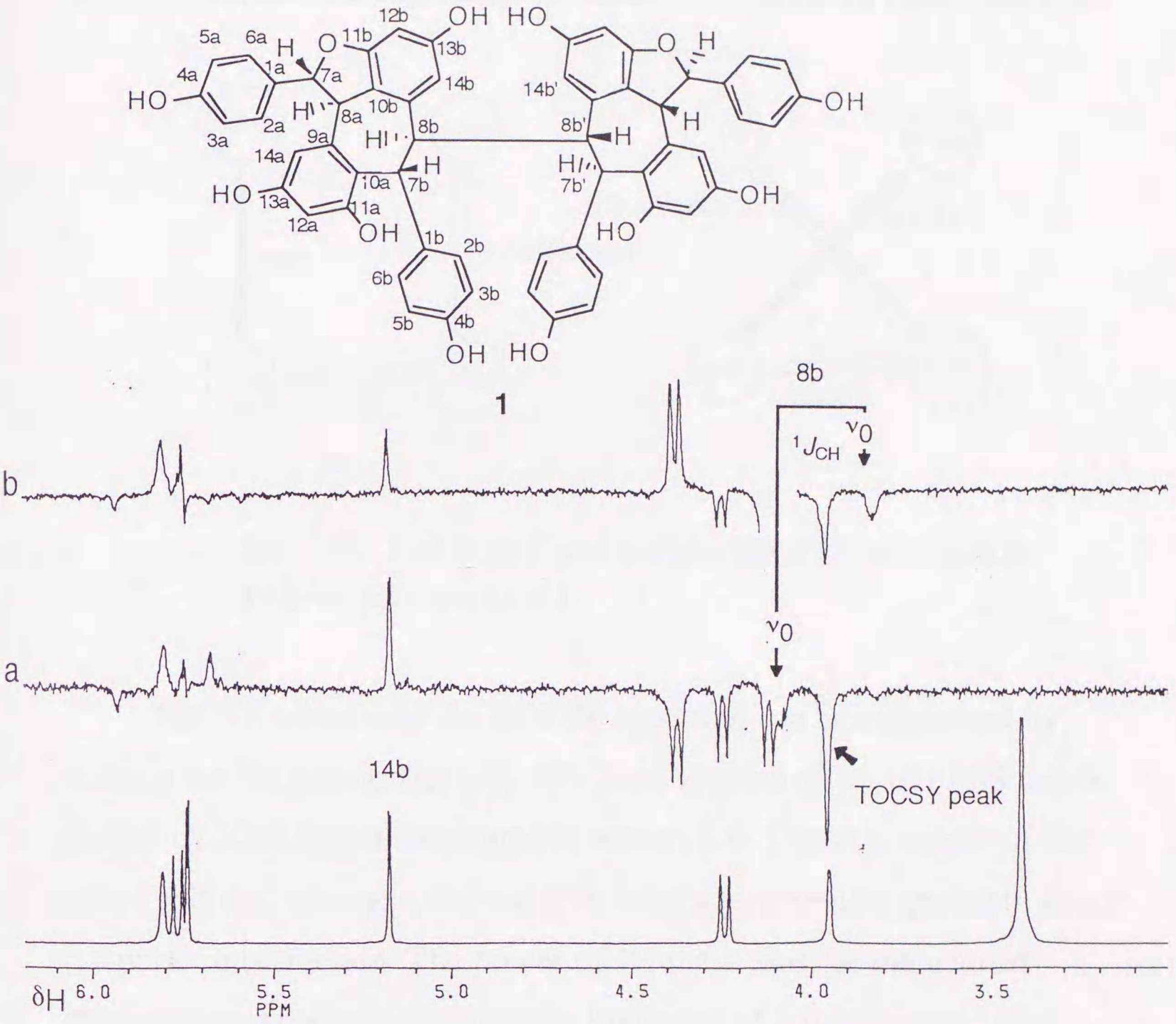


Chart 2.22. Parts of the PASS-ROESY spectra of **1** (50 mg in 0.5 ml of acetone-d_6). Pulse sequence used was Fig. 2.17b. ^{1}H pulses were derived from the high-power output of the decoupler channel attenuated by 18 dB (90° pulse duration was 100 μs). The delays, RD, BD, Δ_1, Δ_2, and τ_m were 0.8s, 0.4 s, 3.88 ms, 1.94 ms ($^1J_{CH}$ = 129 Hz), and 0.4 s, respectively. ^{1}H pulse offset (ν_0) was set on higher (a) and lower (b) frequency signal of ^{13}C satellite of H-7. Each spectrum was accumulated using 2400 transients. The total measuring time was *ca.* 2 h each.

ROESY false peak to H-14b in the similar manner. Both real (H-8b/H-14b') ROESY and false (H-8b→H-8b'→H-14b) TOCSY-ROESY peaks are also overlapped in this case. Thus the existence of TOCSY-ROESY transfer prevents the separate determination of intra- or inter-unit ROE.

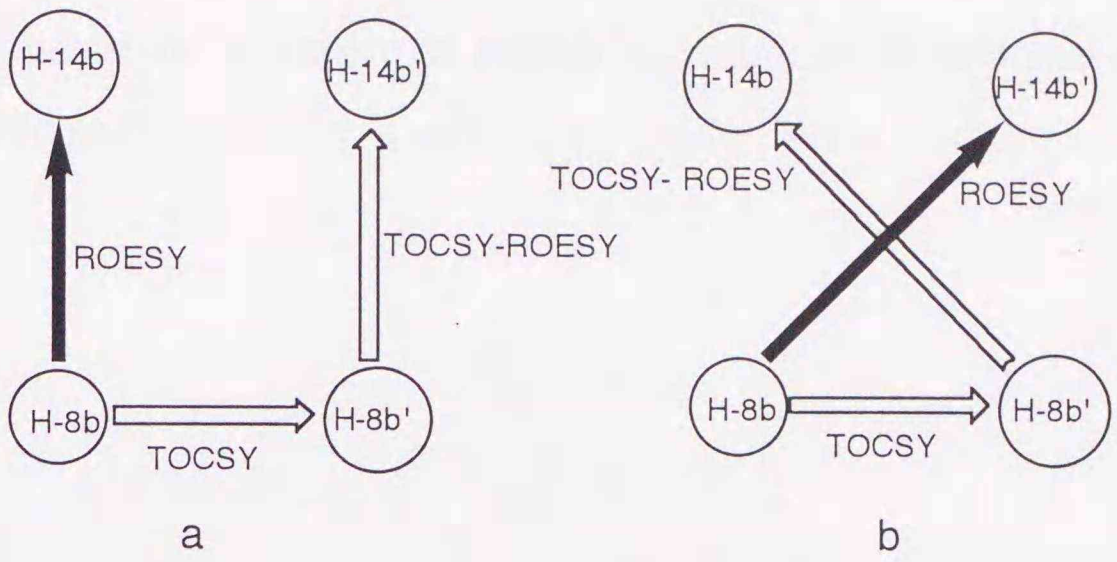


Fig. 2.18. Real ROESY peak and false TOCSY-ROESY peak in PASS-ROESY spectra of **1**.

TOCSY transfer in the ROESY spectrum can be suppressed by shifting the ^{1}H pulse offset (*31*, *48*). The ^{1}H pulse offset of PASS can be shifted by $\pm 2n^1J_{CH}$ as mentioned in section 2.6. The experiment of the offset shifting, however, did not give satisfactory results, probably due to the pulse imperfection. The power of ^{1}H-pulse must be maintained through the experiment because the limitation of hardware does not permit switching it. The power of ^{1}H-pulse used in this experiment (90° pulse duration was 100 μs) was optimized for CW spin-locking. It was, however, supposed to be incompetent for being used for excitation pulse. Although this pulse could excite the signals close to its offset, when this pulse was offset away from the exact satellite position, it might be too weak to excite the satellite signal completely. Thus, in order to use stronger excitation pulse (90° pulse duration is 40 μs), the spin-locking pulse must be changed to DANTE (*49* - *51*), a train of hard pulses with

small flip-angles separated by the short delay instead of CW spin locking by weaker pulse. The pulse sequence was shown in Fig.2.17c. The experiment of the offset shifting now gave satisfactory results. Chart 2.23 shows that the TOCSY peak disappeared by shifting the ^{1}H pulse offset to 1,533 Hz (12 x $^{1}J_{CH}$) down-field of each satellite signal. The resulting spectra indicate the existence of strong intra-unit ROE between H-14b and H-8b (Chart 2.24).

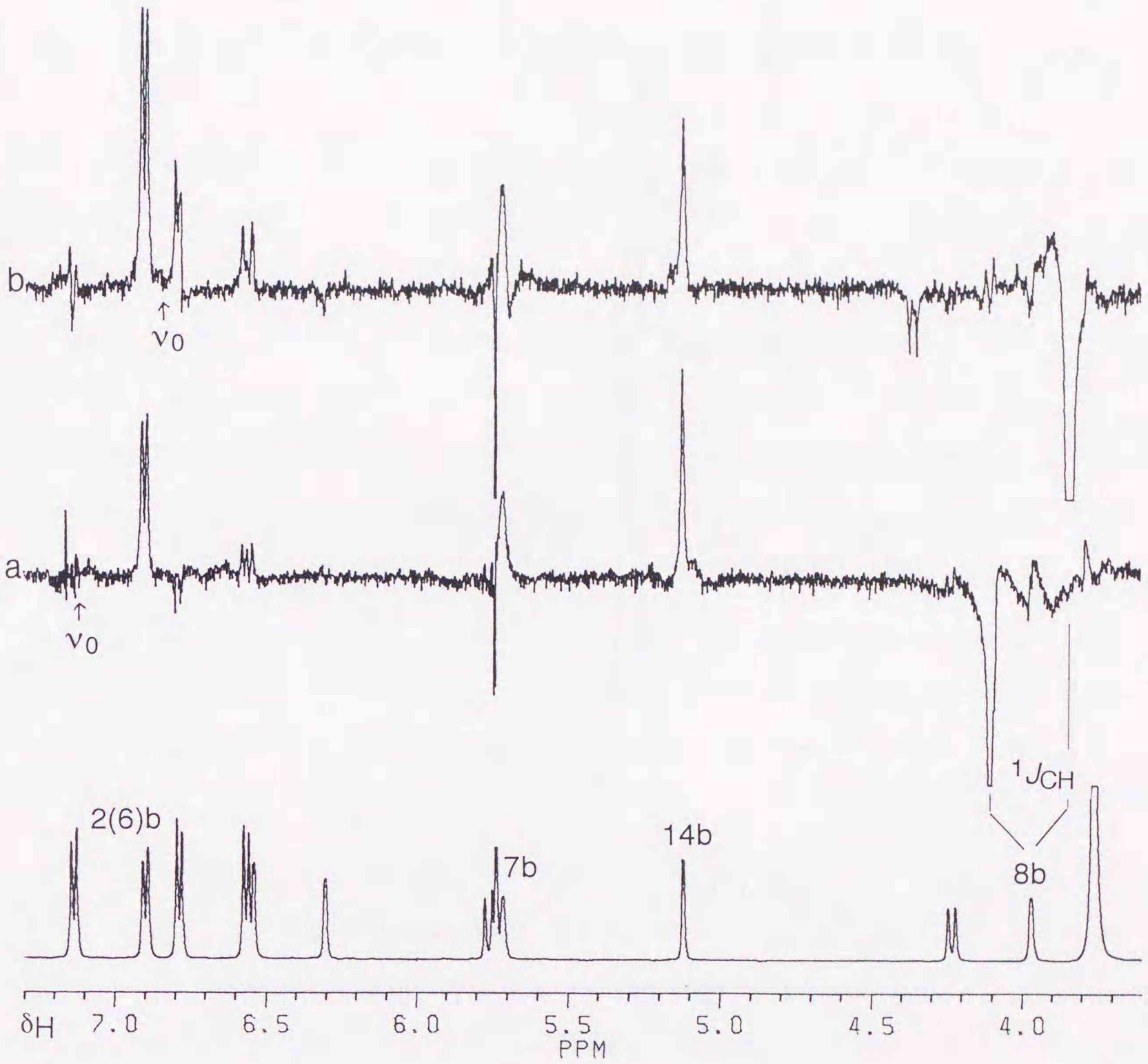


Chart 2.23. Parts of the PASS-ROESY spectra of **1** (50 mg in 0.5 ml of acetone-d_6). Pulse sequence used was Fig. 2.17c. ^{1}H pulses were derived from the high-power output of the decoupler channel attenuated by 12 dB (90° pulse duration was 42 μs), and the duration of selective ^{13}C rectangular pulses was 3.4 ms. The duration of trim pulse was set to 75.6 μs, and DANTE pulse train was composed of 6,000 pulses of flip angle 30° separated with the delays of 53 μs. The delays were the same as those of Chart 2.22. ^{1}H pulse offset (ν_0) was shifted to 1533 Hz (12 x ^1J(C-8b/H-8b)) downfield point of higher (a) and lower (b) frequency signal of ^{13}C satellite of H-7. Each spectrum was accumulated using 27136 transients. The total measuring time was *ca.* 23 h each.

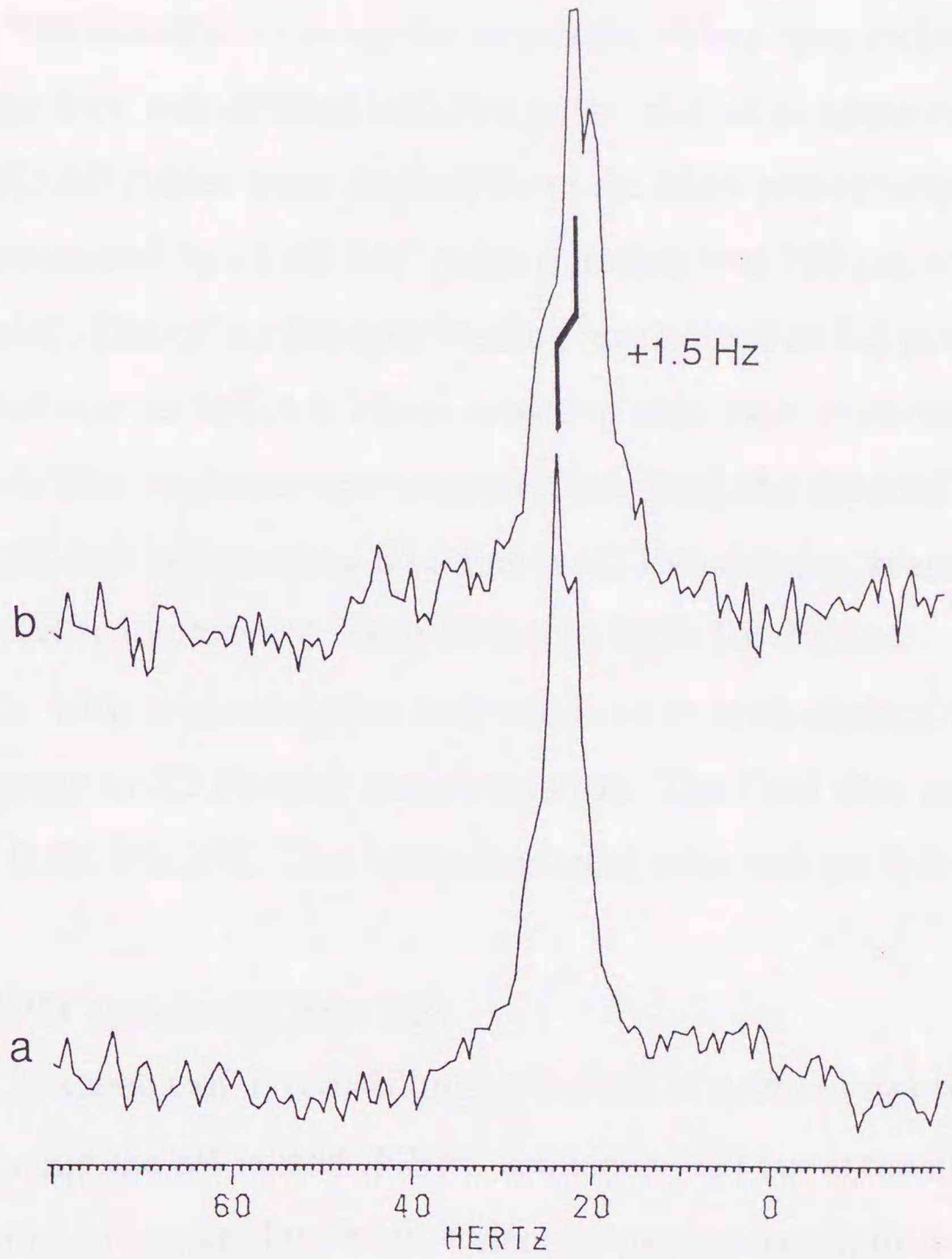


Chart 2.24. H-14b region for Chart 2.23a (a) and b (b).

2.9 Experimental

ROESY spectrum (Chart 2.2)

The phase sensitive ROESY spectrum of **1** (*ca.* 40 mg in 0.5 ml of acetone-d_6) was determined using the sequence: 90°-t_1-spin lock(CW)-t_2 (*31*). CW spin lock was divided into two parts, shifted in phase by +90° and -90° (*36*). All pulses were derived from the high-power output of the decoupler attenuated by 18 dB (90° pulse duration was 100 μs, a 2500 Hz spin-lock field). The offset for spin locking was placed at 3.2 ppm. The spin-lock time was set to 0.4 s. Phase-sensitive data were collected by the TPPI method. The spectrum was measured covering the spectral width of 4761 Hz in 1K data points using 64 scans (with two dummy scans) for each of the 128 t_1 increments. Zero-filling to 0.5K for F_1 and multiplication with squared cosine-bell windows in both dimensions were performed prior to 2D Fourier transformation. The final data matrix consisted of 0.5K x 0.25K. The total measuring time was *ca.* 6 h.

INEPT-LSPD spectra (Chart 2.3)

The LSPD (*5*) spectra of **1** (*ca.* 40 mg in 0.5 ml of acetone-d_6) were determined using the refocused INEPT sequence (*32*) for intensity enhancement of protonated carbons. Selective proton irradiation was carried out using a low-power output of the decoupler channel (0.2 W) attenuated by 60 dB. Both defocusing and refocusing delays were 1.7 ms ($^1J_{CH}$ = 147 Hz). The spectra were recorded with 15000 transients in 32K data points with a sweep width of 15,625 Hz. Resolution enhancement was achieved by zero-filling to 64K and multiplication with a squared sine-bell window shifted by π/32 prior to Fourier transformation. The total measuring time of each experiment was *ca.* 17 h.

COLOC spectra (Chart 2.4)

The COLOC spectra without F_1 decoupling of **1** (*ca.* 40 mg in 0.5 ml of acetone-d_6) were determined using the pulse sequence shown in Fig.2.2b (*33*). The F_2 and F_1 spectral widths were 20833 and 4500(4000) Hz, respectively; 192 scans (with two dummy scans) were accumulated into 2K data points for each of the 116(128) t_1 increments. The defocusing delay Δ_1 was set to 55 and 90 ms, and the refocusing delay Δ_2 to 27.5(45) ms ($^{LR}J_{CH}$ = 9.1 and 5.5 Hz), respectively. Zero-filling to 256 data points for F_1 and multiplication with sine-bell windows (shifted by $\pi/2$ for F_2, not shifted for F_1) were performed prior to 2D Fourier transformation. Absolute-mode calculation gave a data matrix of 1K x 0.25K. The total measuring time of each experiment was *ca.* 14 (15) h.

HMBC spectrum (Chart 2.5)

The HMBC spectrum of **1** (*ca.* 40 mg in 0.5 ml of acetone-d_6) was obtained using the pulse sequence proposed by Bax and Summers (*7*) involving a low-pass *J* filter to suppress correlation due to one-bond couplings. The F_2 spectral width was 4098 Hz, whereas F_1 covered 21008 Hz; 48 scans (with four dummy scans) were accumulated into 2K data points for each of the 472 t_1 increments. The defocusing delay was set to 55 ms ($^{LR}J_{CH}$ = 9.1 Hz). Zero-filling to 1K data points in F_1 and multiplication with squared sine-bell windows shifted by $\pi/4$ in both dimensions were performed prior to 2D Fourier transformation. The resulting absorption mode spectrum consisted of 1K x 1K data matrix. The total measuring time was *ca.* 15 h.

^{13}C-coupled HMQC-NOESY spectra (Charts 2.6 and 2.7a)

The ^{13}C-coupled HMQC-NOESY spectra were determined by the sequence shown in Fig.2.3 (*9*) without ^{13}C-decoupling during acquisition.

The delays, RD, BD, Δ_1, and τ_m were set to 2.0 s, 0.4 s, 3.6 ms ($^1J_{CH}$ = 140 Hz), and 0.4 s, respectively. Chart 2.6 was obtained using a solution containing 21 mg of **2** in pyridine-d_5. The spectrum was measured covering the spectral width of 4116 Hz in 2K data points using 192 transients (with two dummy scans) for each of 128 t_1 increments. Chart 2.7a was obtained using a solution containing 50 mg of **1** in 0.5 ml of acetone-d_6. The spectrum was measured covering the spectral width of 3000 Hz in 2K data points using 224 transients (with two dummy scans) for each of 116 t_1 increments. For each spectrum, zero-filling to 0.5K for F_1 and multiplication with squared cosine-bell windows in both dimensions were performed prior to 2D Fourier transformation. The total measuring time was *ca.* 21 h each.

^{13}C-coupled HMQC-ROESY spectrum (Chart 2.7b)

The ^{13}C-coupled HMQC-ROESY spectrum of **1** (50 mg in 0.5 ml of acetone-d_6) was determined by the sequence shown in Fig.2.6. ^{1}H pulses were derived from the high-power output of the decoupler channel attenuated by 18 dB (90° pulse duration was 100 μs, a 2500 Hz spin-lock field). The carrier frequency was positioned at 6.7 ppm. The spectrum was measured covering the spectral width of 5000 Hz in 2K data points. The other measuring conditions were the same as those of Chart 2.7a.

^{13}C-coupled HMQC(-DQF)-COSY spectra (Charts 2.9 and 2.10)

The two-dimensional ^{13}C-coupled HMQC-COSY and HMQC-DQF-COSY spectra were obtained using the pulse sequences shown in Fig. 2.8a (Chart 2.9a) and 2.8b (Charts 2.9b, 2.10), respectively.

Charts 2.9a and b were obtained using a solution containing 20 mg of **5** in acetone-d_6. The delays, RD, BD, and Δ_1 were set to 3.0 s, 2.3 s, and 3.6 ms ($^1J_{CH}$ = 140 Hz), respectively. Each spectrum was measured

with a spectral width of 1000 Hz in 1K data points using 16 transients (with 2 dummy scans) for each of the 50 t_1 increments. Zero-filling in F_1 dimension and multiplication with squared cosine-bell function in both F_1 and F_2 dimensions were performed prior to 2D Fourier transformation. The resulting data matrix was 0.5 K x 64 data points. The total measuring time was *ca.* 1.5 h.

Chart 2.10 was obtained using a solution containing 30 mg of **6** in chloroform-*d* The delays, RD, BD, and Δ_1 were set to 5.3 s, 3.22 s, and 3.6 ms ($^1J_{CH}$ = 140 Hz), respectively. The spectrum was measured with a spectral width of 3496 Hz in 2K data points using 160 transients (with 2 dummy scans) for each of the 32 t_1 increments. Zero-filling in F_1 dimension and multiplication with squared cosine-bell function in both F_1 and F_2 dimensions were performed prior to 2D Fourier transformation. The resulting data matrix was 1 K x 64 data points. The total measuring time was *ca.* 13 h.

2D ω_1 hetero half-filtered DQF-COSY spectra (Charts 2.11 and 2.12)

The two-dimensional ω_1 hetero half-filtered DQF-COSY spectra were obtained using the pulse sequence shown in Fig. 2.11.

Chart 2.11 was obtained using a solution containing 20 mg of **5** in acetone-d_6. The delays, RD, BD, and Δ_1 were set to 2.0 s, 2.3 s, and 3.6 ms ($^1J_{CH}$ = 140 Hz), respectively. The spectrum was measured with a spectral width of 1200 Hz digitized with 2K data points acquiring eight transients with two dummy scans for each of the 64 t_1 increments. Zero-filling in F_1 dimension and multiplication with squared cosine-bell function in both F_1 and F_2 dimensions were performed prior to 2D Fourier transformation. The resulting data matrix was 1K x 128 data points. The total measuring time was *ca.* 1 h.

Chart 2.12a was obtained using a solution containing *ca.* 50 mg of **1** in 0.5 ml of acetone-d_6. The delays, RD, BD, and Δ_1 were set to 2.0 s, 0.4 s, and 3.6 ms ($^1J_{CH}$ = 140 Hz), respectively. The spectrum was measured with a spectral width of 2000 Hz digitized with 2K data points acquiring 512 transients with four dummy scans for each of the 112 t_1 increments. Zero-filling in F_1 dimension and multiplication with squared cosine-bell function in both F_1 and F_2 dimensions were performed prior to 2D Fourier transformation. The resulting data matrix was 1K x 128 data points. The total measuring time was *ca.* 48 h.

The resolution-enhanced slices of the 2D spectrum (Chart 2.12b and c) were obtained by the sequence of inverse Fourier transformation, zero-filling to 128K, and re-transformation.

2D ω_1 hetero half-filtered TOCSY spectrum (Chart 2.13a)

The two-dimensional ω_1 hetero half-filtered TOCSY spectrum of **7** (30 mg in 0.5 ml DMSO-d_6) was obtained using the pulse sequence shown in Fig.2.9 (*14*). ^{1}H pulses were derived from the high-power output of the decoupler channel attenuated by 11 dB (90° pulse duration was 39 μs). The duration of trim pulses was set to 2.5 ms and the spin-lock time was 43 ms. The delays, RD, BD, and Δ_1 were set to 2.0 s, 1.17 s, and 3.6 ms ($^1J_{CH}$ = 140 Hz), respectively. The spectrum was measured with a spectral width of 2500 Hz digitized with 1K data points acquiring 32 transients with two dummy scans for each of the 128 t_1 increments. Zero-filling in F_1 dimension and multiplication with squared cosine-bell function in both F_1 and F_2 dimensions were performed prior to 2D Fourier transformation. The resulting data matrix is 0.5K x 0.125K. The total measuring time was *ca.* 4.5 h.

The resolution-enhanced slices of the 2D spectrum (Charts 2.13b and c) were obtained by the sequence of inverse Fourier transformation, zero-filling to 8K, and re-transformation.

PASS-TOCSY spectra (Charts 2.13d and e, 2.14 - 2.18) **and 1D HMQC-TOCSY spectrum** (Chart 2.13f)

The PASS-TOCSY spectra and 1D HMQC-TOCSY spectrum were obtained with the pulse sequences shown in Fig.2.15a (Charts 2.13d - f, 2.14, and 2.17a), 2.15b (Charts 2.17b and 2.18), and 2.15c(Charts 2.15 and 2.16). ^{1}H pulses were derived from the high-power output of the decoupler channel attenuated by 11 dB (90° pulse duration was 39 μs). The duration of trim pulses was set to 2.5 ms.

Charts 2.13 d and e, and 2.16 were obtained using a solution containing 30 mg of **7** in 0.5 ml DMSO-d_6. ^{1}H pulse offset was shifted to $+^{2}J$ (C-1/H-1), 276 Hz, upfield points of higher (Charts 2.13d and 2.14a) or lower (Charts 2.13e and 2.14b) frequency signal of ^{13}C satellite of H-1. The delays, RD, BD, Δ_1, Δ_2, and τ_m were 2.0 s, 1.7 s, 3.6 ms, 1.8 ms ($^{1}J_{CH}$ = 140 Hz), and 43 ms, respectively. Each spectrum was measured with the spectral width of 3496 Hz in 16K data points using 128 transients. The total measuring time was 9 min each. In the 1D HMQC-TOCSY (*4*) spectrum (Chart 2.13f), both the delays Δ_1 and Δ_2 were 3.6 ms ($^{1}J_{CH}$ = 140 Hz). The other experimental conditions were the same as those of Chart 2.13d.

Charts 2.15 and 2.16 were obtained using a solution containing 30 mg of **8** in 0.5 ml DMSO-d_6. A few drops of D_2O was added to suppress the OH signal. ^{1}H pulse offset was set onto higher (Charts 2.15a and c, and 2.16a and c) or lower (Charts 2.15b and d, and 2.16b and d) frequency signal of ^{13}C satellite of H-2. τ_m were 31 ms (Charts 2.15, and 2.16a and b) and 88 ms (Charts 2.15, and 2.16c and d). The delays, RD,

BD, Δ_1, and Δ_2 were 4.0 s, 0.86 s, 3.94 ms, and 1.97 ms ($^1J_{CH}$ = 127 Hz), respectively. Each spectrum was measured with the spectral width of 4000 Hz in 16K data points using 512 transients. The total measuring time was *ca.* 1 h each.

Charts 2.17 and 2.18 were obtained using a solution containing *ca.* 50 mg of **1** in 0.5 ml of acetone-d_6. The duration of selective ^{13}C rectangular pulses were 2.1 ms for Chart 2.17 and 3.4 ms for Chart 2.18. ^1H pulse offset was set onto higher (Charts 2.17a and b, and 2.18a and c) or lower (Charts 2.18b and d) frequency signal of ^{13}C satellite of H-8b. The delays, RD, BD, Δ_1, and Δ_2 were 0.1s, 0.4 s, 3.88 ms, and 1.94 ms ($^1J_{CH}$ = 129 Hz), respectively. Each spectrum was measured with the spectral width of 8000 Hz in 16K data points using 4480 transients. τ_m were 71, 111, 18, and 111 ms for Charts 2.17a and b, 2.18a and b, and 2.18c and d, respectively. The total measuring time was *ca.* 1 h each.

PASS-NOESY spectra (Charts 2.19 - 2.21)

The PASS-NOESY spectra were obtained with the pulse sequence shown in Fig.2.17a. ^1H pulse was derived from the high-power output of the decoupler channel attenuated by 12 dB (90° pulse duration was 42 μs).

Chart 2.19 was obtained using a solution containing 35 mg of **9** in 0.5 ml of benzene-d_6. ^1H pulse offset was set onto higher (Chart 2.19a) or lower (Chart 2.19b) frequency signal of ^{13}C satellite of H-7. The delays, RD, BD, Δ_1, Δ_2, and τ_m were 5.0 s, 1.24s, 3.2 ms, 1.66 ms ($^1J_{CH}$ = 156 Hz), and 2.5 s, respectively. Each spectrum was measured with the spectral width of 1000 Hz in 4K data points using 3200 transients. The measuring time was 9 h each.

Charts 2.20 and 2.21 were obtained using a solution containing 40 mg of **2** in 0.5 ml of pyridine-d_5. ^1H pulse offset was set onto higher (Charts 2.20a and 2.21a) or lower (Charts 2.20b and 2.21b) frequency

signal of ^{13}C satellite of H-9. The delays, RD, BD, Δ_1, Δ_2, and τ_m were 1.2 s, 0.4 s, 3.62 ms, 1.81 ms ($^1J_{CH}$ = 138 Hz), and 0.4 s, respectively. Each spectrum was measured with the spectral width of 6024 Hz in 16K data points using 20992 transients. The measuring time was *ca.* 22 h each.

PASS-ROESY spectra (Charts 2.22 - 2.24)

The PASS-ROESY spectra of **1** (50 mg in 0.5 ml of acetone-d_6) were obtained with the pulse sequences shown in Fig.2.17b (Chart 2.22) and 2.17c (Chart 2.23). The delays, RD, BD, Δ_1, Δ_2, and τ_m were 0.8s, 0.4 s, 3.88 ms, 1.94 ms ($^1J_{CH}$ = 129 Hz), and 0.4 s, respectively.

For Chart 2.22, ^1H pulse was derived from the high-power output of the decoupler channel attenuated by 18 dB (90° pulse duration was 100 μs). ^1H pulse offset was set onto higher (Chart 2.22a) or lower (Chart 2.22b) frequency signal of ^{13}C satellite of H-8b. Each spectrum was measured with the spectral width of 6024 Hz in 16K data points using 2400 transients. The measuring time was *ca.* 2 h each.

For Charts 2.23 and 2.24, ^1H pulse was derived from the high-power output of the decoupler channel attenuated by 12 dB (90° pulse duration was 42 μs), and the duration of selective ^{13}C rectangular 90° pulses was 3.4 ms. The duration of trim pulse was set to 75.6 μs, and DANTE pulse train was composed of 6000 pulses of flip angle 30° separated with the delays of 53 μs. ^1H pulse offset was set to 12 x ^1J(C-8b/H-8b), 1533 Hz, downfield point of higher (Charts 2.23a and 2.24a) or lower (Charts 2.23b and 2.24b) frequency signal of ^{13}C satellite of H-8b. Each spectrum was measured with the spectral width of 6024 Hz in 16K data points using 27136 transients. The measuring time was *ca.* 23 h each.

3 NMR analysis of consecutive quaternary carbon systems

3.1 Introduction

Determination of molecular structures by heteronuclear long-range C-H correlation spectroscopies, such as COLOC and HMBC, has a substantial problem in which a carbon carrying no proton within three bonds cannot be assigned since these methods only give correlations between proton and carbon via three and less than three bonds. Hence, the structure elucidation of highly hydrogen-deficient molecules might be a problem since the carbon network could not be completely followed by information from indirect $^{2,3}J_{CH}$. For the structure elucidation of such compounds, direct detection of ^{13}C-^{13}C connectivity is a necessity. In the H-^{13}C-^{13}C relay methods, the C-C relay portion can be tuned for long-range C-C couplings to detect the H-C correlations via four bonds (^{1}H-^{13}C-X-X-^{13}C).

However, there is an inherent serious problem in detecting ^{13}C-^{13}C coupling which is a hopelessly low sensitivity due to quite a low population (0.01%) of the detectable isotopomers . Therefore, the application of sensitivity enhancement techniques should be necessary for the C-C detecting methods to be practically used in natural products analysis. One of the most popular methods for detecting direct C-C connectivities is INADEQUATE (*16*, *17*) proposed some ten years ago. There have been several approaches to enhance its sensitivity including INEPT-INADEQUATE (*52* - *55*), DEPT-INADEQUATE (*56*, *57*), C-relayed H-C INEPT (*53*, *55*), and proton monitoring INADEQUATE (*58*). Although notable sensitivity enhancements were attained by these polarization-transfer methods, another notable defect, a phase-distortion problem depending on resonance-offset effects still remained. These

resonance-offset effects would be a serious problem in examining compounds containing a wide range of carbons by high-field NMR instruments.

Sensitivity loss and phase inversion in ^{13}C-^{13}C satellite spectra due to the resonance-offset effects have long been noticed (*17*, *59*, *60*) and the application of composite pulses to compensate this phenomenon has been reported (*18*, *61* - *64*). Recently, Torres *et al.* found that the utilization of symmetric phase-alternating composite pulses (*43*) to the INADEQUATE sequence was efficient for compensation of the resonance-offset effects (*65*). I propose here a new detection methods for ^{13}C-^{13}C couplings, DEPT C-C relay (*19*), which enables sensitivity enhancement by DEPT polarization transfer and observation of ^{13}C-^{13}C satellites, without any resonance-offset variation of phase distortion through the wide range of ^{13}C resonance, by inclusion of symmetric phase-alternating composite ^{13}C pulses. By this phase-distortionless sequence, it has become possible to apply DEPT spectrum editing to the relayed spectra in order to discriminate CH_3-, CH_2-, CH-C connectivities. Furthermore, accurate J_{CC} values can be determined since constant phase results are available even in high-field instruments. Although there have been several variations of INADEQUATE combined with spectrum editing techniques such as INADEQUATE-SEFT (*66*, *67*) and SEMINA (*68*, *69*), this simple DEPT spectrum editing is a sensitive and easily accessible method for discriminating carbon status according to multiplicities of neighboring carbons.

In addition, I present a 2D version of the sequence, 2D DEPT C-C relay (*20*), which enables well-resolved detection of C-C correlations. In the 2D sequence, the introduction of a second dimension would reduce signal overlapping, and hence, it becomes possible to detect C-C correlation peaks without the interference of unwanted residual signals.

Spectral editing, as used in the corresponding 1D method, is no longer necessary for removing central residual signals since an optional baseline correction sufficiently suppress undesirable F_1 ridges to give a clean 2D map.

Finally, the detection of long-range J_{CC} couplings has been enabled by introducing BIRD pulse to the DEPT C-C relay methods for suppression of unwanted signals. This method gives correlations between proton and carbon via three and four bonds. The latter (^{1}H-^{13}C-X-X-^{13}C) is one-bond further than the detectable ones in conventional long-range C-H correlation methods such as COLOC or HMBC.

3.2 1D DEPT C-C relay

In 1985, it was reported that the detection of CH_n-C_q bonds at quaternary carbon (C_q) sites had been achieved by the sensitivity-enhanced C-relayed INEPT sequence (*53*). It seems that spectrum editing according to multiplicities of adjacent carbons enables one to distinguish CH_3-C_q, CH_2-C_q and CH-C_q bonds by choosing a proper refocusing delay for the INEPT part of the sequence or a proper flip angle of the variable ^{1}H pulse for a corresponding DEPT version. However, severe phase-distortion problem depending on resonance-offset effects because of the wide range of ^{13}C resonances makes it impossible to utilize phase information of the ^{13}C-^{13}C satellite signals for spectrum editing.

The basic DEPT C-C relay sequence is depicted in Fig. 3.1a. To suppress a residual ^{13}C magnetization, a sequence of ^{13}C 90° presaturation pulses is applied before DEPT part (*56*). A sequence of sixteen 90° pulses separated by 0.1 s intervals suppressed artifact sufficiently.

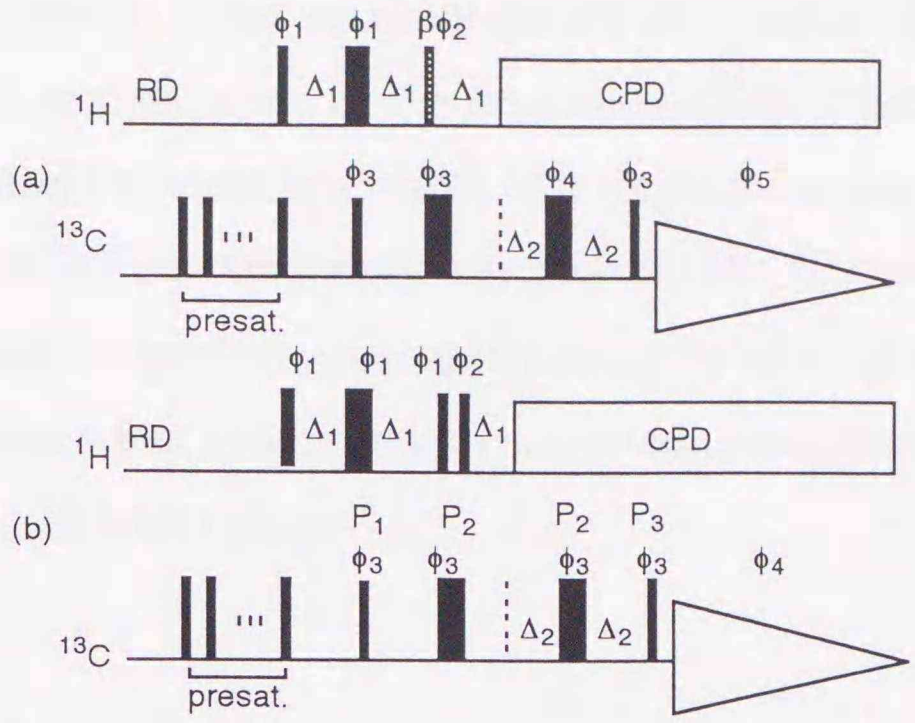


Fig.3.1. Pulse sequences for the basic DEPT C-C relay (a) and composite pulse DEPT C-C relay (b). Hatched bar is a variable pulse with a flip angle of β. P1 - P3 in (b) are composite pulses consisted of (58° -140° 172°), (58° -140° 344° -140° 58°) and (24° -152° 346° -152° 24°), respectively (*43*). The delays, Δ_1 and Δ_2 are $1/2J_{CH}$ and $1/4J_{CC}$-$1/2J_{CH}$, respectively. ^{13}C presaturation pulses are composed of sixteen 90° pulses separated by 0.1 s intervals (*56*). Phase cycling used is as follows: (a) ϕ_1= x; ϕ_2= y,-y; ϕ_3= x,x,y,y,-x,-x, -y,-y; ϕ_4= y,y,-x,-x, -y,-y,x,x; ϕ_5= x, -x,y, -y,-x,x,-y,y; (b) ϕ_1= β, 360°-β; ϕ_2= -x, ϕ_3= x,x,y,y, -x,-x, -y,-y; ϕ_4= x,-x,y,-y,-x,x,-y,y.

The satellite signals of the carbonyl carbon of acetic acid were selected to estimate the resonance-offset effects of RF pulses in this basic sequence. As the transmitter offset frequency was shifted, the phase of the satellites was inverted (Fig. 3.2). Difference in frequency between the methyl and carbonyl carbons of acetic acid is about 19,000 Hz (at 125MHz). ^{13}C pulse width (90°) is 5 μs and the calculated field strength, $\gamma B_1/2\pi$, is 50 kHz for ^{13}C. Under these conditions, tolerable sensitivity was gained only when the transmitter frequency offset was positioned between δ 190 - 110 and 50 - 10 ppm. It should be noted that the phase of the satellite signals of the carbonyl carbon is inverted when the offset

frequency is placed at either maximal sensitivity position. This phenomenon is accounted for by the resonance-offset effects of the transmitter pulse. Efficient bandwidth of a single pulse was estimated as $\Delta\omega/\omega_1 = \pm 0.08$ (*43*), in the present case, ±4000 Hz. Consequently, it is almost impossible to perform spectrum editing by using phase information even when spectral width is limited to the extent of 100 ppm (12,500 Hz at 125 MHz) range.

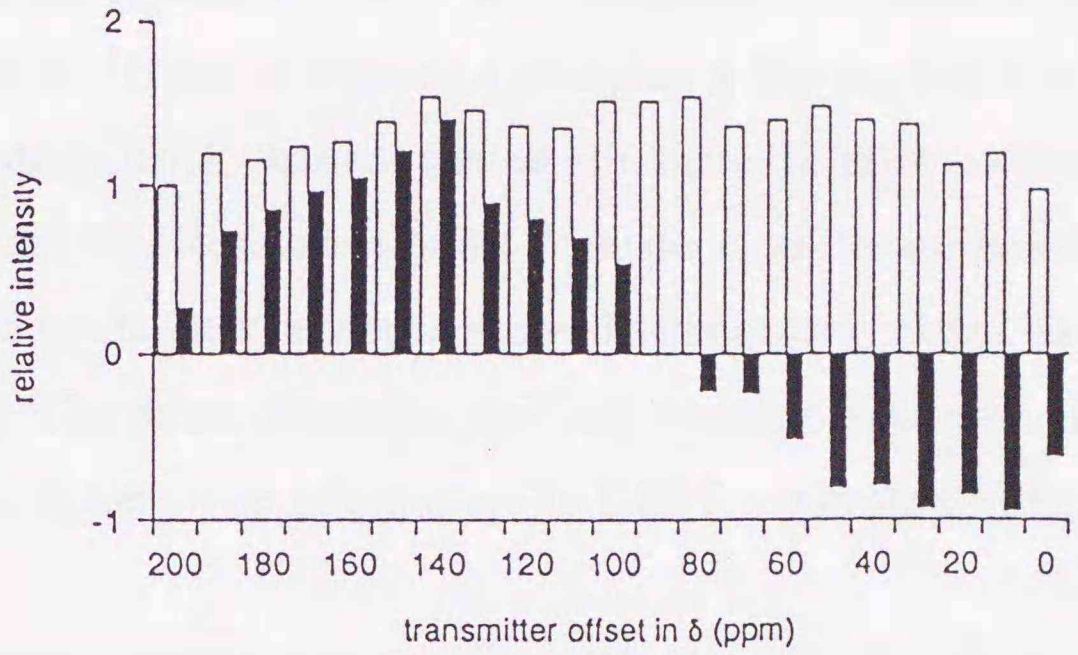


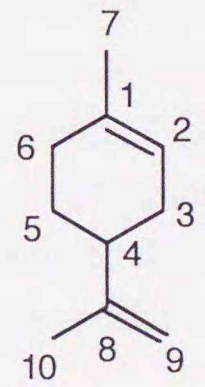
Fig.3.2. Intensity of ^{13}C-^{13}C satellite signals of a carbonyl carbon of acetic acid. Filled and open bars are the results obtained by the pulse sequences, Fig. 3.1a and 3.1b, respectively. Flip or phase angle, β, is 45°, and delays, RD, Δ_1 and Δ_2, were 3.4 s, 3.8 ms, and 0.6 ms, respectively. Horizontal scale is position of the transmitter offset in δ (ppm) and vertical scale is relative intensity of the anti-phase satellite signals given by subtracting the intensity of the low field satellite from that of the high field satellite. The values are calculated in the absolute intensity mode and displayed as relative intensity when the intensity at the lowest transmitter offset by the sequence Fig. 3.1b is 1. 4 transients were accumulated for each spectrum. The total measuring time was 2 min each.

All the carbon pulses were replaced by symmetric phase-alternating composite pulses (*43*), as shown in Fig. 3.1b (*19*). In this sequence, two 180° pulses and the last 90° pulse were replaced by symmetric (58° -140° 344° -140° 58°) and (24° -152° 346° -152° 24°) pulses, respectively, whereas a so-called point-to-point pulse composed of (58° -140° 172°) was used as the first 90° pulse. In these composite pulses, constant-phase bandwidth reaches $\Delta\omega/\omega_1 = \pm 0.35$, ±17,500 Hz in this case, which covers a range of around 280 ppm (at 125 MHz) of the carbon resonance. Furthermore, a phase-shifting DEPT sequence (*61*) which includes phase-shifting of all ^1H pulses instead of changing a flip angle of the variable ^1H pulse in basic DEPT, was adopted to eliminate the effect of the variable pulse width (*70*). Resonance-offset dependency of the carbonyl signal of acetic acid by the new sequence showed satisfactory results, as expected (Fig. 3.2). The phase distortion problem was thus overcome and the utilization of the phase information in DEPT spectrum editing was made possible.

Spectrum editing for selecting CH_3-C_q, CH_2-C_q, and CH-C_q connectivities was achieved by the same concept as basic DEPT, namely, using 45° [CH_3-C_q(+), CH_2-C_q(+), CH-C_q(+)], 90°[CH-C_q(+)] and 135°[CH_3-C_q(+), CH-C_q(+), CH_2-C_q(-)] phase-shifting experiments. The signal intensity modulated by the phase-shifting angle, β (corresponding to the flip angle of the variable proton pulse in basic DEPT) is sinβ for CH-C_q, sin2β for CH_2-C_q and 3/4(sinβ+sin3β) for CH_3-C_q. The CH-C_q subspectrum was obtained by the 90° phase-shifting experiment {90°}, whereas the CH_2-C_q subspectrum was constructed by subtracting the 135° phase-shifting data {135°} from the 45° phase-shifting data {45°}. Finally, the CH_3-C_q subspectrum was calculated by the combination of the three experimental results as {45°}+{135°}-{90°} x 0.707 (*71*).

In order to test the efficiency of the spectrum editing, a mixture of acetic, propionic and isobutyric acids was analyzed. The carbonyl carbon regions of the three subspectra of the acid mixture are shown in Chart 3.1. Each subspectrum contains one pair of the carbonyl satellites, that is, isobutyryl, propionyl and acetyl carbonyls are excited only in the CH-C_q, CH_2-C_q and CH_3-C_q subspectra, respectively. The results clearly show the feasibility of this method. It should be noted that the phase of the satellite signals in the three subspectra is the same and the sensitivity of the signals is reasonable, regardless of the transmitter offset. Qualitative distinction of CH_3-C_q, CH_2-C_q and CH-C_q signals was thus achieved, although quantitative evaluation is not very clear since additional coherence transfer pathways through ^{13}C-^{13}C couplings are included in the DEPT C-C relay sequence.

Application of the method to more complex natural products was next carried out. Three subspectra obtained by the DEPT C-C relay sequence in Fig. 3.1b of a monoterpene hydrocarbon, limonene (**10**) are shown in Chart 3.2. The molecule has two quaternary carbons, C-1 and C-8, and both carbons are attached to CH_3, CH_2 and CH carbons. The three subspectra clearly showed the distinction of CH_3-C_q, CH_2-C_q and CH-C_q bonds. Hence, the coupling constants of the connectivities were separately determined as shown in Table 3.1.



limonene (**10**)

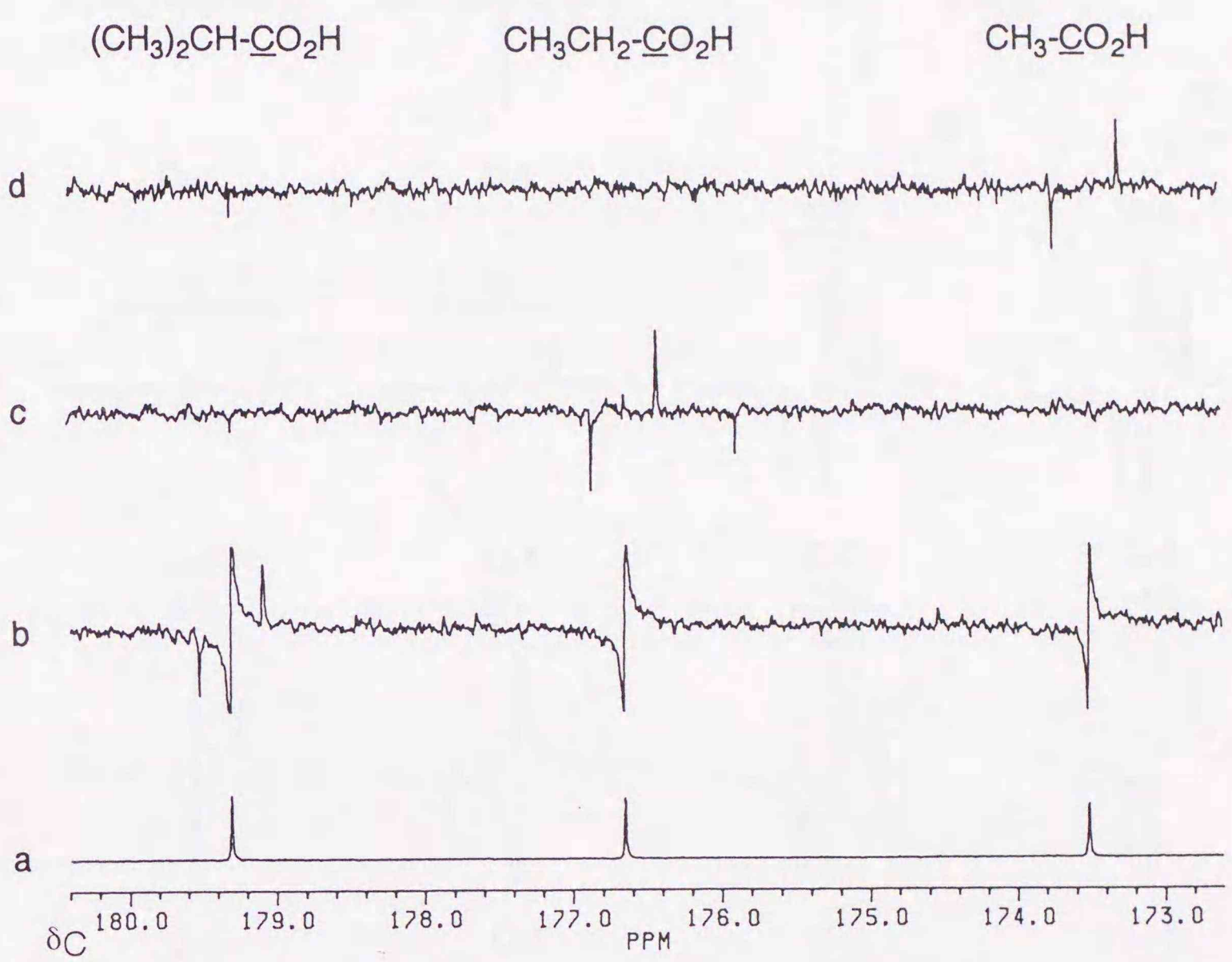


Chart 3.1. Carbonyl region of the edited satellite spectra of the mixture of acetic, propionic and isobutyric acids (1 mmol each in DMSO-d_6. The sample volume was adjusted to *ca.* 0.5 ml) measured by the sequence shown in Fig. 3.1b. Delays, RD, Δ_1, and Δ_2 were 3.4 s, 3.8 ms, and 0.6 ms (J_{CH} = 132, J_{CC} = 57 Hz), respectively. (a): conventional ^{13}C spectrum, (b): CH subspectrum, (c): CH_2 subspectrum and (d): CH_3 subspectrum. Each spectrum was accumulated using 128 transients. The total measuring time was *ca.* 12 min each except (a). The peak intensities are shown in the absolute intensity mode except (a).

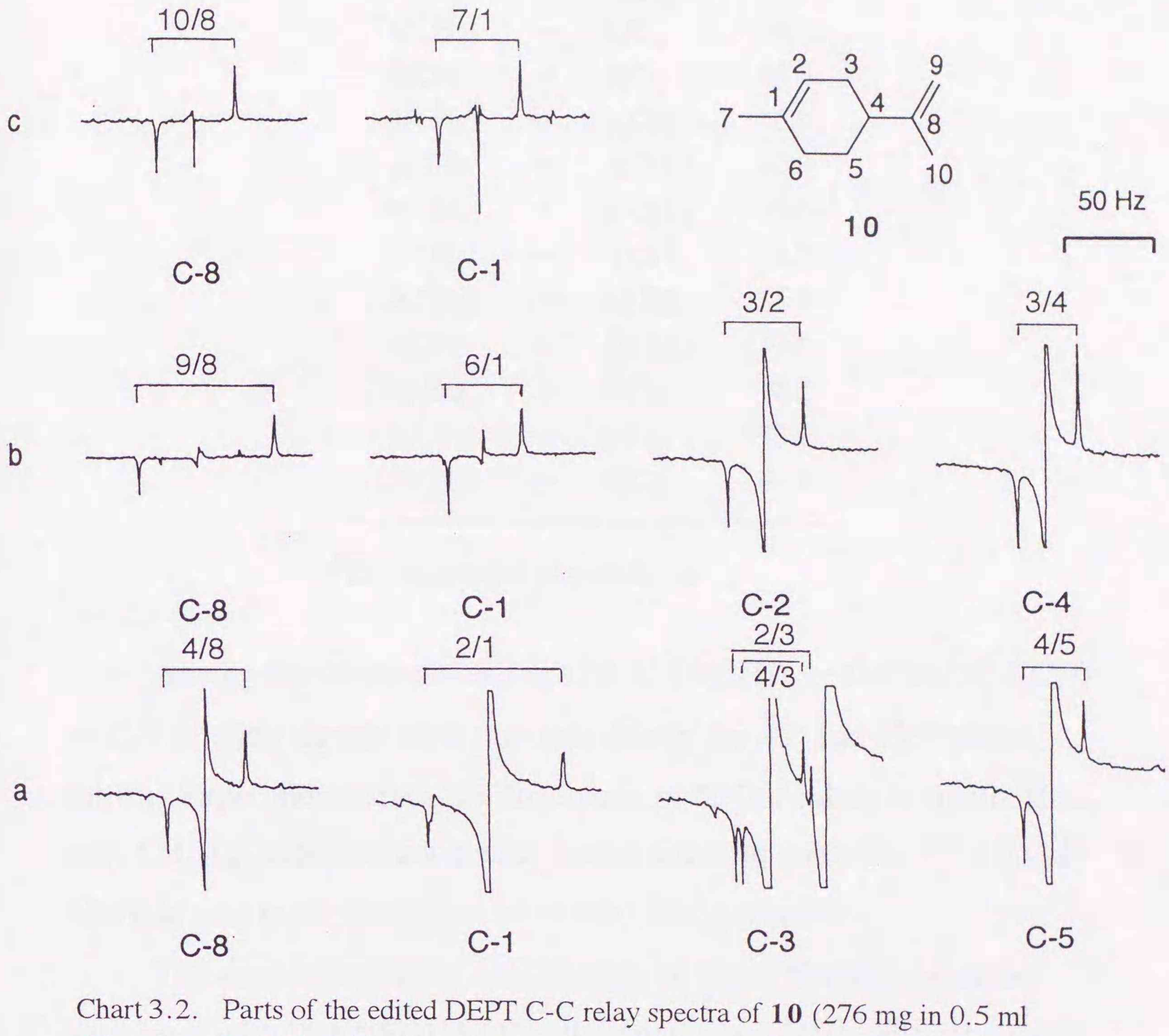


Chart 3.2. Parts of the edited DEPT C-C relay spectra of **10** (276 mg in 0.5 ml chloroform-*d*) obtained by the sequence shown in Fig. 3.1b. Delays, RD, Δ_1 and Δ_2 were set to 2.0 s 3.6 ms, and 2.3 ms ($^1J_{CH}$ = 140, $^1J_{CC}$ = 42 Hz), respectively. Each spectrum was accumulated using 1280 transients. The total measuring time was *ca.* 12 h each (a): CH subspectrum, (b): CH_2 subspectrum and (c): CH_3 subspectrum. All spectra are displayed in the same absolute intensity scale.

Table 3.1. J_{CC} values for limonene determined by DEPT C-C Relay

^{13}C	→	^{13}C	J(Hz)
2(CH)	→	1(C_q)	72.6
6(CH_2)	→	1(C_q)	39.7
7(CH_3)	→	1(C_q)	43.6
3(CH_2)	→	2(CH)	40.9
2(CH)	→	3(CH_2)	40.9
4(CH)	→	3(CH_2)	33.6
3(CH_2)	→	4(CH)	33.3[a]
5(CH_2)	→	4(CH)	33.3[a]
4(CH)	→	5(CH_2)	33.0
4(CH)	→	8(C_q)	42.1
9(CH_2)	→	8(C_q)	72.0
10(CH_3)	→	8(C_q)	41.8

[a] Not resolved at this condition.

Among the connectivities to C-8, C-10(CH_3) → C-8 and C-4(CH) → C-8 satellite signals were unresolvable in the 45° and 135° phase-shifting experiments since the difference in their J values is small. Thus, only CH_3-C_q subspectrum could give an accurate value for J(C-10,C-8) which is free from the influence of the CH-C_q signals.

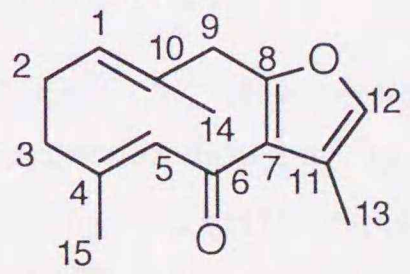
The most outstanding disadvantage of the C-C relay sequences compared with INADEQUATE is the relatively strong residual signals arising from single-quantum coherence in the center of the satellites since no double-quantum selection is included in the pulse sequences. These central signals are especially prominent at protonated carbons, and consequently, observation of the ^{13}C-^{13}C satellite signals is nearly hopeless for these carbons.

When CH_3, CH_2 or CH selection is carried out in the DEPT C-C relay sequence, these strong unwanted signals also undergo the spectrum-

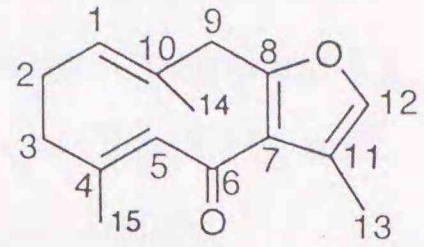
editing effect and thus they would be suppressed. Therefore, at the position of the carbons other than ones selected by the editing, ^{13}C-^{13}C satellite signals can be detected even if they are protonated carbons. For instance, CH_3-CH(or CH_2) couplings are detected at the CH(or CH_2) carbons as well as CH_3-C_q at C_q's in a CH_3-selected subspectrum. From this point of view, β=45° and 135° spectra themselves usually utilized in basic DEPT, are of less use in the relayed sequence since all protonated carbons are excited and, hence, interfere with the observation of small satellites at these carbons in the spectra. The use of CH_3, CH_2 and CH subspectra is strongly recommended for that reason.

Nine of ten ^{13}C-^{13}C couplings present in the **10** could be detected (Chart 3.2). The coupling constants between protonated carbons are also presented in Table 3.1. The only undetermined connectivity was the C-5 → C-6 coupling, where both carbons are CH_2. It is impossible to remove the strong central signal due to the coherence directly transferred from the attached protons when the satellite signals are observed in the CH_2-selection spectrum.

Efficiency of phase-alternating composite pulse and spectrum editing was thus indicated by using strong test sample which was prepared dissolving 2 mmol of **10** in 0.5 ml chloroform-*d*. Next, sensitivity of this method was demonstrated in more practical conditions for natural product analysis. A smaller amount (0.5 mmol) of furanodienone (**11**), a sesquiterpene found in *Curcuma zedoaria* (Zingiberaceae) and *Chloranthus japonicus* (Chloranthaceae) was used and the experimental time was set to 30 min (Chart 3.3).



furanodienone (**11**)



11

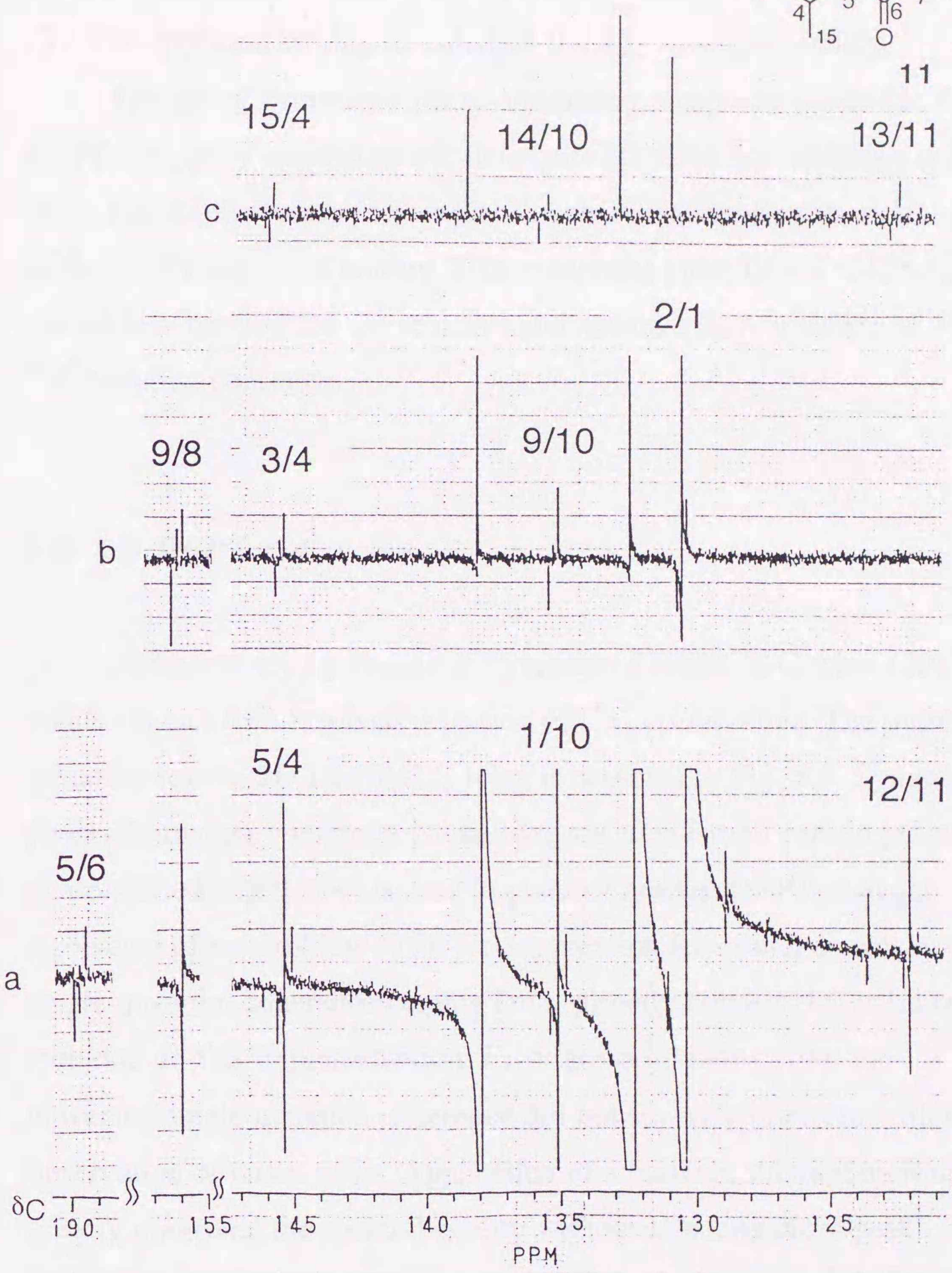


Chart 3.3. Parts of the edited DEPT C-C relay spectra of **11** (115 mg in 0.5 ml chloroform-*d*) obtained by the sequence shown in Fig. 3.1b. Delays, Δ_1 and Δ_2 were set to 3.6 and 1.1 ms ($^1J_{CH}$ = 140, $^1J_{CC}$ = 53 Hz), respectively. Each spectrum was accumulated using 640 transients. The total measuring time was *ca.* 32 min each (a): CH subspectrum, (b): CH_2 subspectrum and (c): CH_3 subspectrum. All spectra are displayed in the same absolute intensity scale.

These conditions are equivalent to those using a 50 μmol sample measured for 50 h, which can be covered by a weekend experiment. Compound **11** has two quaternary carbons, each of which is attached to CH_3, CH_2, and CH. The spectrum editing revealed all the J_{CC} values separately.

The use of symmetric phase-alternating composite pulses for the DEPT C-C relay experiments is thus quite effective for obtaining constant phase results, especially in case that the phase information is critical such as for DEPT spectrum editing. This composite pulse DEPT C-C relay should be a method for the sensitive and accurate determination of ^{13}C-^{13}C coupling constants.

3.3 2D DEPT C-C relay

Furthermore, I present a 2D version of DEPT C-C relay (*20*), which enables well resolved detection of C-C correlations. The pulse sequence for the 2D DEPT C-C relay is depicted in Fig. 3.3. Symmetric phase-alternating composite pulses (*43*) are used for all carbon pulses and phase-shifted DEPT (*64*) is used in place of normal DEPT to avoid resonance-offset problem (*19*). No suppression for center signals due to single-quantum coherence coming from directly bonded H-C pairs is included. In this implementation, F_1 ridges originating from the unwanted single-quantum coherence did not severely interfere with the observation of cross peaks. Application of a baseline subtraction routine greatly improved the spectral quality without affecting cross peak intensities since C-C cross peaks are split into doublets by ^{13}C-^{13}C couplings, leaving vacant space at the center.

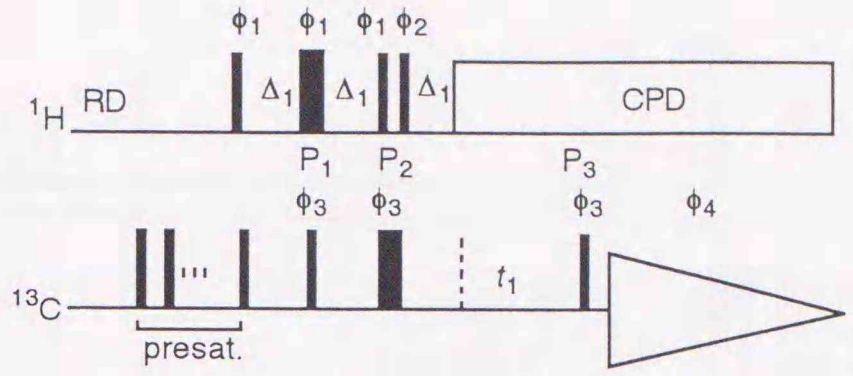
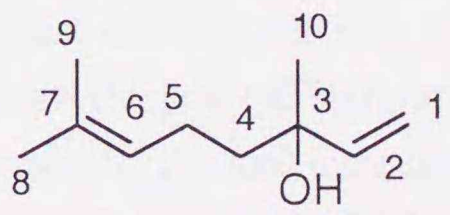


Fig.3.3. Pulse sequences for the 2D DEPT C-C relay. P1 - P3 are composite pulses consisted of (58° -140° 172°), (58° -140° 344° -140° 58°) and (24° -152° 346° -152° 24°), respectively (*43*). The delay Δ_1 is $1/2J_{CH}$. ^{13}C presaturation pulses are composed of sixteen 90° pulses separated by 0.1 s intervals (*56*). Phase cycling used is as follows: ϕ_1= β, 360°-β; ϕ_2= -x; ϕ_3= x,x,y,y,-x,-x,-y,-y; ϕ_4= x,-x,y,-y, -x,x,-y,y.

The 2D DEPT C-C relay spectrum of a monoterpene hydrocarbon, linalool (**12**), is shown in Chart 3.4a. In order to compare sensitivity, the 2D INADEQUATE spectrum of the same sample is shown in Chart 3.4b. Although there has been some discussion concerning the sensitivity loss for the COSY-type presentation of INADEQUATE (*17*, *72*), a significant difference in spectral quality was not actually found in the conventional and COSY-type INADEQUATE experiments in this case. Comparison of the two contour plots clearly demonstrated the enhanced sensitivity of the DEPT C-C sequence. This can be seen more evidently in the F_1 slices of the both spectra depicted in Chart 3.5.



linalool (**12**)

Twelve correlation peaks from nine C-C bonds were clearly detected in the 2D DEPT C-C relay spectrum. Although 18 correlation peaks were expected for the molecule, six relay signals starting from quaternary carbons C-3 and C-7 were undetectable in the spectrum

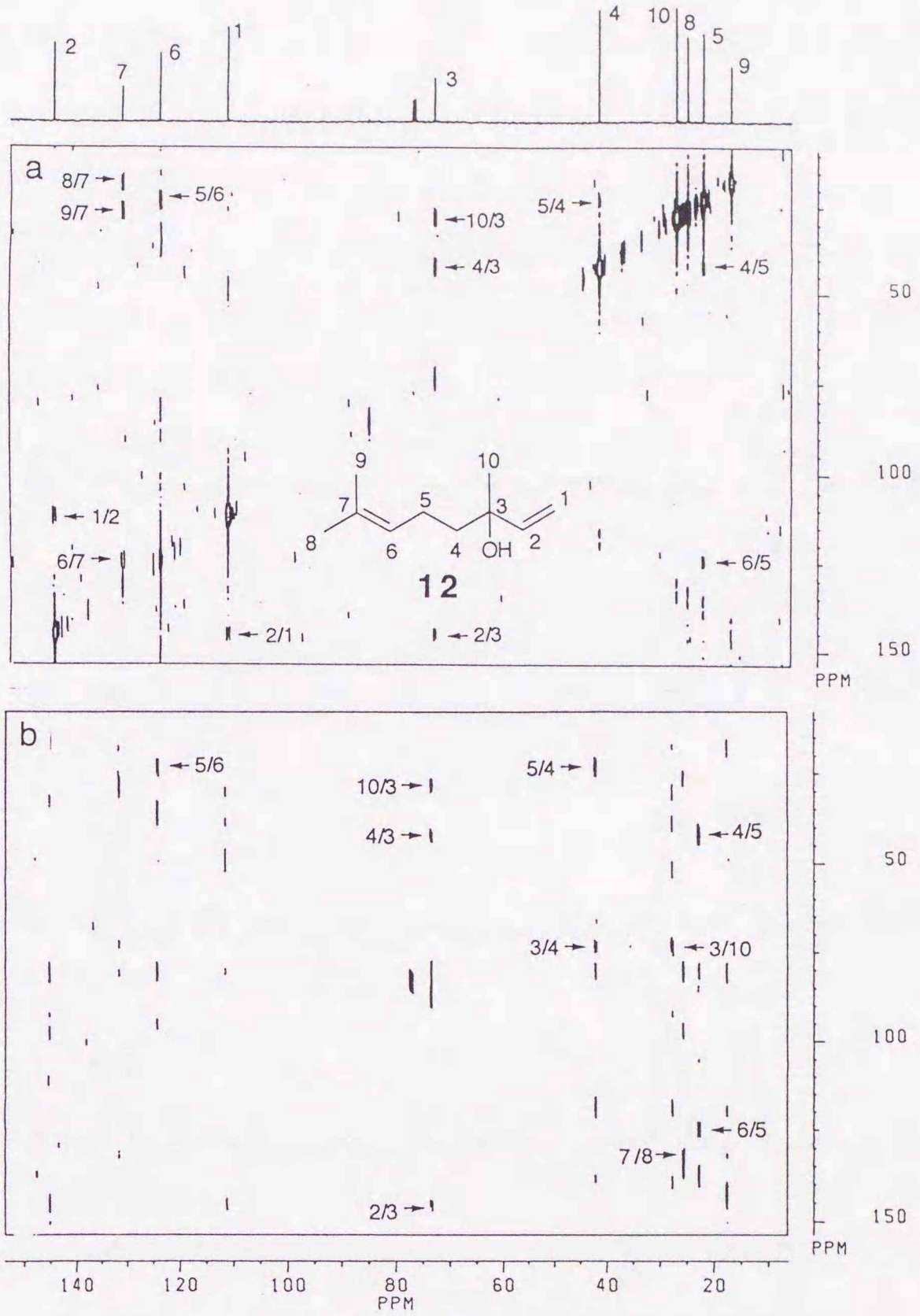


Chart 3.4. The 2D DEPT C-C relay (a) and the 2D INADEQUATE (b) spectra of **12** (61 mg in 0.5 ml chloroform-*d*). The 2D DEPT C-C relay spectrum was obtained by the sequence shown in Fig. 3.3. Phase shift for DEPT, β, was 45°. Delays, RD and $\Delta_1(1/2J_{CH})$ were 2.0 s and 3.6 ms ($^1J_{CH}$ = 140 Hz), respectively. Each 54 t_1 increments was accumulated using 128 transients. The total measuring time was *ca.* 7 h each. The 2D INADEQUATE spectrum was obtained by the Bruker INADSYM.AU program. The delay for creating antiphase C-C magnetization was 11.4 ms ($^1J_{CC}$ = 44 Hz). Baseline correction by the SUB2 routine of the Bruker software was applied to the resulting 2D DEPT C-C relay spectrum. Both spectra are displayed at the contour level just above the thermal noise.

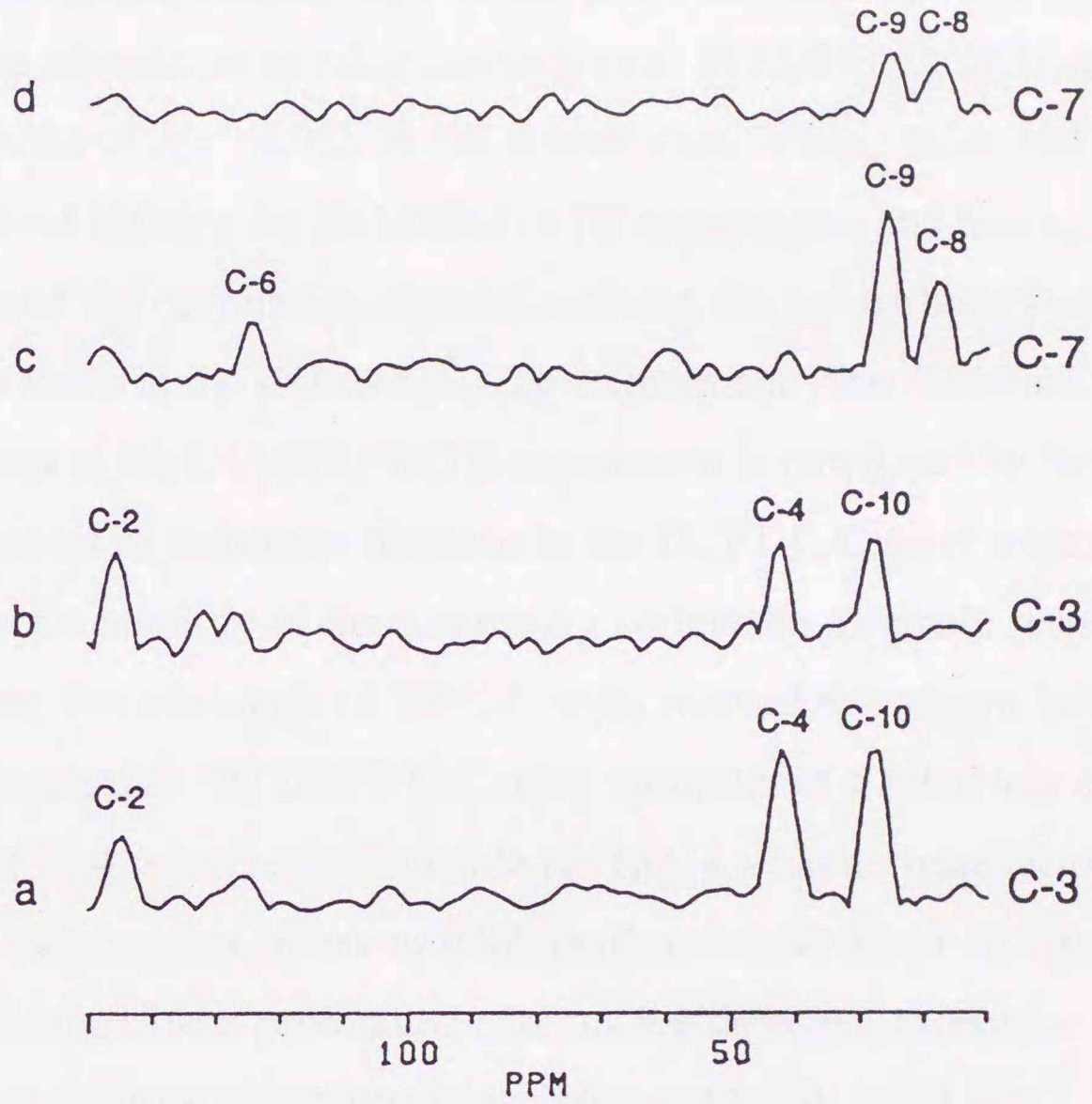
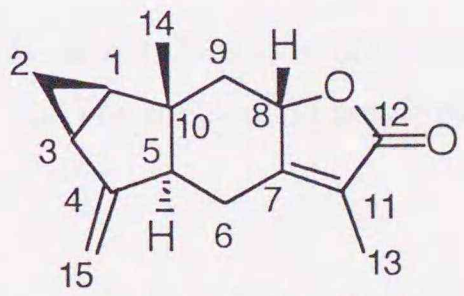


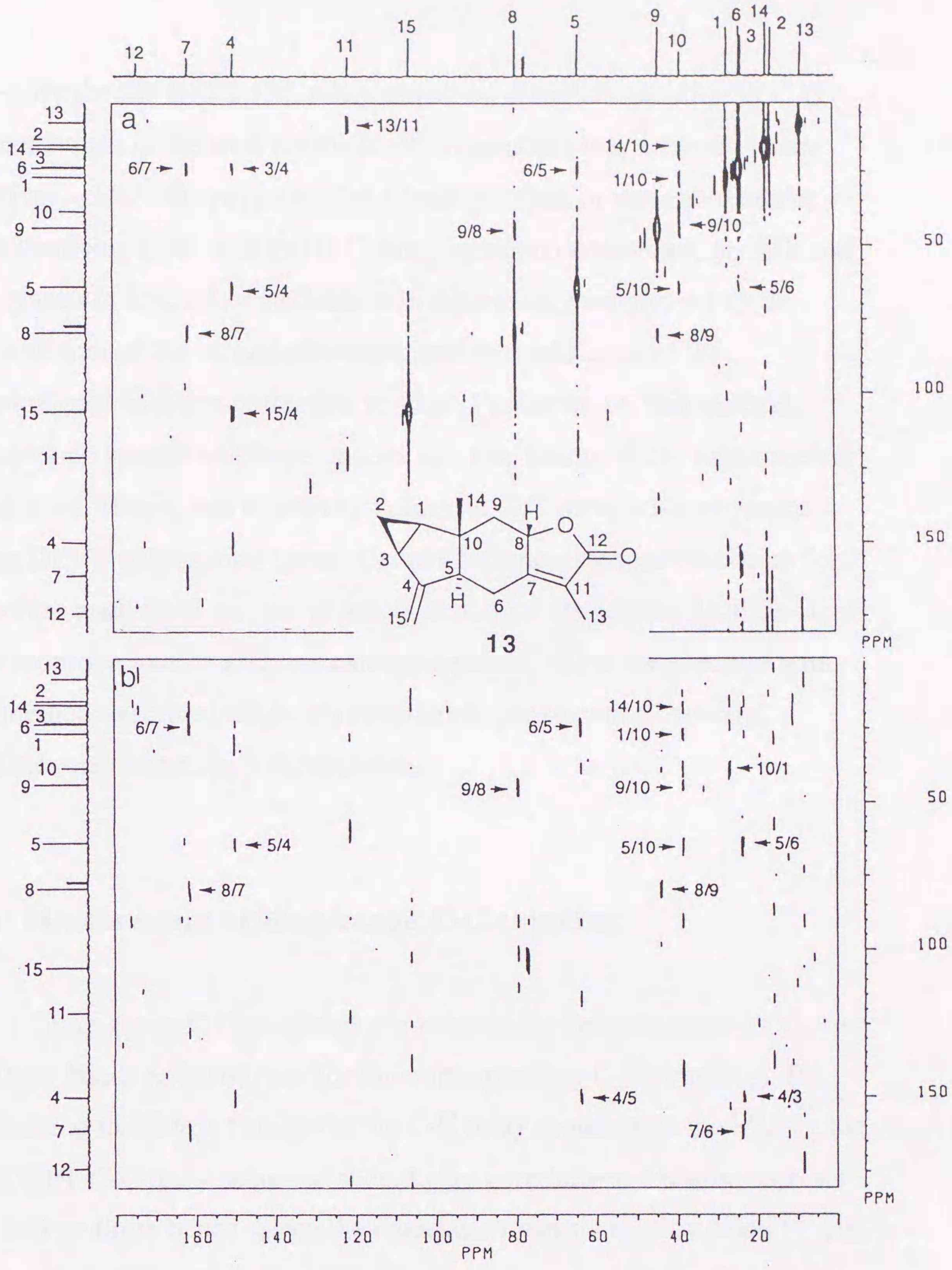
Chart 3.5. Slices in the F_1 dimension of the 2D DEPT C-C relay (a and c), and 2D INADEQUATE (b and d) spectra of **12** obtained as in Chart 3.4.

because of the use of DEPT polarization transfer, hence giving an asymmetrical 2D map. The drawback of lacking cross peaks from the quaternary carbons in the method is, needless to say, offset by the appearance of cross peaks arising from neighboring protonated carbons. This method, however, will have gaps in connectivity networks that will arise when quaternary carbons are adjacent to one another. In the 2D INADEQUATE spectrum, only 10 out of 18 correlations were visible. One of the advantages of relay methods over INADEQUATE is an independence of J_{CC} values. In the present case, $1/4J_{CC}$ value was set to 5.7 ms (J=44 Hz) for the INADEQUATE experiment, and hence, intensities of the correlation signals involving the sp^2 carbons were relatively weak in the INADEQUATE experiment. The drawback for the sp^2 carbons in the INADEQUATE experiment is paralleled by the incomplete set of responses obtained in the DEPT C-C relay experiment caused by the inability of the quaternary carbons to originate responses.

Next, the advantage of 2D C-C relay method was shown by a more complex molecule. 2D DEPT C-C relay spectrum of a relatively small amount of (0.4 mmol) shizukanolide A (**13**), a sesquiterpene lactone found in *Chloranthus japonicus* (Chloranthaceae), is shown in Chart 3.6a. All correlations from protonated carbons are detected, except for those between cyclopropane carbons which have unusually small J_{CC}. Compared with the INADEQUATE spectrum (Chart 3.6b) obtained under the same conditions, The 2D DEPT C-C COSY spectrum gives distinct correlation signals especially in the low-field region.



shizukanolide A (**13**)



13

Chart 3.6. The 2D DEPT C-C relay (a) and the 2D INADEQUATE (b) spectra of **13** (90 mg in 0.5 ml chloroform-*d*). The measuring conditions were the same as those of Chart 3.4.

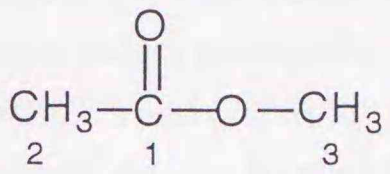
By the 2D DEPT C-C relay sequence, direct observation of C-C connectivities in the well-resolved ^{13}C dimensions was achieved in the relatively clear 2D spectrum. The severe problem of unwanted center signals arising from residual H-C single-quantum coherence, an inherent annoyance of C-C relay methods, was successfully suppressed by an introduction of the second dimension and an application of the conventional baseline-correction routine. Furthermore, this method requires no special hardware options nor fine tuning of the experimental conditions. Hence, this sensitivity-enhanced C-C correlation sequence using DEPT polarization transfer could become a reasonable choice for structure analysis of natural products at natural abundance. Utilization of a microprobe and/or gradient enhanced pulses (*73*) in conjunction with the method described might give further improvement of spectral qualities and sensitivity enhancements.

3.4 Measurement of long-range C-C coupling

Long-range C-C couplings are measurable between carbons via two or three bonds as in the case for the corresponding C-H couplings. By optimizing the delays for J_{CC} in the C-C relay sequence to the $^{LR}J_{CC}$, the 1D DEPT C-C relay sequence should give correlations between carbons via two or three bonds. Since the correlation signals split by small $^{LR}J_{CC}$, they will be seriously suffered from residual central signals. Although spectrum editing is also efficient to eliminate the unwanted signals, a CH-subspectrum can not get the benefit.

The unwanted signal is due to long-range CH couplings ($^{LR}J_{CH}$). For example, in the DEPT C-C relay spectrum of methyl acetate (**14**) optimized to detect directly bonded ^{13}C-^{13}C coupling (Chart 3.7a), the

^{13}C satellite signal is due to the expected magnetization transfer ^{1}J(H-2/C-2) → ^{1}J(C-2/C-1) occurring in the (^{1}H-2)-(^{13}C-2)-(^{13}C-1) isotopomer (Fig.3.4a), whereas the unwanted signal is mainly due to that of ^{2}J(H-2/C-1) in the (^{1}H-2)-(^{12}C-2)-(^{13}C-1) isotopomer(Fig.3.4b) whose population is 100 times larger than that of (^{1}H-2)-(^{13}C-2)-(^{13}C-1).



methyl acetate (**14**)

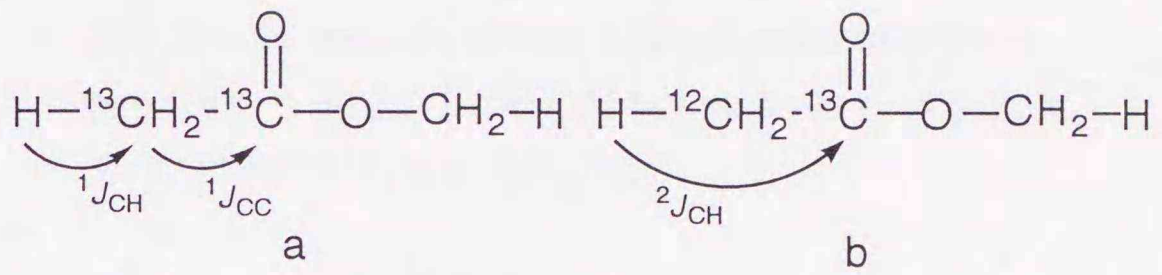


Fig.3.4. Origination of unwanted central signals in 1D DEPT C-C relay spectra of **14**. The population of the species giving unwanted signal (b) is 100 times larger than that giving expected signal (a).

Large dispersive line of this unwanted center signal reaches to ± 10 Hz (Chart 3.7a). To suppress the magnetization transfer due to $^{LR}J_{CH}$, an insertion of BIRD pulses before the pulse sequence was applied.

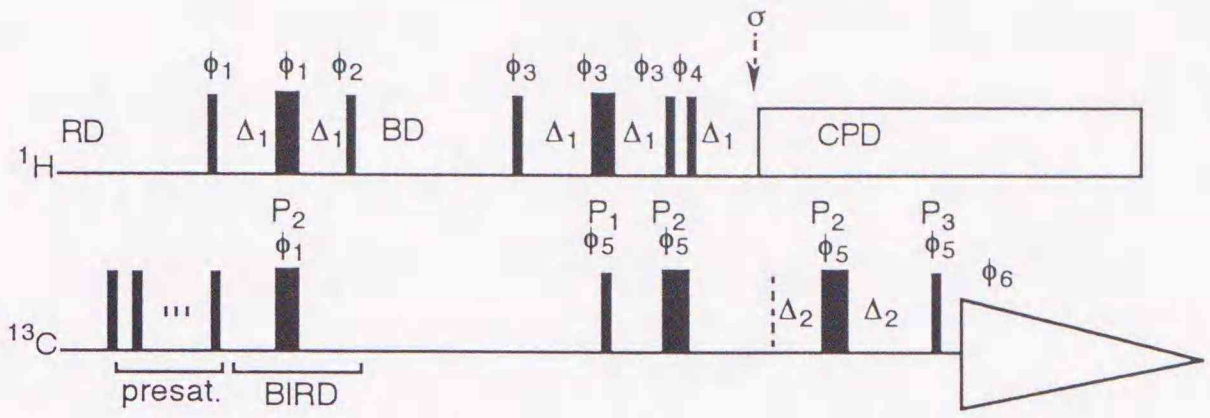
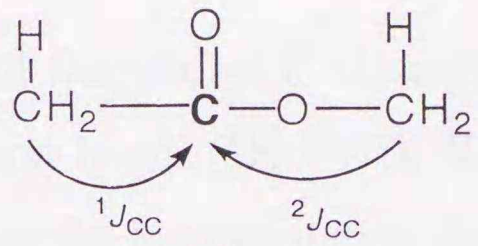


Fig.3.5. Pulse sequence for the BIRD/ DEPT C-C relay. P1 - P3 are composite pulses consisted of (58° -140° 172°), (58° -140° 344° -140° 58°) and (24° -152° 346° -152° 24°), respectively. The delays Δ_1 and Δ_2 are $1/2J_{CH}$ and $1/4J_{CC}$-$1/2J_{CH}$, respectively. ^{13}C presaturation pulses are composed of sixteen 90° pulses separated by 0.1 s intervals (*56*). See the text fot σ. Phase cycling used is as follows: ϕ_1= x; ϕ_2= = -x; ϕ_3= β, 360°-β; ϕ_4= -x, β; ϕ_5= x,x,y,y,-x, -x,-y,-y; ϕ_6= x,-x,y,-y -x,x, -y,y.

The product operator formulae (*42*) before Δ_2 in the resultant BIRD C-C relay sequence (Fig.3.5) is:

$$\sigma = I_Z - I'_Z \cos \pi J 2\Delta - 2I'_X S_Z \sin(\pi J 2\Delta)$$

where I, I' and S represent H-2 of the isotopomer a, H-2 of the isotopomer b, and C-1 of the isotopomer b, respectively in Fig.3.4. J and Δ represent $^{LR}J_{CH}$ and Δ_1, respectively. It shows that BIRD pulse can reduce the magnetization from $^{LR}J_{CH}$. The term $-2I'_X S_Z \sin\pi J 2\Delta$ is negligible because $\pi J 2\Delta$ is small, and the term $-I'_Z \cos\pi J 2\Delta$ is efficiently eliminated by a BIRD delay, Δ_2. In each experiment, Δ_2 was carefully optimized for eliminating the signals originated from this term. Insertion of BIRD pulse cleared away the unwanted signal from the experimental spectrum (Chart.3.7b), resulting plane baseline. Optimization of the delay for ^{13}C-^{13}C evolution to long range coupling gave small doublet in the BIRD C-C relay spectrum (Chart 3.7c). This doublet would be hidden under residual central signal without the aid of BIRD pulse.



14

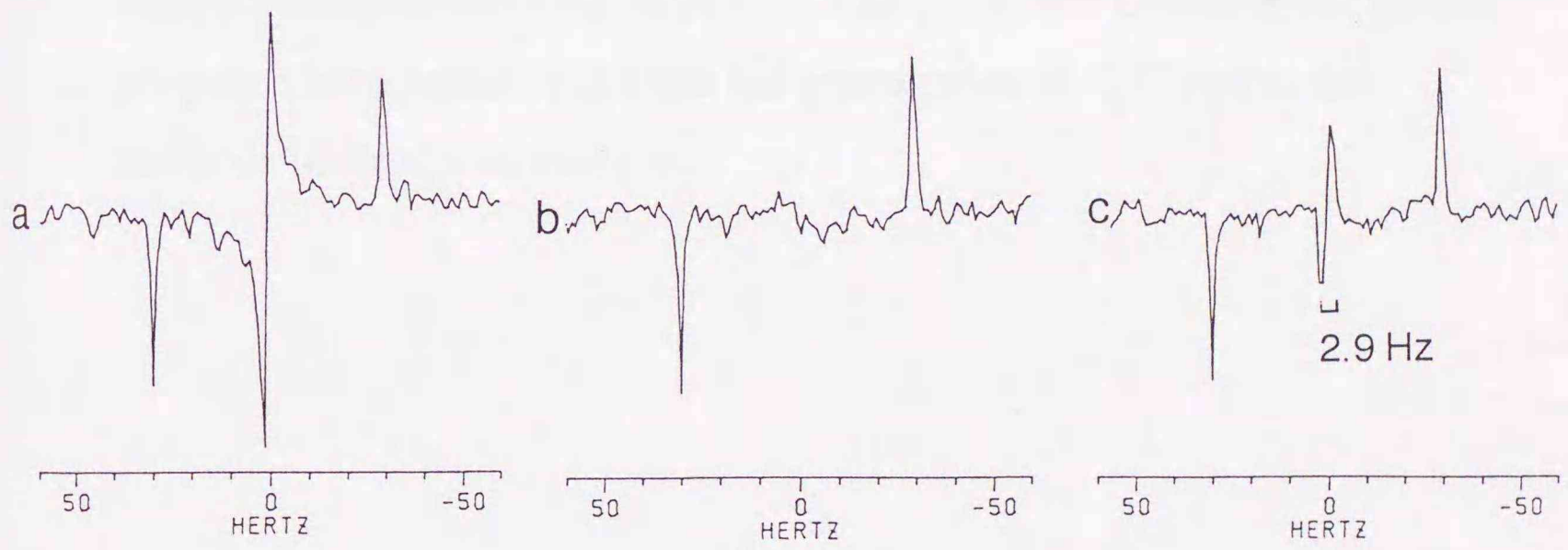
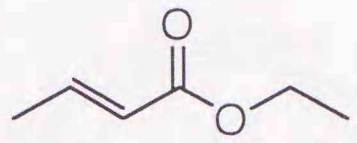


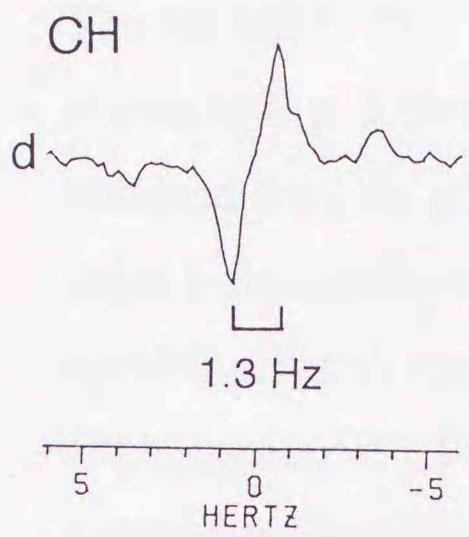
Chart 3.7. Original DEPT C-C relay spectrum (a) and BIRD/DEPT C-C relay spectra (b and c) of **14** (0.5 ml of 1:1 (v/v) solution in chloroform-*d*) obtained by the sequence shown in Fig. 3.3 (a) and 3.5 (b and c).The delays, RD, BD, and Δ_1 were 3.6 s, 1.8 s, and 3.85 ms ($^1J_{CH}$ = 130 Hz), respectively. The delay Δ_2 was 1.15 ms (a) ($^1J_{CC}$ = 50 Hz) and 83.5 ms (b and c) ($^{LR}J_{CC}$ = 2.8 Hz). Each spectrum was accumulated using 32 transients. The total measuring time was *ca.* 4 min each. All spectra are displayed in the same absolute intensity scale.

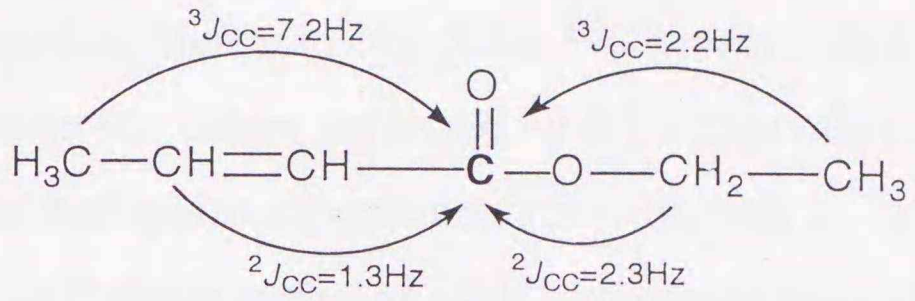
Also for the case of ethyl crotonate (**15**), it was possible to measure $^{LR}J_{CC}$ values in CH_3- (Chart 3.8a) and CH_2- (Chart 3.8b) subspectra of the DEPT C-C relay spectra, and it was impossible to measure that in the CH-subspectrum (Chart 3.8c). The CH-subspectrum of BIRD/DEPT C-C relay gave a clear doublet signal (Chart 3.8d).



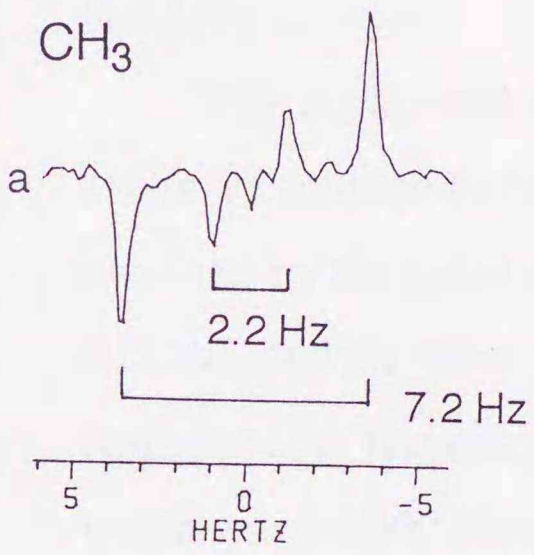
ethyl crotonate (**15**)

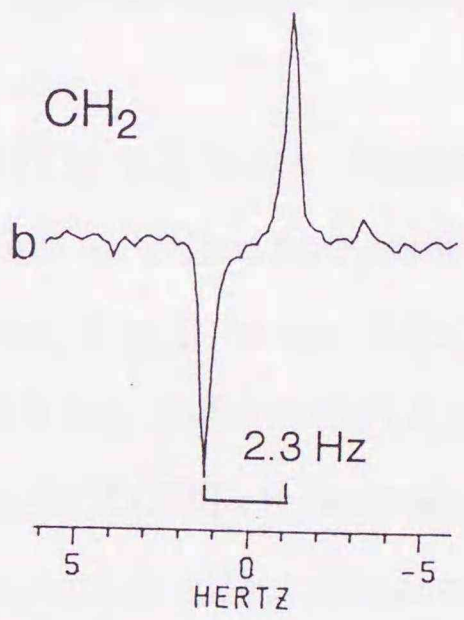
Measurements of long-range C-C coupling realize the detection of H-C correlation via four bonds (^{1}H-^{13}C-X-X-^{13}C). Although sensitivity loss might be caused by the long evolution time adjusted for detecting long-range coupling, this method is attractive for structure elucidation of highly hydrogen-deficient molecules. The sensitivity enhancement method proposed here would contribute the propagation of C-C correlation methods in structural analysis.





15





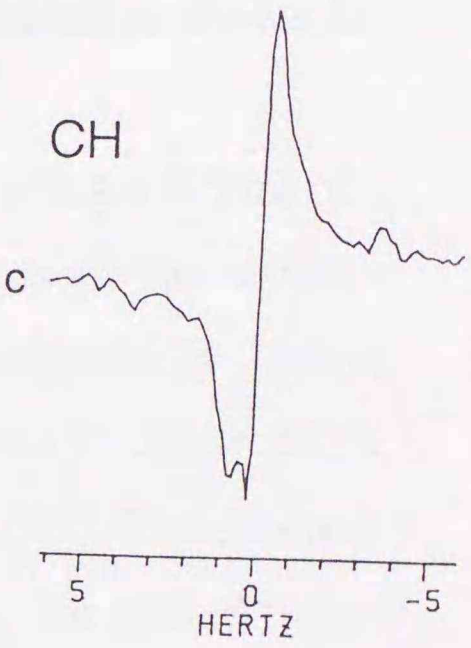


Chart 3.8. Edited (BIRD) DEPT C-C relay spectra of **15** (340 mg in 0.5 ml chloroform-*d*) obtained by the sequence shown in Fig. 3.3 (a-c) and 3.5 (d). Delays, RD, BD, Δ_1 and Δ_2 were 0.1 ms, 1.0 s, 3.6 ms, and 46.4 ms ($^1J_{CH}$ = 140, $^1J_{CC}$ = 5 Hz), respectively. (a): CH_3 subspectrum, (b): CH_2 subspectrum and (c and d): CH subspectrum. All spectra are displayed in the same absolute intensity scale. Each spectrum was accumulated using 192 transients. The total measuring time was *ca.* 30 min each.

3.5. Experimental

1D DEPT C-C relay spectra (Fig. 3.2, Charts 3.1 - 3.3, 3.7a, and 3.8a-c)

The 1D DEPT C-C relay spectra were measured with the pulse sequences shown in Fig. 3.1b except for the Fig.3.2 (filled bars) and Chart 3.7a obtained with the pulse sequences shown in Fig. 3.1a. ^{13}C presaturation pulse train consisted of sixteen 90° pulses separated by 0.1 s intervals was applied prior to starting the multipulse experiments (*56*). In each experiments, 45°, 90° and 135° phase angles of DEPT were accumulated except for Fig. 3.2 and Chart 3.7a. A line-broadening factor of 1 Hz was applied prior to Fourier transformation. CH, CH_2 and CH_3 subspectra were calculated by adding or subtracting the each spectrum as shown in Ref.(*71*).

The acetic acid spectra (Fig.3.2) were obtained using a 0.5 ml of 1:1 (v/v) solution in chloroform-*d*. Filled and open bars are the results obtained by the pulse sequences, Fig. 3.1a and 3.1b, respectively. Delays RD, Δ_1, and Δ_1 were 3.4 s, 3.8 ms, and 0.6 ms (J_{CH} = 132, J_{CC} = 50 Hz), respectively. The phase angle for DEPT, β, was set to 45°. The spectral width was 50,000 Hz and transmitter offset frequency was shifted from δ 200 to 0 ppm by 10 ppm in each experiment. Four scans were accumulated and the data were processed same as that in Chart 3.1. Twenty-one spectra with different transmitter offset frequency were processed with the same phase-correction constants and displayed in the absolute intensity mode. The total measuring time was *ca.* 2 min each.

Chart 3.1 was obtained using the mixture of 1 mmol each of acetic, propionic and isobutyric acids in DMSO-d_6. The sample volume was adjusted to *ca.* 0.5 ml. All delays were the same as for Fig.3.2. Each

spectrum was measured covering the spectral width of 3000 Hz using 128 transients. The total measuring time was *ca.* 12 min each.

Chart 3.2 was obtained using a solution containing 276 mg of **10** in 0.5 ml chloroform-*d*. The delays, RD, Δ_1, and Δ_2 were set to 2.0 s, 3.6 ms, and 2.3 ms ($^1J_{CH}$ = 140, $^1J_{CC}$ = 42 Hz), respectively. Each spectrum was measured covering the spectral width of 20,000 Hz in 128K data points using 1280 transients. The total measuring time was 12 h each. No window function was applied.

Chart 3.3 was obtained using a solution containing 115 mg of **11** in 0.5 ml chloroform-*d*. The delays, RD, Δ_1, and Δ_2 were 2.0 s, 3.6 ms, and 1.1 ms ($^1J_{CH}$ = 140, $^1J_{CC}$ = 53 Hz), respectively. Each spectrum was measured covering the spectral width of 31,250 Hz in 64K data points using 640 transients. The total measuring time was 32 min each. No window function was applied.

Chart 3.7a was obtained using a 0.5 ml of 1:1 (v/v) **14** solution in chloroform-*d*. The delays, RD, Δ_1 and Δ_2 were 3.6 s, 3.85 ms and 1.15 ms ($^1J_{CH}$ = 130, $^1J_{CC}$ = 50 Hz), respectively. The spectrum was measured covering the spectral width of 31250 Hz in 64 K data points using 32 transients. The total measuring time was 4 min. No window function was applied.

Charts 3.8a - c were obtained using a solution containing 340 mg of **15** in 0.5 ml chloroform-*d*. The delays, RD, BD, Δ_1, and Δ_2 were 0.1 ms, 1.0 s, 3.6 ms, and 46.4 ms ($^1J_{CH}$ = 140, $^{LR}J_{CC}$ = 5 Hz), respectively. Each spectrum was measured covering the spectral width of 10,000 Hz in 128 K data points using 192 transients. The total measuring time was 30 min each. Data processing performed was the same as Chart 3.1.

2D DEPT C-C relay spectra (Charts 3.4a, 3.5a and c, and 3.6a)
The 2D DEPT C-C relay spectra were obtained by the sequence in Fig. 3.3. ^{13}C presaturation pulse train consisting of sixteen 90° pulses separated by 0.1 s intervals was applied prior to starting the multipulse experiments (*56*).

Chart 3.4a was obtained using a solution containing 61 mg of **12** in 0.5 ml chloroform-*d*. The delays, RD and Δ_1 were 2.0 s and 3.6 ms ($^1J_{CH}$ = 140 Hz), respectively. Phase shift for DEPT, β, was 45°. The spectrum was measured covering the spectral width of 18,500 Hz in 4K data points using 128 transients (with two dummy scans) for each of 54 t_1 increments. Zero-filing to 128 points for F_1 and multiplication with unshifted sine-bell windows were performed in both dimensions prior to 2D Fourier transformation. The resulting magnitude mode spectrum consisted of 4K x 128 data points with a digital resolution of 4.5 Hz per point in F_2. Baseline correction by the SUB2 routine of the Bruker software was applied to the resulting spectrum. The total measuring time was *ca.* 7 h.

Chart 3.6a was obtained using a solution containing 90 mg of **13** in 0.5 ml chloroform-*d*. The delay RD was 3.6 s. The spectral width was 22,727 Hz. The other measuring and data processing conditions were the same as those of Chart 3.5a.

2D INADEQUATE spectra (Charts 3.4b, 3.5b and d, and 3.6b)
The 2D INADEQUATE spectra were obtained by the Bruker INADSYM.AU program, (RD)-90°-(1/4J_{CC})-180°-(1/4J_{CC})-90°-(t_1/2)-120°-(t_1/2)-t_2, which uses a 120° conversion pulse in the middle of the evolution time to present a COSY-type symmetric 2D map (*72*) and no presaturation was included.

For Charts 3.4b and 3.6b, the delay for creating antiphase C-C magnetization was 11.4 ms ($^1J_{CC}$ = 44 Hz). The other measuring and data processing conditions were the same as those of Charts 3.4a and 3.6a, respectively.

BIRD/DEPT C-C relay spectra (Charts 3.7b and c, and 3.8d)
BIRD/DEPT C-C relay spectra were measured with the pulse sequence shown in Fig. 3.4. ^{13}C presaturation pulse train consisted of sixteen 90° pulses separated by 0.1 s intervals was applied prior to starting the multipulse experiments (*56*).

Charts 3.7b and c were obtained using 0.5 ml of a 1:1 (v/v) solution of **14** in chloroform-*d*. The delay Δ_2 was 83.5 ms ($^{LR}J_{CC}$ = 2.8 Hz). The other measuring conditions were the same as those of Chart 3.7a.

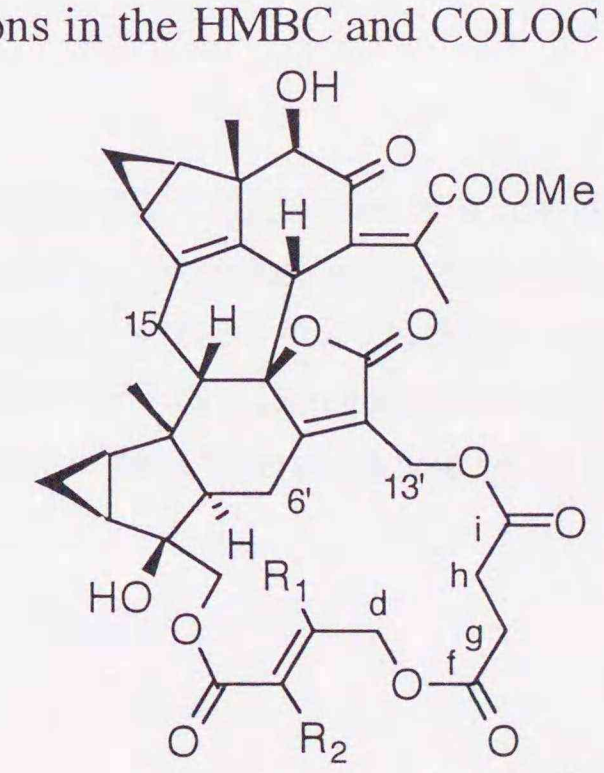
For Chart 3.8d, the delay Δ_2 wwas 46.4 ms ($^{LR}J_{CC}$ = 5 Hz). The other measuring conditions were the same as those of Chart 3.8a.

4 Discrimination of C-H connectivities via two and three bonds

4.1 Introduction

Heteronuclear long-range CH correlation spectroscopies, such as COLOC and HMBC are indispensable tools for structure elucidation of natural products having quaternary carbons. They can detect long-range CH couplings existing between carbon and proton via two (^{13}C-X-H) and three (^{13}C-X-X-H) bonds, where X represents carbon or other heteroatom. The small differences in absolute values between $^{2}J_{CH}$ and $^{3}J_{CH}$, however, result in the difficulty in distinguishing C-H couplings via two and three bonds, which might be in some cases critical in structure elucidation of natural products.

For example, shizukaols, sesquiterpene dimers isolated from *Chloranthus japonicus* (Chloranthaceae), are the case. Shizukaols F(**3**) and B (**4**) have a pendant macrocyclic ester substructure containing succinic acid (*24*, *34*). Two pairs of methylene protons in the succinate residue of **3** and **4** could not be unambiguously assigned by detecting C-H long-range coupling since all the protons in two methylenes gave correlation with both carbonyl carbons in the HMBC and COLOC spectra (Chart 4.1).



	R_1	R_2
3	Me	H
4	H	Me

Shizukaols F(**3**) and B (**4**)

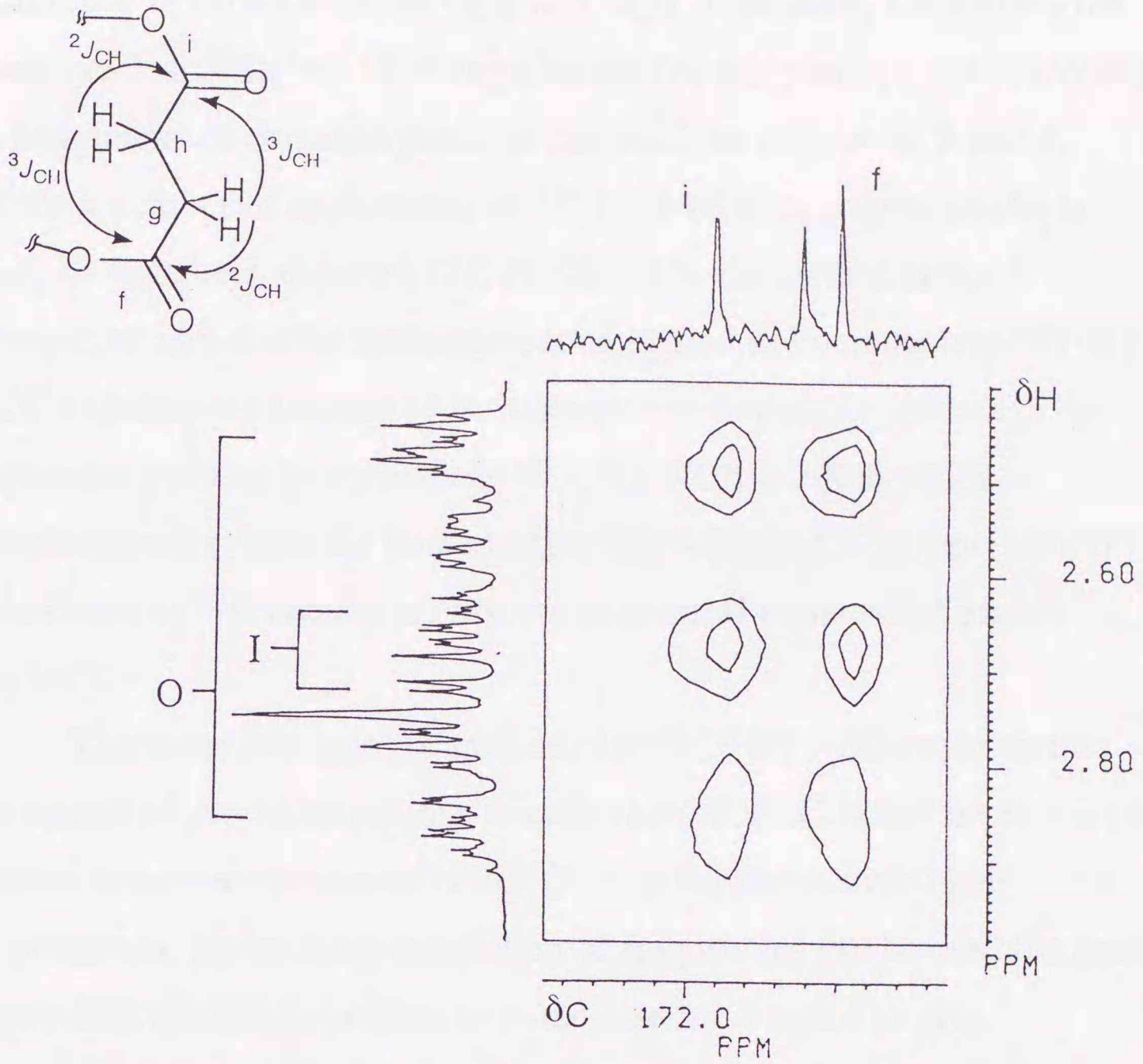


Chart 4.1 Part of the COLOC spectrum of **4** (*ca.* 40 mg in 0.5 ml of chloroform-*d*). The spectrum was were determined using the pulse sequence shown in Fig.2.2a. The delays RD, Δ_1, and Δ_2 were set to 2.0 s, 50 ms, and 25 ms ($^{LR}J_{CH}$ = 10 Hz), respectively. Each of the 128 t_1 increments was accumulated using 224 transients. The total measuring time of each experiment was *ca.* 18 h.

On the other hand, there is remarkable difference in spatial distance of a proton to a carbon via 2- and 3-bond in contrast to the small difference in values between $^{2}J_{CH}$ and $^{3}J_{CH}$. Therefore, I examined the heteronuclear $^{13}C\{^{1}H\}$ NOE experiments for this purpose and succeeded in assignment of two methylenes in the succinate residue of **3** and **4**. While a number of applications of $^{13}C\{^{1}H\}$ NOE to natural products analysis have been reported (*21*, *22*, *74* - *86*), the method is not recognized as a routine measurement compared to homonuclear $^{1}H\{^{1}H\}$ NOE experiments because of its inherent low sensitivity. Although the maximum positive heteronuclear $^{13}C\{^{1}H\}$ NOE is 200% which is fourfold greater than the homonuclear $^{1}H\{^{1}H\}$ case (50%), the natural abundance of ^{13}C nucleus is only 1% in contrast to abundant proton nuclei.

There are two types of methods for $^{13}C\{^{1}H\}$ NOE experiments; saturation of proton transitions (steady-state NOE) (*21*) and inversion of proton transitions (transient NOE) (*22*). In the steady state NOE experiments, the multiple irradiation of frequencies can be used for non-equivalent methylene protons as in the case for **3** and **4** to give satisfactory results (*80*, *81*, *87*). On the other hand, from my preliminary investigation, the transient $^{13}C\{^{1}H\}$ NOE experiment was less sensitive than its steady-state counterpart, and this drawback seems to be the reason why there have been few applications of transient heteronuclear NOE (*86*). Although the irradiation power in the steady state NOE experiments was as low as we could control the instrument to saturate the transitions, the selectivity was still poor, in contrast to the satisfactory selectivity of signal inversion in the transient NOE experiments. The transient NOE therefore seems to be a promising method for the structure analysis of complex natural products if the sensitivity becomes comparable to that of steady-state NOE. Both techniques were applied to assign two pairs of

non-equivalent methylenes in the non-symmetric succinate residue of **3** and **4** (*23*).

4.2 1D heteronuclear $^{13}C\{^1H\}$ NOE

Both of shizukaols F (**3**) and B (**4**) have a non-symmetric succinate unit (Fig. 4.1). Two ester carbonyl carbons (C-i, C-f) in the succinate unit were unambiguously assigned by COLOC (*6*) and/or HMBC (*7*) cross peaks of C-i/H-13' and C-f/H-d (Chart 4.1). The two sets of non-equivalent methylene signals in the succinate residue in **3** are represented by "I"(δ_H 2.86 and 2.78) for the inner pair, and "O"(δ_H 2.94 and 2.62) for the outer pair (Chart 4.2a). The signals of four pairs of non-equivalent methylene protons, H-15, H-6', H-g, and H-h overlap in the proton spectral region of δ 3.0-2.3 ppm in **3** and **4**. In the COLOC spectra, both pairs of methylene protons in the succinate unit ("I" and "O") in each compound showed correlations to both C-f and C-i.

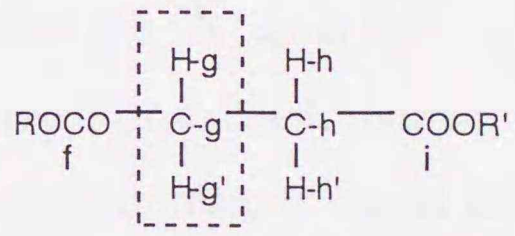


Fig. 4.1. A non-symmetric succinate unit. H-g, H-g', and C-g are a set of methylene. Two methylenes ({H-g, H-g', and C-g} and {H-h, H-h', and C-h}) are non-equivalent. H-g and H-g' are non-equivalent protons.

Assignments of two methylenes in the succinate unit in **3** and **4** were made by the $^{13}C\{^1H\}$ NOE experiments. They have been carried out by two methods; saturation of proton transitions (steady-state NOE)

(Fig. 4.2a) (*21*) and inversion of proton transitions (transient NOE) (Fig. 4.2b) (*22*).

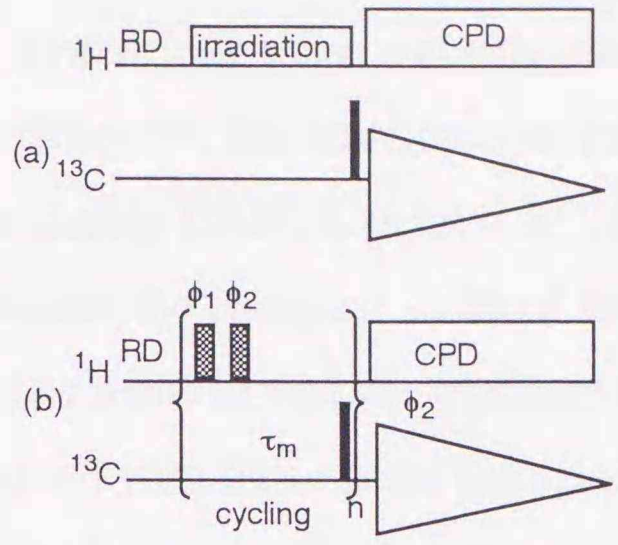


Fig. 4.2. Pulse sequences for the steady-state (a) and transient (b) $^{13}C\{^1H\}$ NOE experiments. Hatched bars represent selective 90° pulses. τ_m represents mixing time. Phase cycling used is as follows: ϕ_1 = x; ϕ_2 = x,-x.

The NOEs from one of the non-equivalent methylene protons in each method did not give enough sensitivity, which seemed to be due to the three-spin effect as indicated previously (*84*). The non-equivalent methylene protons (e.g., H-g and H-g' in Fig. 4.1) are close in space to each other and both close to the ^{13}C atom (C-f). When one of the protons (H-g) was saturated or excited, indirect magnetization transfer (H-g → H-g' → C-f) might diminish or cancel the direct NOE effect (H-g → C-f). Hence the simultaneous saturation (steady-state NOE) or inversion (transient NOE) of both protons of each methylene was examined.

First, the steady-state NOE in **3** was determined. The simultaneous saturation of the two "I" protons (inner pair, δ_H 2.86 and 2.78) by quasi-simultaneous irradiation (*87*) gave an NOE to one of the succinate ester carbonyl carbons, C-i (Chart 4.2c). In the same manner, an NOE from the "O" protons (outer pair, δ_H 2.94 and 2.62) to C-f (Chart 4.2d)was

observed. Consequently the methylene "I" was assigned to H-h and "O" to H-g. Second, the transient NOE experiments were carried out. The simultaneous inversion of the two protons of the methylene "I" could be achieved using a rectangular long pulse since the chemical shifts of the two "I" protons were close. For the simultaneous inversion of "O" protons, however, the double DANTE pulse train (*25*) was needed for selective excitation because the chemical shifts of the two protons were far from each other. The results from the transient NOE experiments (Charts 4.2e and f) agreed with those from the steady-state NOE experiments.

The same procedure was followed for **4** and in this case, heteronucler NOEs from "I" to C-f and from "O" to C-i were unexpectedly observed (Charts 4.3 c - f), which indicates the protons "I" and "O" should be assigned to H-g and H-h, respectively. Problem of poor sensitivity with selective irradiation in the steady-state experiments are observed in trace Charts 4.3c and d.

When assignments of protons are made for related compounds such as **3** and **4**, we tend to assign them by analogy, for example, the "I" (the inner pair) of both compounds to H-g and "O" (the outer pair) to H-h. In **3**, however, "I" is H-h and "O" is H-g, whereas in **4**, "I" is H-g and "O" is H-h. The exchange of the signal position is one of the important information for the conformational analysis of the macrocyclic ester bearing senecioic (**3**) and tiglic(**4**) acids. The importance of the exact assignments of protons by reliable methods should therefore be emphasized to avoid misassignment by uncertain analogy.

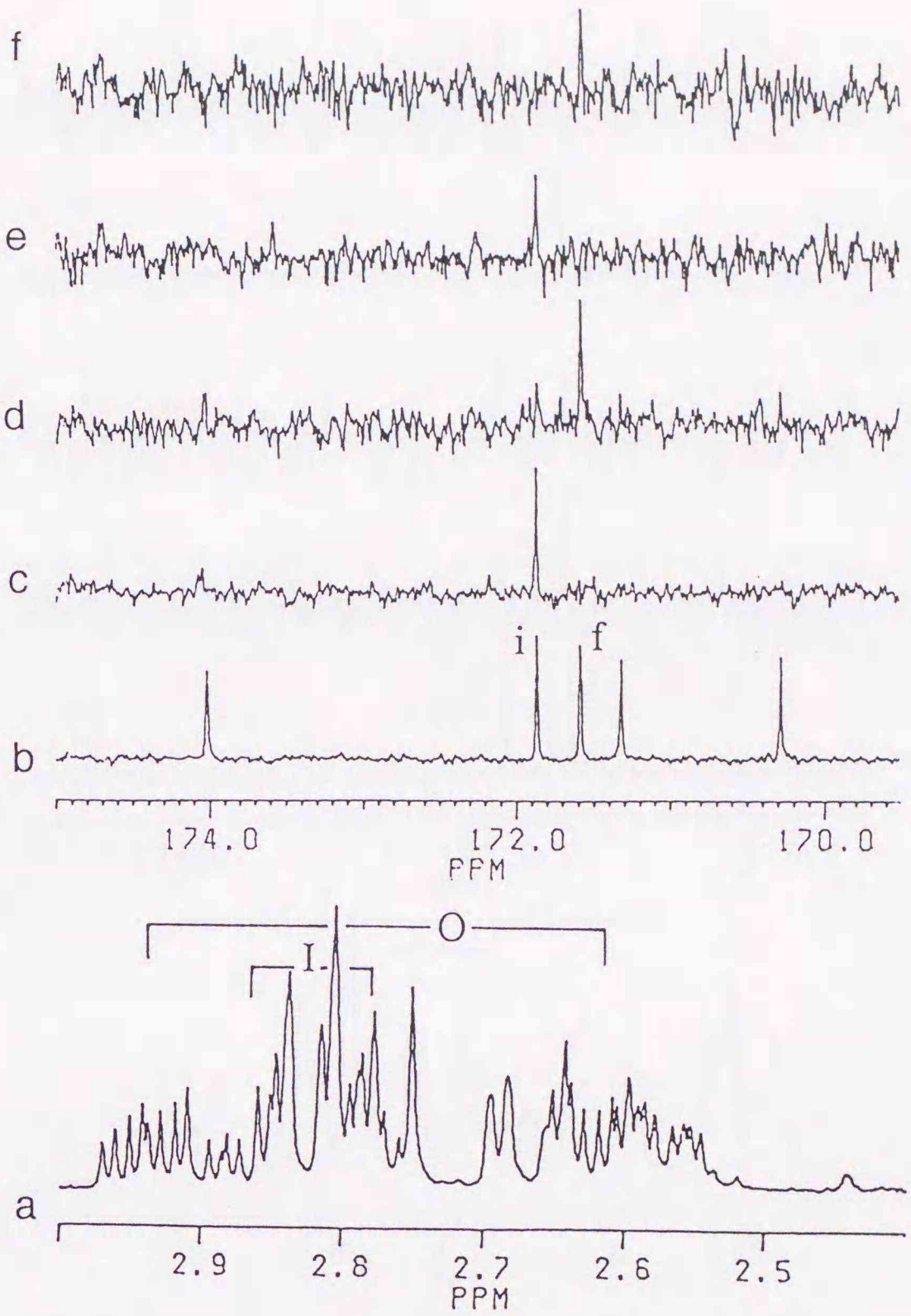


Chart 4.2 $^{13}C\{^{1}H\}$NOE experiments of **3** (*ca.* 100 mg in 0.5 ml chloroform-*d*). (a)Part of the ^{1}H spectrum. (b)Part of the ^{13}C spectrum. (c)Part of the steady-state NOE spectrum obtained from the irradiation of "I" protons. (d)Part of the steady-state NOE spectrum obtained from irradiation of "O" protons. (e)Part of the transient NOE spectrum obtained from inversion of "I" protons. (f)Part of the transient NOE spectrum from inversion of "O" protons. In (e) and (f), $\tau_m$was 1.6 s, and the number of loops was 8. In (c) and (d), 2560 transients were accumulated. The total measuring time was *ca.* 4 h each. In (e), 384 transients were accumulated. The total measuring time was *ca.* 2 h. In (f), 3776 transients were accumulated. The total measuring time was *ca.* 16 h.

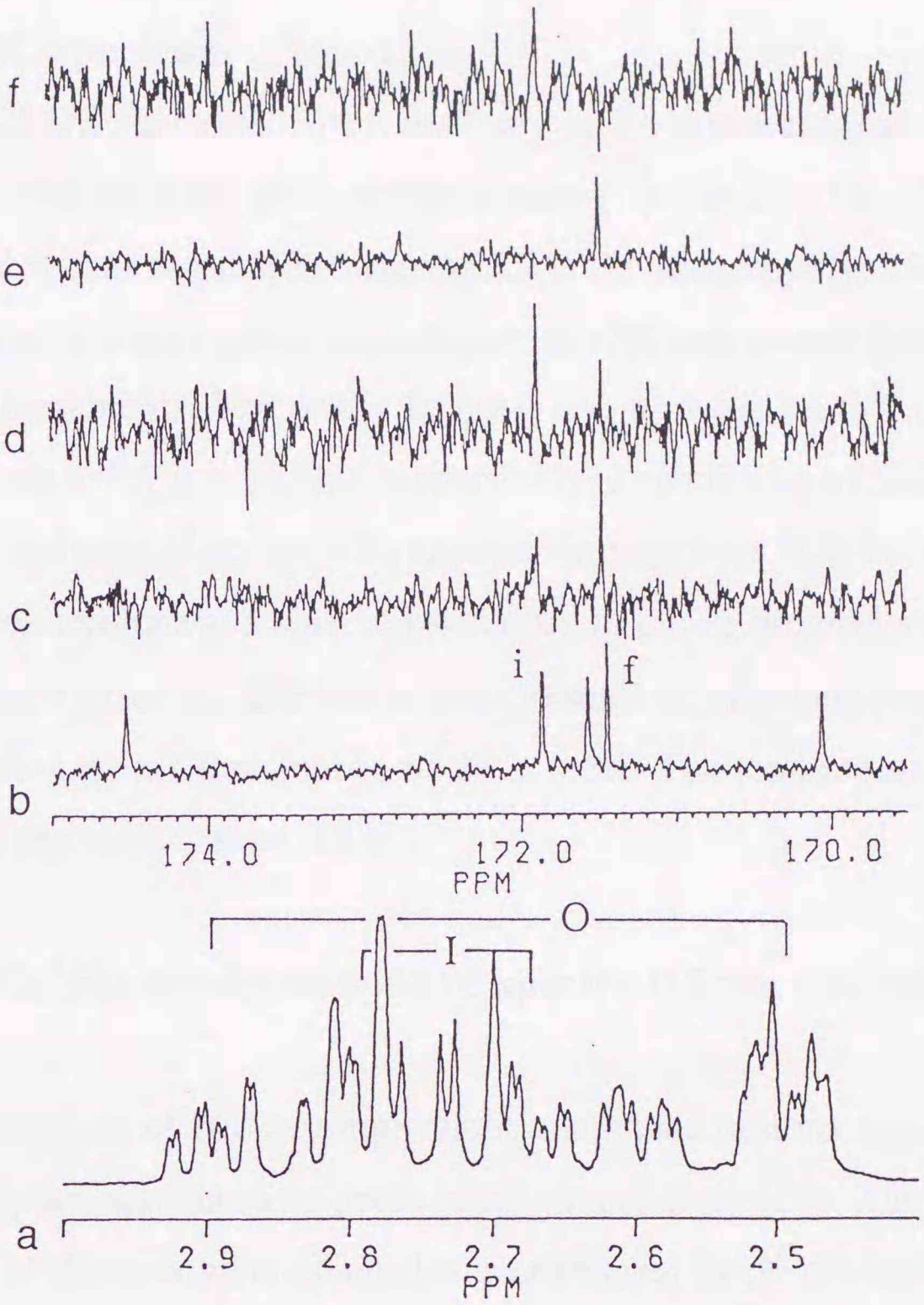


Chart 4.3 $^{13}C\{^{1}H\}$NOE experiments of **4** (*ca.* 40 mg in 0.5 ml chloroform-*d*). (a)Part of the ^{1}H spectrum. (b)Part of the ^{13}C spectrum. (c)Part of the steady-state NOE spectrum obtained from the irradiation of "I" protons. (d)Part of the steady-state NOE spectrum obtained from irradiation of "O" protons. (e)Part of the transient NOE spectrum obtained from inversion of "I" protons. (f)Part of the transient NOE spectrum from inversion of "O" protons. In (e) and (f), $\tau_m$was 1.6 s, and the number of loops was 8. In (c) and (d), 4480 transients were accumulated. The total measuring time was *ca.* 8 h each. In (e), 3456 transients were accumulated. The total measuring time was *ca.* 14 h. In (f), 3328 transients were accumulated. The total measuring time was *ca.* 14 h.

4.3. Experimental

COLOC spectrum (Chart 4.1)

The COLOC spectrum of **4** (*ca.* 40 mg in 0.5 ml of chloroform-*d*) was determined using the pulse sequence shown in Fig.2.2a (*6*). The F_2 and F_1 spectral widths were 26316 Hz and 3500 Hz, respectively; 224 scans (with two dummy scans) were accumulated into 2K data points for each of the 128 t_1 increments. The delays RD, Δ_1, and Δ_2 were set to 2.0 s, 50 ms, and 25 ms ($^{LR}J_{CH}$ = 10 Hz), respectively. Zero-filling to 512 data points for F_1 and multiplication with exponential windows (LB factor = 2) in the F_1 dimensions and sine-bell windows in the F_2 dimensions were performed prior to 2D Fourier transformation. Absolute-mode calculation gave a data matrix of 2K x 0.5K. The total measuring time of each experiment was *ca.* 18 h.

1D $^{13}C\{^1H\}$ steady-state NOE spectra (Charts 4.2c and d, and 4.3c and d)

The multiplets of two non-equivalent methylene protons were irradiated with a quasi-simultaneous preirradiation technique (*87*). The low power output of the decoupler channel was attenuated by 50 dB for irradiation. The center of each multiplet was irradiated for 63.5 ms, and in an interval of 0.5 ms the decoupler frequency was changed to another multiplet. This process was repeated 64 times, and the resulting total irradiation time was 4.5 s. The carbon pulse flip angle was 90°, and RD was 0 s. Each spectrum was measured covering the spectral width of 31250 Hz in 64K data points using 2560 transients (the measurement time was *ca.* 4 h) for **3** (*ca.* 100 mg in 0.5 ml chloroform-*d*) and 4480 transients (the measurement time was *ca.* 8 h) for **4** (*ca.* 40 mg in 0.5 ml chloroform-*d*).

1D $^{13}C\{^{1}H\}$ transient NOE spectra with rectangular long pulse (Charts 4.2e and 4.3e)

The $^{13}C\{^{1}H\}$ transient NOE spectra were determined by the pulse sequence shown in Fig. 4.2b. The simultaneous selective inversion of two non-equivalent methylene protons whose chemical shifts are close to each other was carried out by a rectangular pulse of low power output from a decoupler attenuated by 30 dB (180° pulse duration was 24 ms, effective field strength : 21 Hz). Delay τ_m was 1.6 s, and the number of loops was 8. The carbon pulse flip angle was 90°, and RD was 0 s. The spectra were recorded with 384 transients (the measurement time was *ca.* 2 h) for **3** and 3456 transients (the measurement time was *ca.* 14 h) for **4**. The other measuring conditions were the same as those of the steady-state NOE spectra.

1D $^{13}C\{^{1}H\}$ transient NOE spectra with a double-DANTE pulse (Charts 4.2f and 4.3f)

In the case where the chemical shifts of the multiplets of two non-equivalent methylene protons are separate and other signals exist between them, the simultaneous selective inversion of them was carried out by double-DANTE pulse train (*25*). The double-DANTE sequence was made up of a total of 48 fixed-phase pulses and 48 rotating-phase pulses. The phase increment was $\pi/8$, and a pulse interval was 0.17 ms for **3** and 0.14 ms for **4**. The spectra were recorded with 3776 transients (the measurement time was *ca.* 16 h) for **3** and 3328 transients (the measurement time was *ca.* 14 h) for **4** .The other measuring conditions were the same as those of the transient NOE spectra with rectangular long pulse.

5. Summary

Among the limitations in the conventional NMR method, the following structural problems were overwhelmed by developing some new techniques as well as modification of conventional methods.

1. Distinction of equivalent nuclei in symmetric molecules.

A strategy for the structure elucidation of C_2 symmetric molecules was established from the viewpoint of isotopomeric asymmetry utilizing the low natural abundance (1.11 %) of NMR detectable ^{13}C nucleus. Regarding one pair of equivalent carbons in a C_2 symmetric system, an isotopomer consisted of $\{^{12}C, ^{12}C\}$ is predominant (97.8%), whereas $\{^{13}C, ^{12}C\}$ (2.20%) and $\{^{13}C, ^{13}C\}$ (0.01%) isotopomers are minor. In ^{13}C NMR the major isotopomer is undetectable, and the $\{^{13}C, ^{13}C\}$ species is also excluded owing to its low natural abundance. Hence, the only isotopomer to be considered is the $\{^{13}C, ^{12}C\}$ species, which is not symmetrical. Separate detection of this last species solved structural problems characteristic of symmetric molecules as follows. Connectivity between equivalent carbons, C-8b and C-8b' in (H-8b)-(^{13}C-8b)-(^{12}C-8b')-(H-8b') system of hopeaphenol (**1**), a C_2 symmetric tetrastilbene isolated from *Carex pumila*, was confirmed by detecting long-range couplings between ^{13}C-8b and H-8b' by the LSPD, modified COLOC, and HMBC. NOEs between equivalent protons, H-9 and H-9' in cycloshizukaol A (**2**), a C_2 symmetric sesquiterpene dimer isolated from *Chloranthus serratus*, and H-7b and H-7b' in **1** were observed by the detection of the negative cross-peaks at the center of the split HMQC correlations in the ^{13}C-coupled HMQC-NOESY (ROESY) spectra. In addition, the measurement of *J* couplings between equivalent protons, H-8b and H-8b' in **1**, was achieved by ω_1 hetero half-filtered DQF-COSY

without interference of long-range CH couplings. Next, as a novel concept for conversion of 2D ω_1 hetero half-filtered methods to their 1D variants, PASS (*pa*ired *s*atellite *s*election) has been introduced. The long-range J_{CH} appeared as displacement of signals in the resulting two 1D spectra. In **1**, ^2J(C-8b/H-7b) and ^3J(C-8b/H-7b') were measured separately by PASS-TOCSY for C-8b. PASS-NOESY (ROESY) made it possible to detect intra-unit (H-9/H-1) NOEs in **2**, and intra-unit (H-8b/H-14b) ROEs in **1** by utilizing the difference of two long-range values between J(C-9/H-1) and J(C-9/H-1'), and between J(C-8b/H-14b) and J(C-8b/H-14b'), respectively.

2. Analysis of highly proton-deficient molecules.

As for the structure elucidation of proton-deficient molecules, a new detection method for ^{13}C-^{13}C coupling, DEPT C-C relay has been constructed. This sequence enables spectrum editing to the relayed spectra to discriminate CH_3-, CH_2-, CH-C connectivities. The phase distortion varying with resonance offset, which is especially a problem in high-field instruments, is efficiently compensated by using phase-alternating ^{13}C composite pulses. Accurate J_{CC} values can be determined since constant phase results were available. Furthermore, construction of CH, CH_2 and CH_3 subspectra by DEPT spectrum editing makes it possible to detect the ^{13}C-^{13}C satellite signals even at the protonated carbon sites since the strong contribution of the single quantum coherence derived from $^1J_{CH}$ also undergoes the selection by the editing. In addition, a 2D variant of the sequence was also proposed, which enabled well-resolved detection of C-C correlations including those between protonated carbons. Application of a baseline subtraction routine greatly improves the spectral quality. The advantages of these relay methods over INADEQUATE are independency from J_{CC} values, and no sensitivity loss caused by double-

quantum filtration in INADEQUATE. Moreover, correlations between proton and carbon via 4 bonds (^{1}H-^{13}C-X-X-^{13}C), are obtained by BIRD/DEPT C-C relay methods, tuning the C-C relay part for long-range C-C couplings.

3. Discrimination of CH connectivities via two and three bonds.

The discrimination of CH connectivities via two and three bonds was solved by detection of two-bond connectivities selectively by the application of heteronuclear $^{13}C\{^{1}H\}$ NOE experiments, which revealed the assignments of two methylenes in succinate unit of shizukaols F (**3**) and B (**4**), isolated from *Chloranthus japonicus*. The NOEs from one of the non-equivalent methylene protons in steady-state or transient NOE method did not give enough sensitivity due to the three-spin effect, whereas NOEs from both protons gave satisfactory results. For steady-state NOE, both protons were saturated simultaneously by quasi-simultaneous irradiation. As for transient NOE, two protons whose chemical shifts were close were inverted by rectangular pulse, and inversion of both protons whose chemical shifts were far from each other was performed using a double DANTE pulse train.

6. References

1. T. J. Arnold, S. S. Dharmatti and M. E. Packard, *J. Chem. Phys.* **19**, 507 (1951).
2. A. E. Derome, "Modern NMR Techniques for Chemistry Research.", Pergamon, Oxford, 1987, p.187.
3. L. Müller, A. Kumar and R. R. Ernst, *J. Chem. Phys.* **63**, 5490 (1975).
4. J. Kawabata, E. Fukushi, M. Hara and J. Mizutani, *Magn. Reson. Chem.* **30**, 6 (1992).
5. S. Takeuchi, J. Uzawa, H. Seto and H. Yonehara, *Tetrahedron Lett.* 2943 (1977).
6. H. Kessler, C. Griesinger, J. Zarbock and R. Loosli, *J. Magn. Reson.* **57**, (1984).
7. A. Bax and M. F. Summers, *J. Am. Chem. Soc.* **108**, 2093 (1986).
8. M. F. Summers, L. G. Marzilli and A. Bax, *J. Am. Chem. Soc.* **108**, 4285 (1986).
9. R. C. Crouch, R. B. McFadyen, S. M. Daluge and G. E. Martin, *Magn. Reson. Chem.* **28**, 792 (1990).
10. G. E. Martin and R. C. J. Crouch, *J. Nat. Prod.* **54**, 1 (1991).
11. J. Kawabata, E. Fukushi and J. Mizutani, *Phytochemistry* **32**, 1347 (1993).
12. J. Kawabata, E. Fukushi and J. Mizutani, *J. Am. Chem. Soc.* **114**, 1115 (1992).
13. E. Fukushi and J. Kawabata, *J. Magn. Reson. Ser. A* **108**, 103 (1994).
14. M. Kurtz, P. Schmieder and H. Kessler, *Angew. Chem. Int. Ed. Engl.* **30**, 1329 (1991).
15. U. Wollborn and D. Leibfritz, *J. Magn. Reson.* **98**, 42 (1992).

16. A. Bax, R. Freeman and T. A. Frenkiel, *J. Am. Chem. Soc.* **103**, 2102 (1981).
17. A. Bax, "Two-Dimensional Nuclear Magnetic Resonance in Liquids.", Delft Univ. Press, Delft, 1984, p.157.
18. S. Wimperis and G. Bodenhausen, *J. Magn. Reson.* **71**, 355 (1987).
19. J. Kawabata and E. Fukushi, *J. Magn. Reson. Ser. A* **107**, 173 (1994).
20. J. Kawabata and E. Fukushi, *J. Magn. Reson. Ser. A* **117**, 88 (1995).
21. H. Seto, T. Sasaki, H. Yonehara and J. Uzawa, *Tetrahedron Lett.* **10**, 923 (1978).
22. J. Uzawa and S. Takeuchi, *Org. Magn. Reson.* **11**, 502 (1978).
23. E. Fukushi and J. Kawabata, *Magn. Reson. Chem.* **33**, 909 (1995).
24. J. Kawabata, E. Fukushi and J. Mizutani, *Phytochemistry* **39**, 121 (1995).
25. H. G. Geen, X.-L. Wu, P. Xu, J. Friedrich and R. Freeman, *J. Magn. Reson.* **81**, 646 (1989).
26. L. Poppe and H. van. Halbeek, *J. Magn. Reson.* **93**, 214 (1992).
27. M. Nakagawa, M. Endo, N. Tanaka and L. Gen-Pei, *Tetrahedron Lett.* **25**, 3227 (1984).
28. Y. Kato, N. Fusetani, S. Matsunaga, K. Hashimoto, R. Sakai, T. Higa and Y. Kashman, *Tetrahedron Lett.* **28**, 6225 (1987).
29. I. Kitagawa, M. Kobayashi, T. Katori, J. Tanaka, M. Doi and T. Ishida, *J. Am. Chem. Soc.* **112**, 3710 (1990).
30. A. A. Bothner-By, R. L. Stephens, J. Lee, C. D. Warren and R. W. Jeanloz, *J. Am. Chem. Soc.* **106**, 811 (1984).
31. A. Bax and D. G. Davis, *J. Magn. Reson.* **63**, 207 (1985).
32. O. W. Sørensen and R. R. Ernst, *J. Magn. Reson.* **51**, 477 (1983).
33. S. Prytulla, J. Lauterwein, M. Klessinger and J. Thiem, *Magn. Reson. Chem.* **28**, 888 (1990).

34. J. Kawabata and J. Mizutani, *Phytochemistry* **31**, 1293 (1991).

35. G. Englet, T. Bjornland and S. Liaaen-Jensen, *Magn. Reson. Chem.* **28**, 519 (1990).

36. D. Neuhaus and J. Keeler, *J. Magn. Reson.* **68**, 568 (1986).

37. D. G. Davis, *J. Magn. Reson.* **84**, 417 (1989).

38. Karplus, *J. Chem Phys.* **30**, 11 (1959).

39. Karplus, *J. Am. Chem. Soc.* **85**, 2870 (1963).

40. M. Eberstadt, G. Gemmecker, D. F. Mierke and H. Kessler, *Angew. Chem. Int. Ed. Engl.* **34**, 1671 (1995).

41. L. Lerner and A. Bax, *J. Magn. Reson* **69**, 375 (1986).

42. O. W. Sørensen, G. W. Eich, M. H. Levitt, G. Bodenhausen and R. R. Ernst, *Prog. NMR Spectrosc.* **16**, 163 (1983).

43. A. J. Shaka and A. Pines, *J. Magn. Reson.* **71**, 495 (1987).

44. E. Pretsch, T. Clerc, J. Seibl and W. Simon, "Strukturaufklarung organisher Verbindungen mit spektroskopischen Methoden.", Springer, Berlin, 1981, p.H25.

45. R. C. Crouch, J. P. Shocker and G. E. Martin, *Tetrahedron Lett.* **31**, 5273 (1990).

46. J. Bernassau and J. Nuzillard, *J. Magn. Reson.* **A104**, (1983).

47. E. Pretsch, T. Clerc, J. Seibl and W. Simon, "Strukturaufklarung organisher Verbindungen mit spektroskopischen Methoden.", Springer, Berlin, 1981, p.C235.

48. J. Cavanagh and J. Keeler, *J. Magn. Reson.* **80**, 186 (1988).

49. C. Griesinger and R. R. Ernst, *J. Magn. Reson.* **75**, 261 (1987).

50. H. Kessler, C. Griesinger, R. Kerssebaum, K. Wagner and R. R. Ernst, *J. Am Chem.Soc.* **109**, 607 (1987).

51. A. Bax, *J. Magn. Reson.* **77**, (1992).

52. O. W. Sørensen, R. Freeman, T. Frenkiel, T. H. Mareci and R. Schuck, *J. Magn. Reson.* **46**, 180 (1982).

53. H. Kessler, W. Bermel and C. Griesinger, *J. Magn. Reson.* **62**, 573 (1985).

54. K. S. Lee and G. A. Morris, *J. Magn. Reson.* **70**, 332 (1986).

55. K. E. Köver, D. Uhrin, T. Liptaj and G. Batta, *Magn. Reson. Chem.* **30**, 68 (1992).

56. S. W. Sparks and P. D. Ellis, *J. Magn. Reson.* **62**, 1 (1985).

57. I. S. Podkorytov, *J. Magn. Reson.* **89**, 129 (1990).

58. P. J. Keller and K. E. Vogele, *J. Magn. Reson.* **68**, 389 (1986).

59. J. Buddrus and H. Bauer, *Angew. Chem. Int. Ed. Engl.* **26**, 625 (1987).

60. A. Y. Denisov, A. V. Tkachev and V. I. Mamatyuk, *Magn. Reson. Chem.* **30**, 95 (1992).

61. M. H. Levitt and R. R. Ernst, *Mol. Phys.* **50**, 1109 (1983).

62. R. Tycko, H. M. Cho, E. Schneider and A. Pines, *J. Magn. Reson.* **61**, 90 (1985).

63. K. V. Schenker and W. von. Philipsborn, *J. Magn. Reson.* **66**, 219 (1986).

64. J. Lambert, H. J. Kuhn and J. Buddrus, *Angew. Chem. Int. Ed. Engl.* **28**, 738 (1989).

65. A. M. Torres, T. T. Nakashima and R. E. D. McClung, *J. Magn. Reson.* **99**, 99 (1992).

66. R. Freeman, T. Frenkiel and M. B. Rubin, *J. Am. Chem. Soc.* **104**, 5545 (1982).

67. R. Benn, *J. Magn. Reson.* **55**, 460 (1983).

68. O. W. Sørensen, U. B. Sørensen and H. J. Jakobsen, *J. Magn. Reson.* **59**, (1984).

69. U. B. Sørensen, H. J. Jakobsen and O. W. Sørensen, *J. Magn. Reson.* **61**, 382 (1985).

70. M. R. Bendall, D. T. Pegg, D. M. Doddrell and J. Field, *J. Magn. Reson.* **51**, 520 (1983).

71. A. E. Derome, "Modern NMR Techniques for Chemistry Research.", Pergamon, Oxford, 1987, p.129.

72. D. L. Turner, *J. Magn. Reson.* **58**, 500 (1984).

73. W. Willker and D. Leibfritz, *Magn. Reson. Chem.* **32**, 665 (1994).

74. K. Tori, J. Nishikawa and Y. Takeuchi, *Tett. Lett.* 2793 (1981).

75. J. J. Ford, W. A. Gibbons and N.Nicolai, *J. Magn. Reson.* **47**, 522 (1982).

76. M. A. Khaled, *J. Am. Chem. Soc.* **105**, 3363 (1983).

77. M. F. Aldersly, F. M. Dean and B. E. Mann, *Chem. Commun.* 107 (1983).

78. N. Niccolai, C. Rossi, V. Brizzi and W. A. Gibbons, *J. Am. Chem. Soc.* **106**, 5732 (1984).

79. K. E. Köver and G. Batta, *J. Am. Chem. Soc.* **107**, 5829 (1985).

80. P. Bigler and M. Kamber, *Magn. Reson. Chem.* **24**, 972 (1986).

81. K. E. Köver and G. Batta, *J. Chem. Soc., Chem. Commun.* 647 (1986).

82. von. R. Neidlein, W. Kramer and V. Ullich, *Helv. Chimica Acta* **69**, 898 (1986).

83. P. Bigler and C. Müller, *J. Magn. Reson.* **79**, 45 (1988).

84. L. Poppe and H. van. Halbeek, *Magn. Reson. Chem.* **29**, 355 (1991).

85. C. Müller, H. R. Bircher and P. Bigler, *Magn. Reson. Chem.* **30**, 466 (1992).

86. D. Canet, N. Mahieu and P. Takely, *J. Am. Chem. Soc.* **114**, 6190 (1992).

87. K. E. Köver, *J. Magn. Reson.* **59**, 485 (1984).

7. Summary in Japanese

ルーチン1Dおよび2DNMR法によって複雑な天然有機化合物の構造が次々と明らかにされるいっぽう，通常の手法では解決できない構造をもつ化合物が取り残されている．そのなかで以下の問題点について，新たなNMR法の開発および既存の手法の改良による解決を試みた．

1. 対称な分子における等価な核の区別

C_2対称化合物は等価な二つのユニットから成り，各ユニットに含まれる一組の等価な核は^{1}H,^{13}C NMRスペクトルにおいて同一のシグナルを与える．このため既存のNMR法ではC_2対称化合物の等価なユニットの区別が困難で，構造解析をすすめる上で問題となる．このようなC_2対称化合物に特有の構造解析上の問題点を，NMRで観測可能な^{13}C核の天然存在比が低い(1.11%)ことを利用して解決した．C_2対称化合物の一組の等価な炭素に着目すると，ここが{^{12}C,^{12}C}であるアイソトポマー(異なる同位体を含んでいる異性体)が最も多く(97.8%)，{^{12}C,^{13}C}のもの(2.20%)と{^{13}C,^{13}C}のもの(0.01%)は少ない．存在比の高い{^{12}C,^{12}C}のアイソトポマーは^{13}C-NMRでは検出できず，また{^{13}C,^{13}C}のものはごく少ないため除外することができる．すなわち非対称な{^{13}C,^{12}C}のアイソトポマーのみの観測が可能である．^{13}C/^{1}H間には異種核スピンカップリングが存在し，そのカップリング定数は1本の結合を介した$^{1}J_{CH}$では120Hz以上，2,3本の結合を介した遠隔カップリング($^{LR}J_{CH}$)では15Hz以下であり，^{12}C/^{1}H間にはカップリングは存在しない．ほとんどの異種核相関法ではデカップリングを行うためこれらの分裂は観測できない．そこでデカップリングを含まない手法を作成し異種核スピンカップリングを検出することによって，{^{13}C,^{12}C}アイソトポマーの非対称性を利用した構造解析が可能となった．

まずコウボウシバ(*Carex pumila*)から得られたC_2対称なスチルベン四量体hopeaphenol(**1**)の中心結合部分((H-8b)-(C-8b)-(C-8b')-(H-8b'))の等価な炭素間の結合(C-8b/C-8b')を，LSPD，改良COLOC，HMBCによってC-8b/H-8b'間の遠隔カップリング($^{2}J_{CH}$)をC-8b/H-8bのカップリング($^{1}J_{CH}$)と区別して検出することにより証明した．つ

いで，フタリシズカ(*Chloranthus serratus*)より得られたC_2対称なセスキテルペン二量体 cycloshizukaol A(**2**)の等価なプロトン(H-9/H-9')間のNOEおよび**1**の等価なプロトン(H-7b/H-7b')間のROEを，^{13}Cカップル HMQC-NOESY(ROESY)スペクトルにおいて分裂したHMQCシグナル(**2**では^1J(^{13}C-9/H-9)，**1**では^1J(^{13}C-7b/H-7b))の中央にNOE相関ピークを検出することにより観測した．ついで2D ω_1 hetero half-filtered DQF-COSYにより**1**の等価なプロトン間(H-8b/H-8b')のJカップリングの値を^2J(C-8b/H-7b)と分離して得た．さらに，2D ω_1 hetero half-filtered 法を1D化する新しい手法としてPASS(paired satellite selection)を開発し，二つの1Dスペクトルのピークのずれから正確な$^{LR}J_{CH}$を得た．PASS-TOCSYによりひとつのカーボンと等価な二つのプロトントの間の二種類のJ値，たとえば**1**の^2J(C-8b/H-7b)と^3J(C-8b/H-7b')を別々に得た．また**2**のPASS-NOESYではJ(C-9/H-1)とJ(C-9/H-1')の差を利用してユニット内NOE(H-9/H-1)を観測できた．同様に**1**のユニット内ROE(H-8b/H-14b)をPASS-ROESYにより観測した．

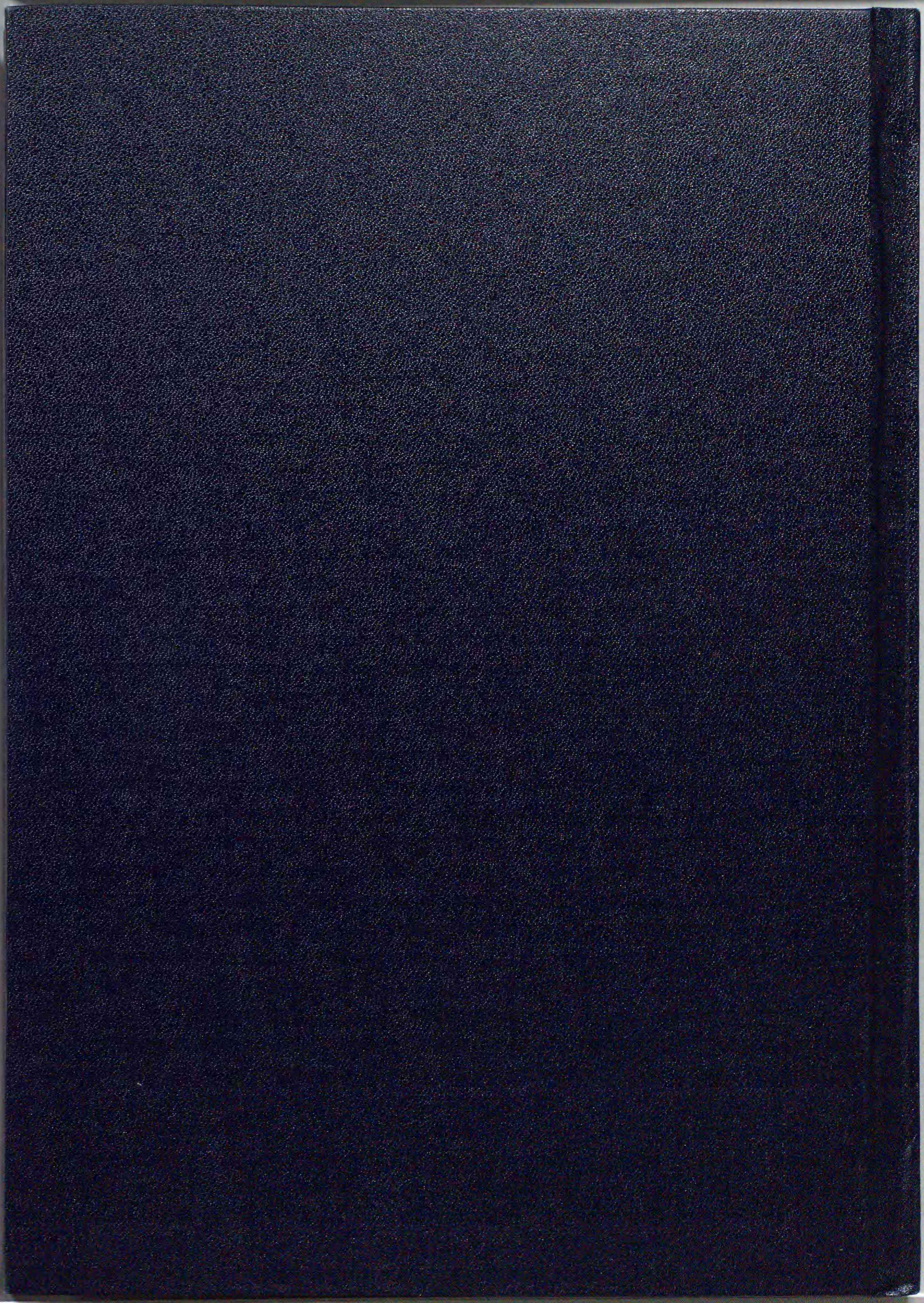
2. プロトンの少ない分子の構造解析

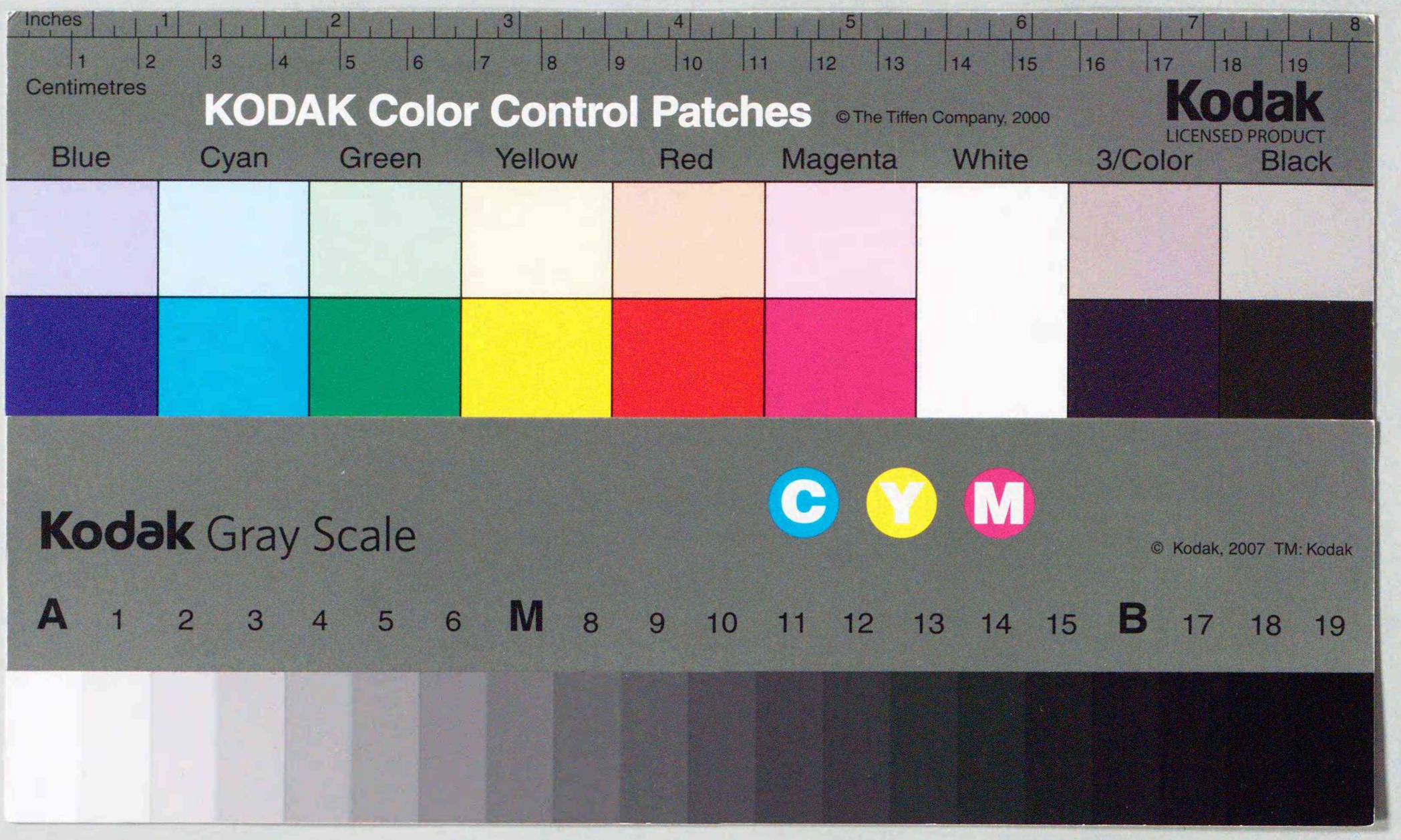
プロトンの少ない化合物の構造解析に際しては^{13}C-^{13}C 結合を直接観測する必要があるが，^{13}C-^{13}C結合を含むアイソトポマーの存在比は非常に少なく測定感度が問題となる．そこで新たな感度増大^{13}C-^{13}C結合検出法のひとつとしてDEPT C-C relayを作成した．特に高磁場の装置で問題になるオフレゾナンス効果による位相の歪みは位相交替複合パルスによって補償した．これにより正しい位相でのスペクトル編集が可能となりCH_3, CH_2, CHからの相関の区別観測に成功した．また二量子フィルターを用いないことにより問題となる，目的シグナルの100倍強い$^1J_{CH}$由来の不要シグナルもこの編集により相殺され，プロトン化炭素における^{13}C-^{13}Cサテライト観測も部分的に可能となった．リモネン(**10**)では10本のCC結合のうちスペクトル編集で不要シグナルを除去できないCH_2-CH_2結合を除く9個のJ_{CC}値を正確に求めることができた．また，本法を2D化して2D DEPT C-C relayを作成した．2D法ではF_1軸にそって強い一量子コヒーレンス由来のノイズが生じるが，大部分は適当なベースライン補正により消去できた．F_1軸方向に相関シグナルが分離することによって四級炭素だけでなくプロトン化炭素同士の相関も検出できた．さらに，BIRDパルスの導入によって厳密にセンターシグナルを除去

したBIRD/DEPT C-C relay法によって$^{3}J_{CC}$リレーシグナルの観測を試みた．C-C展開を遠隔カップリングに最適化することで通常の遠隔CH相関スペクトルで検出できるCH相関よりさらに遠くの，4本の結合を隔てたCH相関(^{1}H-^{13}C-X-X-^{13}C)が得られ，DEPTによるスペクトル編集も可能であった．

3． 2本，および3本の結合を介したプロトン-カーボン結合の区別

遠隔C-H相関では区別できない2本(^{1}H-X-^{13}C)あるいは3本(^{1}H-X-X-^{13}C)の結合を介したC-H結合の区別を，$^{13}C\{^{1}H\}$NOEにより前者のみを選択的に観測することで行った．ヒトリシズカ(*Chloranthus japonicus*)から得られたセスキテルペンラクトンshizukaol F(**3**)およびB(**4**)のコハク酸ユニットの二組のメチレンの帰属では，非等価メチレンの一つのプロトンからのNOEは三スピン効果により十分な感度が得られなかったため，double DANTEなどによって二つのプロトンを同時に励起または照射しNOEを得た．




Inches
Centimetres
KODAK Color Control Patches
© The Tiffen Company, 2000
Kodak
LICENSED PRODUCT
Blue
Cyan
Green
Yellow
Red
Magenta
White
3/Color
Black
Kodak Gray Scale
C
Y
M
© Kodak, 2007 TM: Kodak
A 1 2 3 4 5 6 M 8 9 10 11 12 13 14 15 B 17 18 19